

110
113
119P

COMPUTED POTENTIAL ENERGY SURFACES FOR CHEMICAL REACTIONS

Periodic Research Report

for the period

January 1, 1993 - August 31, 1993

for

Cooperative Agreement NCC2-478

Submitted to

National Aeronautics and Space Administration
Ames Research Center
Moffett Field, California 94035

Computational Chemistry Branch
Dr. Stephen R. Langhoff, Chief and Technical Officer

Thermosciences Division
Dr. Jim Arnold, Chief

Prepared by

ELORET INSTITUTE
1178 Maraschino Drive
Sunnyvale, CA 94087
Phone: 408 730-8422 and 415 493-4710
Telefax: 408 730-1441

Dr. K. Heinemann, President and Grant Administrator
Dr. Stephen P. Walch, Principal Investigator
Dr. Eugene Levin, Co-Principal Investigator

12 October, 1993

N94-20169

Unclas

G3/25 0190871

(NASA-CR-194600) COMPUTED
POTENTIAL ENERGY SURFACES FOR
CHEMICAL REACTIONS Periodic
Research Report, 1 Jan. - 31 Aug.
1993 (Eloret Corp.) 119 p

Computed Potential Energy Surfaces for Chemical Reactions

Investigator: Dr. Stephen Walch

In the previous 6 month progress report, calculations of potential energy surfaces (PES's) for $\text{CH}_3 + \text{OH}$ [1], CH_3O [2], $\text{CH}(^2\Pi) + \text{N}_2$ [3], and for $\text{NH}_2 + \text{NO}$ [4] were described. This work has since been accepted for publication. In addition, calculations of the PES for $\text{NH}_2 + \text{O}$ have been published [5], and calculations of the PES for $\text{CH}_3 + \text{O}_2$ [6] have been submitted for publication. (Reprints or preprints of refs. 1-6 are included in the appendix.)

During the time period from 1 January 1993 to 31 August 1993 several new projects have been undertaken. In collaboration with A. Kuppermann (Cal Tech) a new global potential energy surface is being generated for



This surface is being fit using the rotated Morse oscillator method, which was used to fit the previous POL-CI surface (Walch, Dunning, and Wagner 1980). The new surface is expected to be more accurate and also includes a much more complete sampling of bent geometries. To date, 350 points have been generated for the $^3A'$ and $^3A''$ components of the $^3\Pi$ surface. These 350 points should be sufficient to generate the initial fit. The resulting PES will be used in benchmark coupled-channel calculations for this system.

A new study has been undertaken of the reaction



which had been studied previously at Ames (Walch and Jaffe 1987). The new studies have focused on the region of the surface near a possible minimum corresponding to the peroxy form of NOO. The previous work of Walch and Jaffe had indicated a shallow minimum on the PES for NOO at the CASSCF level, but subsequent externally contracted CI calculations, along a somewhat constrained minimum energy path, showed no minimum. More recently, Meredith and Schaefer found a minimum for NOO using CISD gradient methods, in apparent contra-

diction to the earlier work of Walch and Jaffe. The new studies use the internally contracted CI methodology of Werner and Knowles (MOLPRO), which permits much more extensive CI calculations than were possible in 1987. The new calculations show a very shallow minimum, corresponding to NOO; however, there is a saddle point leading to NO + O in close proximity to the minimum, and the barrier to formation of NO + O is less than 1 kcal/mol. Since the vibrational zero point energy is ≈ 4 kcal/mol, the minimum supports no bound vibrational levels. It may be that the flat region of the surface corresponding to the NOO minimum is important in photodetachment from NOO⁻.

During the course of this work, a large portion of the PES for reaction (2) has been mapped out. Since state to state cross sections for reaction (2) are important in the chemistry of high temperature air, these studies will probably be extended to permit generation of a new global potential for reaction (2).

Recently, there have been new experimental studies by Valentini and coworkers of the product ro-vibrational distributions in the abstraction channel of the CH₄ + H reaction. In order to help understand the new experimental results, a joint theoretical study is being carried out in collaboration with Muckerman (Brookhaven) and Valentini (Columbia). One feature of the new potential for CH₅, which had not been appreciated before, is that while the saddle point for H abstraction is of C_{3v} symmetry (approaching H collinear with a CH bond), at larger H to CH₄ separations the C_{3v} constrained approach is a maximum and the energy decreases if the symmetry is lowered. It appears that the minimum energy path involves initial approach toward a three fold hole, i.e. collinear with a CH bond but on the opposite side of the carbon, with subsequent switch to collinear with one CH bond at closer separations. These new features of the potential may help explain the correlations of product rotational and vibrational levels observed in the experiments.

Work is continuing on the HNO system in collaboration with Schatz (Northwestern). The potential functions for the ¹A', ³A'', and ¹A'' surfaces are essentially complete and preliminary studies have been carried out for the reaction



which occurs on the $^3A''$ surface of HNO. Both the thermal rate constant and product ro-vibrational distributions are in good agreement with experiment. These studies will be extended to the reaction



and will predict the relative probability of reaction (4a) or (4b) (i.e. the product branching ratio) and will enable testing of approximate methods for predicting product branching ratios.

In the remaining funding period, it is planned to begin studies of the reactions of singlet methylene with N_2 and acetylene. The reaction with N_2 may be important in "prompt" NO_x and the reaction with acetylene is believed to be important as an initiating step in soot formation.

References.

1. Theoretical Characterization of the Reaction $CH_3 + OH \rightarrow CH_3OH \rightarrow$ products: The $^1CH_2 + H_2O$, $H_2 + HCOH$, and $H_2 + H_2CO$ Channels, S.P. Walch, J. Chem. Phys., **98**, 3163(1993).
2. Computed Barrier Heights for $H + CH_2O \leftrightarrow CH_3O \leftrightarrow CH_2OH$, S.P. Walch, J. Chem. Phys., **98**, 3076(1993).
3. Characterization of the Minimum Energy Path for $CH(X^2\Pi) + N_2(X^1\Sigma^+) \rightarrow HCN(X^1\Sigma^+) + N(^4S)$, S.P. Walch, Chem. Phys. Lett., **208**, 214(1993).
4. Theoretical Characterization of the Reaction $NH_2 + NO \rightarrow$ products, S.P. Walch, J. Chem. Phys., in press
5. Theoretical Characterization of the Reaction: $NH_2 + O \rightarrow$ products, S.P. Walch, J. Chem. Phys., **99**, 3804(1993).
6. Characterization of the Potential Energy Surface for $CH_3 + O_2 \rightarrow$ products, S.P. Walch, Chem. Phys. Lett., submitted.

Transport Properties of Gases

Investigator: Dr. Eugene Levin

During the time period from 1 January 1993 to 31 August 1993 work continued on the determination of the transport properties of gases (e.g., viscosity, diffusion, thermal conductivity, etc.) from the collision cross-sections of the constituent species. This work was carried out in collaboration with NASA scientists Stallcop, Partridge (and others).

The results for H-H₂O completed during the prior reporting period was presented at a poster session of the 14th Annual West Coast Theoretical Chemistry/Statistical Mechanics Conference June 17-19, 1993. The paper entitled "H-H₂O potential energy surfaces and transport properties" by James R. Stallcop, Harry Partridge and Eugene Levin was presented by Dr. Stallcop of NASA. A formal submission to the Journal of Chemical Physics is in preparation. Similarly, the work on H-H₂ interactions reported during the last time period resulted in a new paper, which has been accepted for publication by the Journal of Chemical Physics [1].

During the present time period, computations were completed for H₂-H₂ and H₂-N₂. Cross section calculations for N₂-N₂ were completed based on a preliminary set of potentials. More accurate *ab initio* potentials have now been obtained by Dr. Partridge. Calculation of new cross sections and transport properties are awaiting adjustment of the new interaction potentials to form a smooth junction with the long-range forms.

Work has been continuing on the comparison of the semi-classical and quantum mechanical methods for the calculation of collision cross sections at low collision energies. The results indicate that the difference is insignificant for repulsive potentials even at low reduced mass of the collision partners and low collision energies. However, for bound potentials, the quantum mechanical calculations must be used to obtain accurate collision integrals for temperatures below about 1500 K even for collision partners with a reduced mass as large as 10. This indicates that prior work for N-N, O-O, and N-O should be revised for such temperature regimes.

During the next time period the results for the comparison of semi-classical and quantum mechanical methods will be documented and submitted for publication. The cross section, collision integral and transport property calculations for N_2-N_2 will be completed as soon as the adjusted potentials are received from Dr. Stallcop. A long-delayed report on a five-species model for air is still awaiting collision cross section or collision integral data for N-e and O-e.

References.

1. *Ab initio* potential energy surface for H-H₂, H. Partridge, C. W. Bauschlicher, Jr., J. R. Stallcop and E. Levin, J. Chem. Phys., in press

Theoretical characterization of the reaction $\text{CH}_3 + \text{OH} \rightarrow \text{CH}_3\text{OH} \rightarrow \text{products}$: The $^1\text{CH}_2 + \text{H}_2\text{O}$, $\text{H}_2 + \text{HCOH}$, and $\text{H}_2 + \text{H}_2\text{CO}$ channels

Stephen P. Walch^{a)}

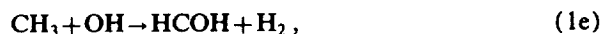
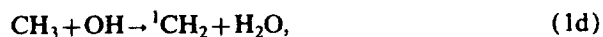
ELORET Institute, Palo Alto, California 94303

(Received 15 September 1992; accepted 10 November 1992)

The potential energy surface (PES) for the CH_3OH system has been characterized for the $^1\text{CH}_2 + \text{H}_2\text{O}$, $\text{H}_2 + \text{HCOH}$, and $\text{H}_2 + \text{H}_2\text{CO}$ product channels using complete-active-space self-consistent-field (CASSCF) gradient calculations to determine the stationary point geometries and frequencies followed by CASSCF/internally contracted configuration-interaction (CCI) calculations to refine the energetics. The $^1\text{CH}_2 + \text{H}_2\text{O}$ channel is found to have no barrier. The long range interaction is dominated by the dipole-dipole term, which orients the respective dipole moments parallel to each other but pointing in opposite directions. At shorter separations there is a dative bond structure in which a water lone pair donates into the empty a'' orbital of CH_2 . Subsequent insertion of CH_2 into an OH bond of water involves a non-least-motion pathway. The $\text{H}_2 + \text{HCOH}$, and $\text{H}_2 + \text{H}_2\text{CO}$ pathways have barriers located at -5.2 and 1.7 kcal/mol, respectively, with respect to $\text{CH}_3 + \text{OH}$. From comparison of the computed energetics of the reactants and products to known thermochemical data it is estimated that the computed PES is accurate to ± 2 kcal/mol.

I. INTRODUCTION

The $\text{CH}_3 + \text{OH}$ reaction has at least six possible product channels:



The role of reaction (1d) has been controversial. The room temperature rate for the reverse of reaction (1d) has been measured by Hatakeyama *et al.*¹ as $\approx 3 \times 10^{-12}$ $\text{cm}^3 \text{ molecule}^{-1} \text{ cm}^{-1}$, while Hack *et al.*² obtained 3.5×10^{-11} $\text{cm}^3 \text{ molecule}^{-1} \text{ cm}^{-1}$, or about an order of magnitude faster. The latter rate is approximately gas kinetic and implies no barrier. Using currently accepted heats of formation,³ and a singlet-triplet splitting for methylene of 9 kcal/mol, reaction (1d) is exothermic by 0.7 kcal/mol at 0 K. Thus the forward reaction is also expected to be very fast.

Dean and Westmoreland⁴ have used a variant of Rice-Ramsperger-Kassel-Marcus (RRKM) theory called QRRK theory to model the product distributions in the $\text{CH}_3 + \text{OH}$ reaction. In this work the parameters for reactions (1b) and (1c) were based on estimated rates for the reverse reaction. The parameters for reaction (1f) were taken from calculations⁵ and the rate for reaction (1d) was taken from Ref. 1. According to these studies, at room temperature and moderate pressure CH_3OH is the domi-

nant product, while at flame temperatures reaction (1b) is thought to take over. The $\text{HCOH} + \text{H}_2$ channel does not appear to have been considered in these studies, though theory⁵ indicates essentially no barrier with respect to $\text{CH}_3 + \text{OH}$. This study indicated that production of $^1\text{CH}_2$ [reaction 1(d)] is a minor channel. By contrast a model proposed by Pilling and co-workers⁶ which makes use of the rate for the reverse of reaction (1d) due to Hack *et al.*² indicates that reaction (1d) is the dominant channel above room temperature.

Recently Smith⁷ has also reported RRKM calculations for $\text{CH}_3 + \text{OH}$. These calculations as well as the work of Pilling *et al.*⁶ have indicated a need for more accurate potential energy surface (PES) information for the $^1\text{CH}_2 + \text{H}_2\text{O}$, $\text{H}_2 + \text{HCOH}$, and $\text{H}_2 + \text{H}_2\text{CO}$ product channels. The most accurate previous theoretical study of these channels in the CH_3OH system was carried out by Harding, Schlegel, Krishnan, and Pople⁵ using Møller-Plesset perturbation theory with a 6-31G** basis set. Although these calculations were carefully carried out, there is probably considerable uncertainty in the energetics; by current standards, both the basis set and treatment of electron correlation can be improved upon. More recently the bond dissociation energies of CH_3OH have been computed by Bauschlicher, Langhoff, and Walch⁸ using the modified coupled-pair functional method. Similar calculations were carried out by Pople and co-workers⁹ using the G2 method, which includes some empirical corrections. These calculations accurately determined the heats of formation of the CH_3O and CH_2OH species, but they did not consider the portions of the PES leading to the $^1\text{CH}_2 + \text{H}_2\text{O}$, $\text{H}_2 + \text{HCOH}$, and $\text{H}_2 + \text{H}_2\text{CO}$ product channels. Thus these regions of the PES are reexamined here.

Qualitative features of the potential energy surfaces are discussed in Sec. II, the computational method is discussed in Sec. III, the results are presented in Sec. IV, and the conclusions are given in Sec. V.

^{a)}Mailing address: NASA Ames Research Center, Moffett Field, CA 94035.

TABLE II. Computed energies and zero-point corrections.

(a)	Energy ^a	$\text{CH}_3\text{OH} \rightarrow \text{CH}_2\text{O} + \text{H}_2$ Zero-point energy ^b	ΔE^c
CH_3OH	-115.513 97 (-0.54566)	0.052 58	0.0
$\text{CH}_2\text{O}-\text{H}_2$	-115.356 03 (-0.39071)	0.044 07	91.9
$\text{CH}_2\text{O} + \text{H}_2$	-115.472 15 (-0.50189)	0.037 68	18.1
(b)	$\text{CH}_3\text{OH} \rightarrow {}^1\text{CH}_2 + \text{H}_2\text{O}$		
CH_3OH	-115.513 97 (-0.54566)	0.052 58	0.0
$\text{CH}_2-\text{H}_2\text{O}$	-115.369 31 (-0.40561)	0.043 66	82.3
$\text{CH}_2 + \text{H}_2\text{O}$	-115.359 89 (-0.39040)	0.038 84	88.8
(c)	$\text{CH}_3\text{OH} \rightarrow \text{HCOH} + \text{H}_2$		
CH_3OH	-115.505 89 (-0.54231)	0.052 58	0.0
$\text{HCOH}-\text{H}_2$	-115.358 03 (-0.39640)	0.042 25	85.0
$\text{HCOH} + \text{H}_2$	-115.378 23 (-0.41465)	0.038 28	71.1

^aEnergy in hartree. The first energy is the CCI energy, while the energy in parenthesis includes a multireference Davidson correction and is with respect to -115. hartree.

^bZero-point energy in hartree.

^cRelative energy in kcal/mol including zero-point energy and a multireference Davidson's correction.

and ${}^1\text{CH}_2 + \text{H}_2\text{O}$, (denoted as $\text{CH}_2\text{O}-\text{H}_2$, $\text{HCOH}-\text{H}_2$, and $\text{CH}_2-\text{H}_2\text{O}$, respectively) and for the $\text{CH}_2 + \text{H}_2\text{O}$ dative bonded structure (denoted as $\text{CH}_2 \cdot \text{H}_2\text{O}$) are also given in Table III. The stationary point corresponding to $\text{CH}_2 \cdot \text{H}_2\text{O}$ is a minimum on the PES, but there is one very small frequency (26 cm^{-1}), which corresponds to a hindered rotation of the CH_2 and H_2O with respect to each other.

The computed energy separations discussed here, in each case, involve breaking two bonds and forming two new bonds; thus the errors in the individual bond strengths cancel and the computed energetics are expected to be accurate. However, in Ref. 2 it was shown that, for calculations of about the same quality as reported here, the error in the C-O bond strength in CH_3OH is 6.5 kcal/mol. Thus in order to compute energies with respect to $\text{CH}_3 + \text{OH}$, the experimental 0 K value of 90.2 kcal/mol¹⁸ was used for the C-O bond strength. The locations of the $\text{H} + \text{CH}_3\text{O}$ and $\text{H} + \text{CH}_2\text{OH}$ asymptotes were taken as the best-estimate values from Ref. 2. This places $\text{H} + \text{CH}_3\text{O}$ and

$\text{H} + \text{CH}_2\text{OH}$ at 14.8 and 6.0 kcal/mol above $\text{CH}_3 + \text{OH}$, respectively. The experimental locations of ${}^1\text{CH}_2 + \text{H}_2\text{O}$ and $\text{CH}_2\text{O} + \text{H}_2$ with respect to CH_3OH were derived from the JANAF³ heats of formation of H_2 , CH_2O , CH_3 , OH , $\text{H}_2\text{O}(g)$, and ${}^3\text{CH}_2$, plus a singlet-triplet splitting in CH_2 of 9.0 kcal/mol and the value for the C-O bond strength in CH_3OH given above.

From Table I it is seen that the computed $\text{CH}_3\text{OH} \rightarrow {}^1\text{CH}_2 + \text{H}_2\text{O}$ separation is 0.7 kcal/mol smaller than experiment, while the computed $\text{CH}_3\text{OH} \rightarrow \text{CH}_2\text{O} + \text{H}_2$ separation is 0.6 kcal/mol smaller than experiment. It is also seen that the computed results of Harding *et al.*⁵ are 5.4 kcal/mol larger and 2.3 kcal/mol smaller, respectively, for the same separations. The com-

TABLE III. Computed saddle point frequencies and rotational constants (cm^{-1}).

	$\text{CH}_2\text{O}-\text{H}_2$	$\text{HCOH}-\text{H}_2$	$\text{CH}_2 \cdot \text{H}_2\text{O}$	$\text{CH}_2-\text{H}_2\text{O}$
ω_1	3195	4130	3860	3723
ω_2	2295	3199	3744	3319
ω_3	1740	2323	3187	3222
ω_4	1574	1564	3113	2091
ω_5	1429	1498	1691	1560
ω_6	1369	1347	1515	1524
ω_7	916	1291	802	1119
ω_8	2877i	1122	610	949
ω_9	3278	934	337	703
ω_{10}	1273	622	334	438
ω_{11}	1211	513	161	387
ω_{12}	1065	1414i	26	1850i
<i>A</i>	3.345	3.042	4.117	4.640
<i>B</i>	0.944	0.839	0.358	0.496
<i>C</i>	0.863	0.764	0.349	0.478

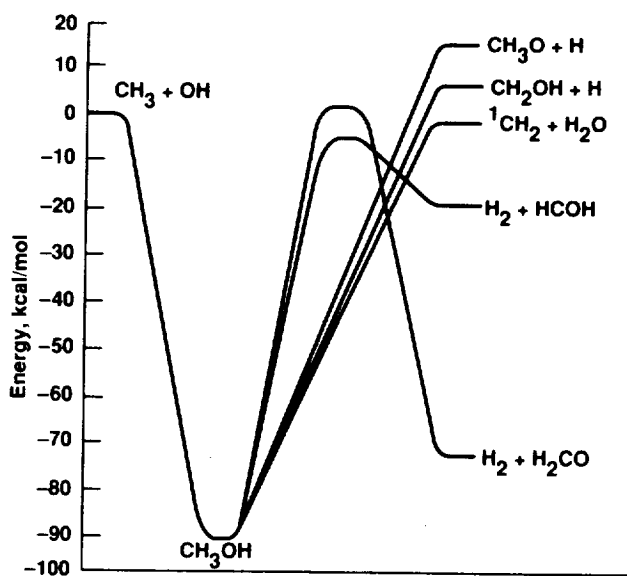


FIG. 1. Schematic diagram of the potential energy surface for $\text{CH}_3 + \text{OH}$. The location of the $\text{CH}_3 + \text{OH}$ asymptote with respect to CH_3OH is taken from experiment, while the locations of the $\text{CH}_2\text{OH} + \text{H}$ and $\text{CH}_3\text{O} + \text{H}$ asymptotes are from previous calculations.

TABLE V. Computed dipole and quadrupole moments.^a

	μ	Q_{xx}	Q_{yy}	Q_{zz}
H_2O	0.768	-1.987	1.955	0.032
$\text{CH}_2^1A_1$	0.679	1.187	0.496	-1.683

^aProperties are in a.u. Quadrupole moment is with respect to the center of mass. The molecule is in the YZ plane with the C_2 axis in the Z direction.

equilibrium geometries and oriented with the planes of the molecule parallel to each other and the CO bond perpendicular to both molecular planes in the orientation shown in Fig. 2. For this geometric orientation, r_{CO} was varied and the resulting energies at the CCI level are also included in Fig. 2.

The main features of Fig. 2 are a shallow minimum followed by a small barrier to formation of CH_3OH . However, the barrier is below the $^1\text{CH}_2 + \text{H}_2\text{O}$ asymptote and therefore the bottleneck on the vibrationally adiabatic curve is expected to occur in the entrance channel region. The main feature responsible for the entrance channel bottleneck is the building in of bending modes, which arise from electrostatic (dipole-dipole, dipole-quadrupole, and quadrupole-quadrupole) interactions. In order to define this interaction, dipole and quadrupole moments (about the center of mass) were computed for $^1\text{CH}_2$ and H_2O and are given in Table V. The experimental values¹⁹ for H_2O (in a.u.) are $\mu = 0.73$, $Q_{xx} = -1.859$, $Q_{yy} = -1.955$, and $Q_{zz} = -0.097$; which are in reasonable agreement with the computed values.

V. CONCLUSIONS

The potential energy surface (PES) for the CH_3OH system has been characterized for the $^1\text{CH}_2 + \text{H}_2\text{O}$, $\text{H}_2 + \text{HCOH}$, and $\text{H}_2 + \text{H}_2\text{CO}$ product channels using complete-active-space self-consistent field (CASSCF) gradient calculations to determine the stationary point geometries and frequencies followed by CASSCF/internally contracted configuration-interaction (CCI) calculations to refine the energetics.

The $\text{H}_2 + \text{H}_2\text{CO}$, and $\text{H}_2 + \text{HCOH}$ pathways have barriers located at 1.7 and -5.2 kcal/mol with respect to $\text{CH}_3 + \text{OH}$. The $^1\text{CH}_2 + \text{H}_2\text{O}$ channel is found to have no barrier in the absence of vibrational zero-point effects. However, the long range interaction is dominated by a

dipole-dipole term and the zero-point effects due to this interaction are expected to lead to a bottleneck on the vibrationally adiabatic minimum energy path. The $^1\text{CH}_2 + \text{H}_2\text{O}$ asymptote is computed to be 1.4 kcal/mol below $\text{CH}_3 + \text{OH}$. Thus all three of these channels are expected to be accessible at moderate temperatures.

From comparison of the computed energetics of the reactants and products to known thermochemistry it is estimated that the computed PES is accurate to ± 2 kcal/mol.

ACKNOWLEDGMENT

S. P. W. was supported by NASA Cooperative Agreement Number NCC2-478.

- S. Hatakeyama, H. Bandow, M. Okuda, and H. Akimoto, *J. Phys. Chem.* **85**, 2249 (1981).
- W. Hack, H. Gg. Wagner, and A. Wilms, *Ber. Bunsenges. Phys. Chem.* **92**, 620 (1988).
- M. W. Chase, Jr., C. A. Davies, J. R. Downey, Jr., D. J. Frurip, A. A. McDonald, and A. N. Syverud, *J. Phys. Chem. Ref. Data* **14**, Suppl. 1 (1985).
- A. M. Dean and P. R. Westmoreland, *Int. J. Chem. Kinet.* **19**, 207 (1987).
- L. B. Harding, H. B. Schlegel, R. Krishnan, and J. A. Pople, *J. Phys. Chem.* **84**, 3394 (1980).
- N. J. Green, A. R. Pereira, M. J. Pilling, and S. H. Robinson, presented at the 23rd Symposium (International) on Combustion, 1990; poster.
- G. P. Smith, 203rd ACS National Meeting, San Francisco, April 1992.
- C. W. Bauschlicher, Jr., S. R. Langhoff, and S. P. Walch, *J. Chem. Phys.* **96**, 450 (1991).
- L. A. Curtiss, L. D. Kock, and J. A. Pople, *J. Chem. Phys.* **95**, 4040 (1991).
- T. H. Dunning, Jr. and L. B. Harding, *Theory of Chemical Reaction Dynamics*, edited by M. Baer (CRC, Boca Raton, 1985), pp. 1-69.
- W. A. Goddard III, *J. Am. Chem. Soc.* **94**, 793 (1972).
- T. H. Dunning, Jr. and P. J. Hay, in *Methods of Electronic Structure Theory*, edited by H. F. Schaefer III (Plenum, New York, 1977).
- T. H. Dunning, Jr., *J. Chem. Phys.* **90**, 1007 (1989).
- SIRIUS is an MCSCF program written by H. J. Jensen and H. Agren and ABACUS is an MCSCF derivatives program written by T. Helgaker, H. J. Jensen, P. Jørgensen, J. Olsen, and P. R. Taylor.
- H.-J. Werner and P. J. Knowles, *J. Chem. Phys.* **89**, 5803 (1988).
- P. J. Knowles and H.-J. Werner, *Chem. Phys. Lett.* **145**, 514 (1988).
- S. R. Langhoff and E. R. Davidson, *Int. J. Quantum Chem.* **8**, 61 (1974).
- D. D. Wagman, W. H. Evans, V. B. Parker, S. H. Schumm, I. Halow, S. M. Bailey, K. L. Churney, and R. L. Nutall, *J. Phys. Chem. Ref. Data* **11**, Suppl. 1 (1982).
- C. G. Gray and K. E. Gubbins, *Theory of Molecular Fluids*, Vol. 1 (Clarendon, Oxford, 1984).

Computed barrier heights for $\text{H} + \text{CH}_2\text{O} \leftrightarrow \text{CH}_3\text{O} \leftrightarrow \text{CH}_2\text{OH}$

Stephen P. Walch^{a)}

ELORET Institute, Palo Alto, California 94303

(Received 4 September 1992; accepted 28 October 1992)

The barrier heights (including zero-point effects) for $\text{H} + \text{CH}_2\text{O} \rightarrow \text{CH}_3\text{O}$ and $\text{CH}_3\text{O} \rightarrow \text{CH}_2\text{OH}$ have been computed using complete active space self-consistent field (CASSCF)/gradient calculations to define the stationary point geometries and harmonic frequencies and internally contracted configuration-interaction (CCI) to refine the energetics. The computed barrier heights are 5.6 and 30.1 kcal/mol, respectively. The former barrier height compares favorably to an experimental activation energy of 5.2 kcal/mol.

The CH_3O radical is important in combustion and atmospheric chemistry.¹ In addition, recent experiments have studied individual rovibrational states of CH_3O above the $\text{H}-\text{CH}_2\text{O}$ dissociation threshold by stimulated emission pumping.² The interpretation of these experiments depends critically on the barriers to the decomposition of CH_3O to $\text{H} + \text{CH}_2\text{O}$ and rearrangement to CH_2OH . Previous studies of these barrier heights include the work of Saebø, Radom, and Schaefer,³ who used Møller-Plesset perturbation theory through third order with small basis sets up through 6-31G**. More recently, Page, Lin, He, and Choudhury⁴ reported somewhat more accurate calculations using multireference configuration-interaction (MRCI) with polarized triple zeta basis sets. In the present paper more accurate calculations are reported which make use of larger basis sets and extensive CI.

Two different basis sets were used in this work. For the complete active space self-consistent field (CASSCF) gradient calculations the polarized double zeta set of Dunning and Hay⁵ was used. The basis set for C and O is a (9s5p)/[3s2p] basis augmented by a single set of 3d functions with exponents of 0.75 and 0.85 for C and O, respectively. The H basis is (4s)/[2s] augmented with a single set of 2p functions with exponent 1.00. The basis set used in the CI calculations is the Dunning correlation consistent triple zeta double polarization basis set.⁶ This basis is [4s3p2d1f] for C and O and [3s2p1d] for H and is described in detail in Ref. 6.

The calculations were carried out in C_s symmetry for a wave function of ${}^2A'$ symmetry. From the Hessian matrix in the diagonal representation, the stationary points obtained in C_s symmetry are the minimum for $\text{CH}_2\text{O} + \text{H}$, the saddlepoint for $\text{CH}_2\text{O} + \text{H} \rightarrow \text{CH}_3\text{O}$, the CH_3O minimum, and the saddlepoint for $\text{CH}_3\text{O} \rightarrow \text{CH}_2\text{OH}$. For CH_3O the ${}^2A'$ state corresponds to one component of the 2E state in C_{3v} symmetry. According to the calculations of Saebø *et al.*,³ the Jahn-Teller stabilization energy in this system is 0.56 kcal/mol and the Jahn-Teller splitting is 0.12 kcal/mol, with the ${}^2A'$ component lower. CH_2OH is found to have no symmetry and the use of a mirror plane of symmetry would not be appropriate. However, the separation between CH_3O and CH_2OH has been accurately computed

by Bauschlicher, Langhoff, and Walch⁷ and further calculations for CH_2OH were not carried out here.

The CASSCF calculations consisted of five electrons and five orbitals. The active electrons for CH_3O included the CO bond pair, one CH bond pair (the CH bond in the molecular plane), and the a' O 2p like orbital. These orbitals correspond to the CO σ and π bonds plus a H 1s orbital for $\text{CH}_2\text{O} + \text{H}$. The remaining electrons, which are inactive, include the other two CH bond pairs, the a'' O 2p like orbital and the O 1s, O 2s, and C 1s like orbitals. In generating the set of reference configurations for the subsequent internally contracted CI (CCI) calculations, no more than two electrons were permitted in the weakly occupied CASSCF orbitals. All but the O 1s and C 1s electrons were correlated in the CCI calculation. A multireference analog of Davidson's correction⁸ was added to the CCI energies.

The CASSCF/gradient calculations used the SIRIUS/ABACUS system of programs,⁹ while the CCI calculations were carried out with MOLPRO.^{10,11} The calculations were carried out on the NASA Ames Cray Y-MP.

TABLE I. Computed stationary point harmonic frequencies (cm^{-1}), rotational constants (cm^{-1}), bond lengths (\AA), and bond angles (degrees).

	CH_3O	$\text{CH}_3\text{O} \rightarrow \text{CH}_2\text{OH}$	$\text{H}-\text{CH}_2\text{O}$	$\text{H} + \text{CH}_2\text{O}$
ω_1	3216	3261	3190	3174
ω_2	2921	2378	1657	1766
ω_3	1608	1556	1471	1589
ω_4	1471	1101	1220	1213
ω_5	1103	1037	605	
ω_6	997	2254 _i	1435 _i	
ω_7	3284	3391	3297	3272
ω_8	1491	1159	1281	1304
ω_9	1050	1015	770	
A	5.180	5.718	3.927	9.548
B	0.885	0.929	1.007	1.263
C	0.884	0.900	0.962	1.115
$r_{\text{C-H}_a}$	1.092	1.086	1.094	1.097
$r_{\text{C-H}_b}$	1.122	1.275	1.668	
$r_{\text{C-O}}$	1.412	1.418	1.259	1.226
$r_{\text{O-H}_b}$		1.237	2.292	
$\angle \text{H}_a\text{CH}_b$	111.5	119.1	117.1	117.2
$\angle \text{H}_b\text{CH}_b$	108.2	117.1	91.2	
$\angle \text{H}_a\text{CO}$	111.7	116.5	120.3	121.4
$\angle \text{H}_b\text{CO}$	105.3	54.4	102.2	

^{a)}Mailing address: NASA Ames Research Center, Moffett Field, California 94035.

Characterization of the minimum energy path for $\text{CH}(X^2\Pi) + \text{N}_2(X^1\Sigma_g^+) \rightarrow \text{HCN}(X^1\Sigma^+) + \text{N}(^4\text{S})$

Stephen P. Walch¹

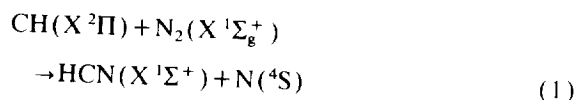
ELORET Institute, 3788 Fabian Way, Palo Alto, CA 94303, USA

Received 22 March 1993

Previous work by Manaa and Yarkony has characterized the doublet–quartet crossing region for the title reaction. In the present work, the minimum energy pathways for addition of $\text{CH}(^2\Pi)$ to N_2 on the doublet surface and for dissociation of HCNN to $\text{HCN} + \text{N}(^4\text{S})$ on the quartet surface are characterized using complete active space SCF(CASSCF) and internally contracted CI(ICCI) methods. The doublet–quartet crossing region is found to be separated from reactants by a barrier of ≈ 18 kcal/mol and from products by a barrier of ≈ 23 kcal/mol.

1. Introduction

The reaction



is believed to be the initiating step for formation of “prompt” NO in hydrocarbon combustion [1]. Measurements of the rate of reaction (1) have been summarized by Miller and Bowman [1]. There is a considerable variation of the measured rate among the different experiments; from the rate expressions the activation energy varies from ≈ 11 kcal/mol to ≈ 20 kcal/mol. The A factor for the reaction is reported [1] to be about a factor of 100 smaller than would be expected for a similar reaction which was spin allowed.

Manaa and Yarkony [2,3] have used a constrained analytical gradient search algorithm to locate regions of the doublet–quartet crossing hypersurface and have also computed the spin–orbit matrix element coupling the two surfaces. They find that the lowest energy point on the doublet–quartet crossing hypersurface corresponds approximately to a C_{2v} configuration (CH bond perpendicular to the mid-

point of a stretched N_2 bond). This region is estimated to be ≈ 7.5 kcal/mol above the $\text{CH}(^2\Pi) + \text{N}_2$ reactants. These workers also characterized a C_{2v} minimum on the doublet surface, denoted $\text{min}(C_{2v})$, which is similar to the structure of the crossing region except for a shorter NN bond, and another minimum, denoted as $\text{min}(\text{dative})$, on the same surface. These authors suggest the formation of an intermediate metastable complex structurally similar to $\text{min}(C_{2v})$ which repeatedly traverses the doublet–quartet crossing region resulting ultimately in the formation of $\text{HCN} + \text{N}(^4\text{S})$ products. Fig. 1 of ref. [3] suggests a pathway in which the barrier to reaction is at the doublet–quartet crossing, but no barriers separate this region from reactants or products. Bair [4], in an unpublished account, suggested the formation of $\text{min}(\text{dative})$ involved no barrier, but no detailed calculations had been carried out to determine whether entrance or exit channel barriers existed.

More recently, Martin and Taylor [5] have applied the same methods used in the present work to this system. They considered an entrance channel pathway in which $\text{CH}(^2\Pi) + \text{N}_2$ initially form $\text{min}(\text{dative})$ and then convert to $\text{min}(C_{2v})$ leading to the doublet–quartet crossing region studied by Manaa and Yarkony. However, they find a very large barrier (≥ 40 kcal/mol) separating $\text{min}(\text{dative})$ from $\text{min}(C_{2v})$. They also find an exit channel bar-

¹ Mailing address: NASA Ames Research Center, Moffett Field, CA 94035, USA.

rier of the same magnitude. They conclude "that the reaction mechanism is different from what has been previously suggested" (i.e. Manaa and Yarkony significantly underestimated the barrier between $\text{min}(\text{dative})$ and $\text{min}(\text{C}_{2v})$); however, they were not able to find an alternative low-energy pathway.

The failure to find a low-energy pathway for insertion of $\text{CH}(^2\Pi)$ into N_2 is surprising, since $\text{CH}(^2\Pi)$ is similar electronically to $^1\text{CH}_2$, which typically inserts into bonds with little or no barrier. However, previous experience with the $\text{CH}(^2\Pi) + \text{H}_2$ reaction [6,7] shows that insertion by a least-motion path involves a high barrier, while non-least-motion pathways involve a small barrier. The pathway involved in the latter reaction may be understood in terms of the orbital phase continuity principle (OPCP) proposed by Goddard [8]. In section 2 we show that use of the OPCP predicts that the CH addition pathway studied by Martin and Taylor (trans orientation) will have a high barrier, while a cis orientation leads to addition with a low barrier.

2. Qualitative features

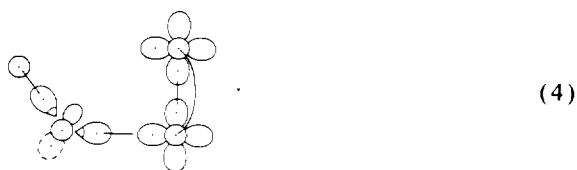
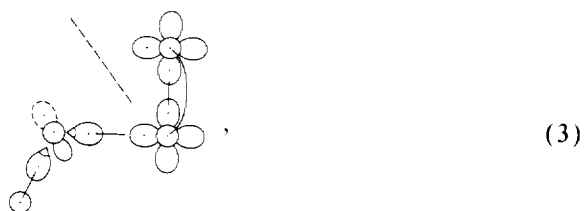
The $X^2\Pi$ state of CH may be represented by



i.e. the two orbitals corresponding to the C lone pair are singlet paired. If these orbitals are solved for self consistently in a generalized valence bond wavefunction the overlap integral between them is ≈ 0.7 . Thus, the $X^2\Pi$ state of CH may be characterized as a singlet biradical, but the orbitals of the lone pair have a substantial overlap, which must be maintained while inserting into a single bond if the process is to occur without a substantial barrier. In terms of multiconfigurational self-consistent-field (MCSCF) theory, the biradical character in the $X^2\Pi$ state of CH arises because of a near degeneracy effect between an sp hybrid lone pair and an empty $2p$ -like orbital.

A complete discussion of the OPCP is beyond the scope of this Letter and the reader is referred to the original paper by Goddard [8] and also to the dis-

ussion of the $\text{CH}(^2\Pi) + \text{H}_2$ reaction in ref. [7]. In the case of the $\text{CH}(^2\Pi) + \text{N}_2$ reaction, for approach in a trans orientation (the pathway considered by Martin and Taylor) (eq. (3), see below), it is seen that transfer of the C lone pair to become a CN bond pair leads to a nodal plane between the upper N $2p$ orbital of the N_2 in plane π bond and the other N $2p$ orbital, which evolves into a singly occupied orbital on C. (In eqs. (3) and (4) below positive orbital lobes are indicated by solid lines, negative orbital lobes are indicated by dashed lines, and the straight dashed line in eq. (3) indicates a nodal surface which results from overlap of orbitals of opposite phase.) Thus, this pathway involves breaking of one bond and is expected to have a high barrier, as Martin and Taylor found. The alternative cis approach path (eq. (4)), permits orbital phases consistent with transferring both bond pairs simultaneously, and this pathway should involve a much smaller barrier,



3. Computational details

Two different basis sets were used in this work. For the CASSCF geometry optimizations, which were performed using analytical first and second derivative methods, the polarized double zeta set of Dunning and Hay [9] was used. The basis set for C and N is a $(9s5p)/[3s2p]$ basis augmented by a single set of $3d$ functions with exponents of 0.75 and 0.80 for C and N, respectively. The H basis is $(4s)/[2s]$ augmented with a single set of $2p$ functions with exponent 1.00. The basis set used in the CI calculations

Table 2
Computed stationary point energies ^{a)}

	ICCI(ICCI+Q+147.)	ZPE ^{b)}	ICCI+Q+147.+ZPE	ΔE ^{c)}
react	-147.58272(-0.59243)	0.01119	-0.58124	0.0
dsp1	-147.54932(-0.56830)	0.01603	-0.55227	18.2
dmin1	-147.57896(-0.59738)	0.02014	-0.57724	2.5
dsp2	-147.56897(-0.59201)	0.01768	-0.57433	4.3
dmin2	-147.60531(-0.62126)	0.01976	-0.60150	-12.7
qmin1	-147.57758(-0.59285)	0.01843	-0.57442	4.3
qsp1	-147.54642(-0.56127)	0.01643	-0.54484	22.8

^{a)} Energies in E_h unless otherwise noted.

^{b)} Zero-point energy based on harmonic CASSCF frequencies.

^{c)} Relative energy (kcal/mol).

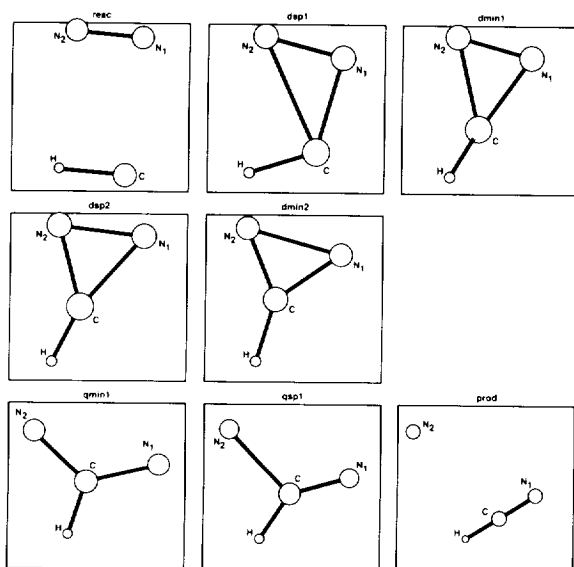


Fig. 1. Stationary point geometries along the minimum energy path for reaction (1). Note that dsp1, dmin1, and dsp2 are non-planar (see table 1).

imposed in the calculations.

From fig. 1 it is seen that the CH and N_2 approach each other in a cis orientation consistent with eq. (4). An unexpected feature of this surface is the presence of the minimum denoted by dmin1. This is a short NN structure with C_s symmetry (the CH bond lies in a plane perpendicular to the $C-N_1-N_2$ plane and passing through the C and midpoint of the NN bond). From fig. 2 it is seen that dmin1 is only a

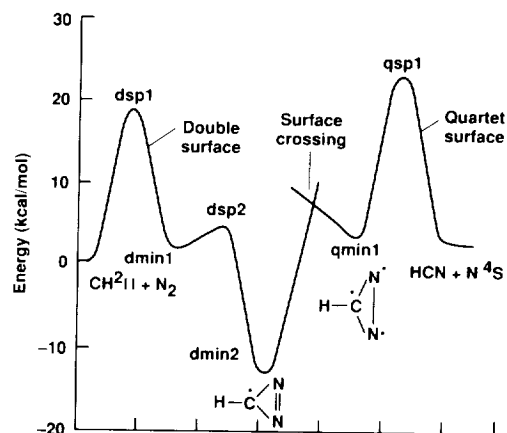
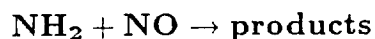


Fig. 2. Schematic representation of the minimum energy path for reaction (1). The energies are from ICCI calculations correlating eleven electrons. The location of the doublet-quartet surface crossing is taken from the work of Manaa and Yarkony [2,3].

shallow minimum connected by dsp2 to dmin2, which is a planar C_{2v} structure with a long NN bond. dmin2 is the same as Manaa and Yarkony's min(C_{2v}) and Martin and Taylor's D3 structure. Thus, the key feature of the present work is a pathway connecting $CH^2\Pi + N_2$ to Manaa and Yarkony's min(C_{2v}) with a barrier of only ≈ 18 kcal/mol. By contrast, the pathway via Manaa and Yarkony's min(dative) structure involves a trans approach and has a barrier > 40 kcal/mol in the calculations of Martin and Taylor. It is probable that, while formation of the min(dative) structure occurs with no barrier, the large barrier separating it from min(C_{2v}) means that this pathway does not lead to products.

Theoretical Characterization of the Reaction



Stephen P. Walch^a
ELORET Institute
3788 Fabian Way
Palo Alto, Ca. 94303

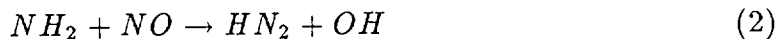
Abstract. The potential energy surface for $\text{NH}_2 + \text{NO}$ has been characterized using complete active space self consistent field (CASSCF)/ derivative calculations to determine the stationary point geometries and frequencies followed by internally contracted configuration interaction (ICCI) calculations to determine the energetics. Production of $\text{N}_2 + \text{H}_2\text{O}$ is found to involve a complex mechanism. The initially formed NH_2NO undergoes a 1,3-hydrogen shift to give an HNNOH isomer (with the substituents trans about the NN bond and cis about the NO bond) which undergoes subsequent cis-trans isomerizations about the NN and NO bonds before decomposing to $\text{N}_2 + \text{H}_2\text{O}$. The saddle point for production of $\text{N}_2 + \text{H}_2\text{O}$ has an approximately rectangular arrangement of one H atom, the two N atoms, and the O atom. This process does not involve a barrier with respect to $\text{NH}_2 + \text{NO}$. Formation of $\text{HN}_2 + \text{OH}$ can occur from any of the isomers of HNNOH with no barrier, but the overall process is endothermic by 0.7 kcal/mol (based on the computed ΔH_f^0 (0K) of HN_2).

The results obtained in this work are qualitatively the same as previous work, but both the stationary point geometries and energies should be more reliable due to the use of larger basis sets and more extensive inclusion of electron correlation effects.

^aMailing Address: NASA Ames Research Center, Moffett Field, CA 94035.

I. Introduction.

The thermal deNO_x process [1-4], in which the addition of NH₃ to combustion processes reduces the production of NO_x, may be useful in reducing NO_x emissions from jet engines. The reaction of NH₂ + NO is believed to be a key reaction in this process, but the product branching ratio at flame temperatures is not known. The two major channels which have been considered are:



The experimental literature on this reaction has been discussed by Silver and Kolb [5]. The product branching ratio $\alpha = k_2/(k_1 + k_2)$ (where k_1 and k_2 are rate coefficients for reactions (1) and (2), respectively) has ranged from > 0.65 to < 0.13 at room temperature [6-10], although most recent determinations [9-10] have converged toward lower values (0.13 [9], < 0.13 [10], and 0.12 [5]). Note that in ref. 5, Silver and Kolb reevaluated their earlier results [6] to correct for OH production from the reaction



The value of the branching ratio (α) is critical in the mechanism of the thermal deNO_x process, because production of radical species via reaction (2) feeds chain reactions. Attempts to model the thermal deNO_x process have required a value of α of 0.29-0.4 to model measurements under combustion conditions [11-16]. The work of Kimball-Linne and Hanson [17] implied that α varies with temperature from 0.48 at 1050K to >0.8 at 1400K. No direct experimental determinations exist at flame temperatures.

It is also possible to obtain the branching ratio (α) from theory. This would require accurate characterization of the potential energy surface (PES) for $\text{NH}_2 + \text{NO}$. There have been several previous theoretical studies of the PES for $\text{NH}_2 + \text{NO}$. Casewit and Goddard [18] used the generalized valence bond - configuration interaction (GVB-CI) method with a polarized double-zeta basis set to study nine isomers of formula $\text{N}_2\text{H}_2\text{O}$. In these studies the geometries were obtained using restricted Hartree-Fock (RHF) theory with a 4-31G basis set. One minor problem in this work was that a planar structure was found for NH_2NO (N-nitrosamide). Later studies by Harrison et al. [19] showed that addition of polarization functions leads to a non-planar structure.

Melius and Binkley [20] carried out an extensive series of calculations on this system using the bond additivity corrected / fourth order Møller-Plesset perturbation theory (BAC-MP4) method with a split-valence plus polarization basis set. In addition to the large bond additivity corrections (10-20 kcal/mol per bond) applied in these calculations, there are also corrections for spin contamination in the unrestricted Hartree-Fock (UHF) calculations. In previous studies on the PES for $\text{NH} + \text{NO}$ [21] it has been shown that, while the BAC-MP4 method gives results in qualitative accord with the results of multireference configuration interaction calculations, there are differences in the detailed energetics as large as 8 kcal/mol.

In a subsequent paper, Harrison and coworkers [22] carried out a study using MP2 through MP4 theory with a 6-31G* basis set. In addition to characterizing the minima on the surface, they also located a number of saddle points. These calculations differed from those of Melius and Binkley in that no empirical corrections were used. Comparison of the results obtained using this approach to MRCI [23] results for the singlet surface of CH_3OH indicates errors as large as 5 kcal/mol in the detailed energetics.

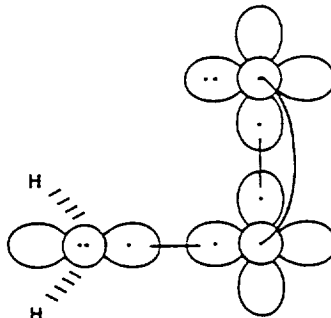
In order to improve on the energetics of the $\text{NH}_2 + \text{NO}$ reaction calculations were carried out here using CASSCF/derivative and ICCI methods with large basis sets. Section II presents some qualitative features of the calculations, Section III discusses the technical details of the calculations, Section IV presents the results and the conclusions are given in Section V.

II. Qualitative Features.

The ground state of NH_2 is 2B_1 , while the 2A_1 state is a low-lying excited state.



Combining the ground state of NH_2 with the $^2\Pi$ state of NO is most favorable for a non-planar approach



← leading to the NH_2NO species (denoted as min1) with a pyramidal geometry about the NH_2 N atom.

Fig. 1 shows the electronic structure of the stable minima on the potential energy surface. In order to consistently describe the making and breaking of bonds over the whole surface, it is necessary to correlate the two NH bonds, the NN σ bond, the NO σ bond, and the NO π bond of min1. Note that these orbitals ultimately evolve to an NN σ bond, two NN π bonds, and two OH σ bonds in the $\text{N}_2 + \text{H}_2\text{O}$ product channel. This choice of correlated orbitals is also able to describe dissociation to $\text{HN}_2 + \text{OH}$.

While min1 is non-planar, the remaining structures shown in Fig1 as well as the saddle points connecting them were found to be planar.

III. Computational Details.

Two different basis sets were used in this work. For the CASSCF derivative calculations the polarized double zeta set of Dunning and Hay [24] was used. The basis set for N and O is a (9s5p)/[3s2p] basis augmented by a single set of 3d functions with exponents of 0.80 and 0.85 for N and O, respectively. The H basis is (4s)/[2s] augmented with a single set of 2p functions with exponent 1.00. The basis set used in the CI calculations is the Dunning correlation consistent triple zeta double polarization atomic natural orbital basis set [25]. This basis is [4s3p2d1f] for N and O and [3s2p1d] for H and is described in detail in Ref. 25.

For the planar structures (min2-min4) the CASSCF/derivative calculations had 10 electrons distributed among 10 orbitals (denoted by 10/10). The active electrons correspond to the electrons in singly occupied orbitals in Fig. 1. Calculations were also carried out using a smaller CASSCF calculation which had 8 electrons distributed among 6 orbitals (denoted by 8/6). For min1 the active electrons include the upper NH σ bond, the in plane O 2p lone pair, the NO π bond, and the N 2p like lone pair. This active space is found to be adequate for describing structures min1 through min4 and the saddle points connecting them, but cannot describe dissociation to the $N_2 + H_2O$ or $HN_2 + OH$ product channels. Finally, a calculation was carried out to determine the NN bond strength for the min1 structure. The CASSCF calculation in this case had 6 electrons distributed among 6 orbitals (denoted by 6/6). The active electrons correspond to the NN σ bond, the NO σ bond, and the NO π bond for min1. In the subsequent internally contracted configuration interaction (ICCI) calculations, the N 1s and O 1s electrons were not correlated. These CI calculations were based on the 10/10, 8/6, or 6/6 CASSCF active spaces,

respectively. The reference space for the ICCI calculations was restricted to no more than two electrons in the weakly occupied CASSCF orbitals.

The CASSCF/derivative calculations used the SIRIUS/ABACUS system of programs [26], while the ICCI calculations were carried out with MOLPRO [27-30]. A multi-reference analog of the Davidson's correction [31] was added to the ICCI energies and is denoted by +Q.

IV. Discussion

Tables I, II, and III give computed ICCI energies, zero-point energies (based on harmonic CASSCF frequencies) and relative energies in kcal/mol based on the (8/6), (10/10), and (6/6) CAS active spaces, respectively. The energetics given in Tables I-III are also shown graphically in Fig. 2, while the geometries corresponding to the stationary points are given in Fig. 3.

The relative energies in Table I are given both with respect to min2 and with respect to $\text{NH}_2 + \text{NO}$. The location of the $\text{NH}_2 + \text{NO}$ asymptote is derived from Table II using the computed separation between min2 and $\text{H}_2 + \text{N}_2\text{O}$ plus the experimental separation [32] between $\text{H}_2 + \text{N}_2\text{O}$ and $\text{NH}_2 + \text{NO}$. Since the $\text{H}_2 + \text{N}_2\text{O}$ and min2 structures involve the same number of bonds (sometimes referred to as an isodesmic reaction), this computed separation is more accurate than that obtained by direct computation of the energy to dissociate min1 to $\text{NH}_2 + \text{NO}$, as in Table III. Table II also gives the energy of the $\text{H}_2\text{O} + \text{N}_2$ asymptote, computed with respect to $\text{H}_2 + \text{N}_2\text{O}$. The computed separation of 124.0 kcal/mol compares well to an experimental separation [32] of 124.5 kcal/mol. Comparing the energy for min1 given in Table I to the directly computed value given in Table III, indicates the directly computed NN bond strength in the min1 structure is too small by 5.9 kcal/mol. This is a reasonable value, since an estimate of 7.2 kcal/mol is obtained from 2/3 of the error in the N_2 dissociation energy with the same basis set.

From Tables I and II the separation between min2 and min3 is 1.5 kcal/mol with the 8/6 CASSCF active space and 1.2 kcal/mol with the 10/10 CASSCF active space. This indicates that the 8/6 active space provides an adequate description of the structures min1 to min4, as asserted in Section III.

From Fig. 2 it is seen that the saddle points in the pathway leading to $\text{N}_2 + \text{H}_2\text{O}$ are all lower in energy than the $\text{NH}_2 + \text{NO}$ asymptotic energy. The largest barrier is for the saddle point separating min3 and min4. From Fig. 3 it is seen that this is a planar saddle point, and may be thought of as an inversion process about N1. An alternative pathway involving rotation about the NN bond is found to be much higher in energy, in agreement with Fig. 1, where it is seen that min2 and min3 both have an NN double bond. The saddle point separating min2 and min3 corresponds to rotation about the NO bond and has a low barrier, in agreement with the bonding structures given in Fig. 1. Saddle point sp1 for the 1,3-hydrogen transfer also has a large barrier, but smaller than for sp3. From Fig. 1 it is seen that this process is complex, involving the simultaneous transfer of an NH bond pair to become an OH bond pair and transfer of an O 2p like lone pair to become a lone pair on N1.

From Fig. 2 it is also seen that structures min2, min3, or min4 can dissociate to $\text{HN}_2 + \text{OH}$ with no barrier other than the exothermicity. From the computed $\Delta H_f^0(0\text{K})$ of HN_2 [33] and the known heats of formation of the other species [32] reaction (2) is computed to be endothermic by ≈ 1 kcal/mol.

Reaction (1), on the other hand is exothermic by 124.5 kcal/mol and has no barriers with respect to $\text{NH}_2 + \text{NO}$. This would suggest that reaction (1) should dominate at low temperatures, but reaction (2) may also be important at higher temperatures. This is consistent with the bulk of the recent experimental information, particularly ref. 17 which implies that α is 0.48 at 1050K and > 0.8 at

1400K.

The geometric parameters of the structures shown in Fig.3 are given in Table IV. Comparing the geometries for the minima to the corresponding structures found by Harrison et al. [22] shows the expected trends, i.e. the CASSCF bond lengths are consistently larger than the SCF bond lengths. The saddle point structures found here differ more from the structures found by Harrison et al. This probably reflects the expected difficulty in describing the process of elongating chemical bonds with SCF theory.

Table V gives computed frequencies and rotational constants for the stationary points obtained in this work. Comparing the frequencies obtained here to those obtained by Harrison et al. indicates the expected trends, i.e. the CASSCF frequencies are all smaller than the SCF frequencies. Once again this well known effect derives from incorrect dissociation of chemical bonds at the SCF level of theory. This is commonly corrected for by an empirical scaling of the frequencies by 0.89. This is found to be unnecessary for CASSCF frequencies [21].

Table VI compares the energetics obtain in the present work with those obtained by Melius et al. [20] and by Harrison et al. [22]. In Table VI the results obtained here are referenced to $\text{NH}_2 + \text{NO}$. This is done in two ways. In the results denoted by ref1 the energies were computed with respect to $\text{H}_2 + \text{N}_2\text{O}$ and the $\text{NH}_2 + \text{NO}$ asymptote was positioned from experiment. In the results denoted by ref2 the energies are directly computed with respect to $\text{NH}_2 + \text{NO}$. As discussed above the results denoted ref1 are more reliable. The ref2 results are also included for comparison to the work of Harrison et al., which was done in the same way.

Comparing our ref1 results to the BAC-MP4 results of Melius et al., it is seen that the BAC-MP4 results for the stationary points min1 - sp4 vary from 5.3 kcal/mol deeper (sp1) to -0.3 kcal/mol shallower (sp3). Since the BAC-MP4 method uses

rather large (10-20 kcal/mol) bond additivity corrections, it is encouraging that the present results are on the average in fairly good agreement with the BAC-MP4 results (average error 2.4 kcal/mol more shallow). It is a bit surprising that the relative energies of structures min1 - sp4 are not in better agreement with the present results. What would be expected is that the relative energies of structures min1 - sp4 should be quite accurate in the present calculations but might be shifted somewhat with respect to $\text{NH}_2 + \text{NO}$. It is probable that the energy with respect to $\text{NH}_2 + \text{NO}$ is accurate to ± 2 kcal/mol and the relative energies should be good to similar accuracy. This suggests that there are disagreements between the present work and the BAC-MP4 results that are larger than the expected error in the present calculations. On the other hand the BAC-MP4 results do give a realistic semiquantitative picture of the PES for this system.

We now compare to the work of Harrison et al. The column of Table VI labeled ICCI+Q is computed from direct calculation with respect to $\text{NH}_2 + \text{NO}$ and without zero-point energy for comparison to the results quoted in their paper. Comparing these numbers to those quoted by Harrison et al. it is seen that our results are deeper by 3.4 - 10.6 kcal/mol (average 7.0 kcal/mol). Note that our results obtained by direct calculation with respect to $\text{NH}_2 + \text{NO}$ are in turn shallower by 5.9 kcal/mol than the results based on a calculation with respect to $\text{H}_2 + \text{N}_2\text{O}$ and use of the experimental separation between $\text{H}_2 + \text{N}_2\text{O}$ and $\text{NH}_2 + \text{NO}$. Thus, our results are deeper than those of Harrison et al. by ≈ 13 kcal/mol on an average basis. This difference reflects both the use of a larger basis set and a more consistent CASSCF/ICCI treatment of the electron correlation problem in the present calculations.

Finally, we compare to the work of Casewit and Goddard [18]. Casewit and Goddard used a GVB-CI with the Dunning polarized valence double zeta basis set

[24]. Their heats of formation were computed with respect to the sum of separate calculations on N_2 and H_2O . Since this is an isodesmic approach, their results should be compared to our results computed with respect to $H_2 + N_2O$. From Table VI it is seen that there are substantial errors, ranging from 13.8 kcal/mol to 15.1 kcal/mol for min1 - min4. These errors are surprisingly large. Part of the error must be due to the relatively small basis set, but another possible problem is the use of separate calculations on N_2 and H_2O . A supermolecule calculation would have been more appropriate and might have given more accurate heats of formation.

V. Conclusions.

The PES for $NH_2 + NO$ has been characterized using CASSCF/derivative methods to locate the stationary points followed by CASSCF/ICCI calculations using a [4s3p2d1f/3s2p1d] correlation consistent atomic natural orbital basis set to determine the energetics. Production of $N_2 + H_2O$ is found to involve a complex mechanism, which, however, has no barrier with respect to $NH_2 + NO$. This pathway is exothermic by 124.5 kcal/mol. Production of $HN_2 + OH$ can occur with no barrier other than the exothermicity from any of three isomers of $HNNOH$. Using the computed heat of formation of HN_2 this channel is endothermic by ≈ 1 kcal/mol. This suggests that the $N_2 + H_2O$ channel will dominate at low temperatures, but the $HN_2 + OH$ channel will be important at higher temperatures, in agreement with the bulk of recent experimental information.

The present calculations are in semiquantitative agreement with the BAC-MP4 results of Melius and Binkley, but there are differences which are larger than the estimated uncertainty of the present results. The present PES is deeper with respect to $NH_2 + NO$ by ≈ 13 kcal/mol as compared to the results of Harrison et al. This difference arises from two causes. First the present calculations use larger basis sets and more extensive treatment of electron correlation. Secondly it is found that

computing the location of the $\text{NH}_2 + \text{NO}$ asymptote by computing the energy of the bound species with respect to $\text{H}_2 + \text{N}_2\text{O}$ and then using the experimental $\text{H}_2 + \text{N}_2\text{O}$ to $\text{NH}_2 + \text{NO}$ separation is more accurate than direct computation with respect to $\text{NH}_2 + \text{NO}$ as was done in the Collins et al. work. The latter method is found to lead to an error of ≈ 6 kcal/mol ($\text{NH}_2 + \text{NO}$ too low with respect to the rest of the surface).

Acknowledgement. SPW was supported by NASA cooperative agreement number NCC2-478.

References

1. J.A. Miller, M.C. Branch, and R.J. Kee, *Combust. Flame*, **43**, 81(1981).
2. R.K. Lyon, Sandia Laboratories Report No. SAND70-8635, 1970.
3. R.K. Lyon, U.S. Patent 3,900,544, August 1975.
4. R.K. Lyon, *Int. J. Chem. Kinet.*, **8**, 315(1976).
5. J.A. Silver and C.E. Kolb, *J. Phys. Chem.* **91**, 3713(1987).
6. J.A. Silver and C.E. Kolb, *J. Phys. Chem.* **86**, 3240(1982).
7. P. Andresen, A. Jacobs, C. Kleinermanns, and J. Wolfrum, Nineteenth Symposium (International) on Combustion; The Combustion Institute; Pittsburgh, PA, 1982
8. L.J. Steif, W.D. Brobst, D.F. Nava, R.P. Borkowski, and J.V. Michael, *J. Chem. Soc., Faraday Trans. 2*, **78**, 1391(1982).
9. J.L. Hall, D. Zeitz, J.W. Stephens, J.V.V. Kasper, G.P. Glass, R.F. Curl, Jr., and F.K. Tittel, *J. Phys. Chem.*, **90**, 2501(1986).
10. D.A. Dolson, *J. Phys. Chem*, **90**, 6714(1986).
11. S. Salimian and R.K. Hanson, *Combust. Sci. Technol.*, **23**, 225(1980)
12. J.A. Silver, *Combustion Flame*, **53**, 17(1983).
13. J.A. Miller, M.D. Smooke, R.M. Green, and R.J. Kee, *J. Combust. Sci. Technology*, **34**, 149(1983).
14. S. Salimian, R.K. Hanson, and C.H. Kruger, *Combustion Flame*, **56**, 83(1984).
15. J.A. Miller, M.C. Branch, W.J. McLean, D.W. Chandler, M.D. Smooke, and R.J. Kee, Twentieth Symposium (International) on Combustion; The Combustion Institute; Pittsburgh, PA, 1984

16. A.M. Dean, M.-S. Chow, and D. Stern, *Int. J. Chem. Kinet.* **16**, 633(1984).
17. M.A. Kimball-Linne and R.K. Hanson, *Combust. Flame*, **64**, 377(1986).
18. C.J. Casewit and W.A. Goddard III, *J. Amer. Chem. Soc.*, **104**, 3280(1982).
19. J.A. Harrison, R.G.A.R. Maclagan, and A.R. Whyte, *Chem. Phys. Lett.*, **130**, 98(1986).
20. C.F. Melius and J.S. Binkley, Twentieth Symposium (International) on Combustion; The Combustion Institute; Pittsburgh, PA, 1984
21. S.P. Walch, *J. Chem. Phys.*, **98**, 1170(1993)
22. J.A. Harrison, R.G.A.R. Maclagan, and A.R. Whyte, *J. Phys. Chem.* **91**, 3713(1987).
23. S.P. Walch, *J. Chem. Phys.*, in press
24. T.H. Dunning, Jr. and P.J. Hay in *Methods of Electronic Structure Theory*, H.F. Schaefer III ed., Plenum Publishing, 1977
25. T.H. Dunning, Jr., *J. Chem. Phys.*, **90**, 1007(1989).
26. SIRIUS is an MCSCF program written by H.J. Jensen and H. Agren and ABACUS is an MCSCF derivatives program written by T. Helgaker, H.J. Jensen, P. Jørgenson, J. Olsen, and P.R. Taylor.
27. H.-J. Werner and P.J. Knowles, *J. Chem. Phys.* **89** (1988)5803.
28. P.J. Knowles and H.-J. Werner, *Chem. Phys. Lett.* **145** (1988)514.
29. H.-J. Werner and P.J. Knowles, *J. Chem. Phys.* **82** (1985)5053.
30. P.J. Knowles and H.-J. Werner, *Chem. Phys. Lett.* **115** (1985)259.
31. S.R. Langhoff and E.R. Davidson, *Int. J. Quantum Chem.*, **8**, 61(1974).
32. M.W. Chase, Jr., C.A. Davies, J.R. Downey, Jr., D.J. Frurip, A.A. McDonald, and A.N. Syverud, *J. Phys. Chem. Ref. Data*, **14**, Suppl. 1(1985).
33. S.P. Walch, R.J. Duchovic, and C.M. Rohlfing, *J. Chem. Phys.*, **90**, 3230(1989).

Table I. Computed energies and zero-point corrections.

ICCI calculations based on an (8/6) CASSCF

	Energy ^a	zero-point energy ^b	ΔE^c		
min1	-185.56699	0.03494	-0.53205	1.7	-44.0
sp1	-185.51535	0.03040	-0.48495	31.3	-14.4
min2	-185.57044	0.03562	-0.53482	0.0	-45.7
sp2	-185.55371			≈ 10.0	≈ -35.7
min3	-185.56798	0.03554	-0.53244	1.5	-44.2

^a ICCI +Q energy in E_H .

^b zero-point energy in E_H , obtained from the harmonic CASSCF frequencies.

^c First column ICCI +Q energy plus zero-point energy + 185. Second column energy in kcal/mol relative to min2. Third column energy in kcal/mol relative to $\text{NH}_2 + \text{NO}$.

Table II. Computed energies and zero-point corrections.

ICCI calculations based on an (10/10) CASSCF

	Energy ^a	zero-point energy ^b	ΔE^c		
H ₂ + N ₂ O	-185.57072	0.02075	-0.54997	0.0	-47.2
H ₂ O + N ₂	-185.69880	0.02643	-0.67237	-76.8	-124.0
min2	-185.58060	0.03303	-0.54757	1.5	-45.7
min3	-185.57839	0.03278	-0.54561	2.7	-44.5
sp3	-185.51521	0.02873	-0.48648	39.8	-7.4
min4	-185.57971	0.03242	-0.54729	1.7	-45.5
sp4	-185.53541	0.02568	-0.50973	25.3	-21.9

^a ICCI +Q energy in E_H.

^b zero-point energy in E_H, obtained from the harmonic CASSCF frequencies.

^c First column ICCI +Q energy plus zero-point energy + 185. Second column energy in kcal/mol relative to H₂ + N₂O. Third column energy in kcal/mol relative to NH₂ + NO.

Table III. Computed energies and zero-point corrections.

ICCI calculations based on an (6/6) CASSCF

	Energy ^a	zero-point energy ^b	ΔE^c	
NH ₂ + NO	-185.50010	0.02278	-0.47732	0.0
min1	-185.57294	0.03494	-0.53800	-38.1

^a ICCI +Q energy in E_H .

^b zero-point energy in E_H , obtained from the harmonic CASSCF frequencies.

^c First column ICCI +Q energy plus zero-point energy + 185. Second column relative energy in kcal/mol.

Table IV. Computed stationary point geometries ^{a b}.

	min1	sp1	min2	min3	sp3	min4	sp4
$r_{H_1N_1}$	1.029	1.308					
$r_{H_2N_1}$	1.003	1.007	1.045	1.046	0.991	1.052	1.124
$r_{N_1N_2}$	1.344	1.260	1.255	1.253	1.193	1.247	1.175
r_{N_2O}	1.201	1.258	1.404	1.423	1.606	1.440	1.941
r_{H_1O}		1.376	0.983	0.976	0.981	0.977	0.986
r_{H_2O}							1.633
$\angle H_1N_1N_2$	113.9	81.2					
$\angle H_2N_1N_2$	112.2	118.5	104.4	103.3	174.5	108.7	104.7
$\angle N_1N_2O$	113.5	104.5	110.5	107.8	109.3	110.5	88.0
$\angle N_1H_1O$		95.7					
$\angle H_1ON_2$		78.6	104.4	101.5	100.3	102.4	139.4
ϕ_1^c	20.7						
ϕ_2^d	155.4						

^a bond lengths in Å and angles in degrees.

^b min1 and sp1 are from an 8/6 CAS, while the remaining results are from a 10/10 CAS.

^c angle between the $H_1N_1N_2$ and N_1N_2O planes.

^d angle between the $H_2N_1N_2$ and N_1N_2O planes.

Table V. Computed frequencies and rotational constants (cm^{-1}) ^a.

	min1	sp1	min2	min3	sp3	min4	sp4
ω_1	3871	3791	3660	3757	4030	3753	3601
ω_2	3490	2160	3313	3296	3688	3216	2100
ω_3	1792	1642	1623	1651	1793	1650	1793
ω_4	1709	1562	1466	1462	1194	1454	1174
ω_5	1368	1348	1405	1366	595	1346	801
ω_6	1207	1006	912	884	389	838	473
ω_7	712	1207	652	637	576	624	998
ω_8	647	629	959	970	344	997	330
ω_9	542	1990 <i>i</i>	509	364	1359 <i>i</i>	353	1150 <i>i</i>
A	2.669	2.416	2.504	2.737	2.455	2.318	1.660
B	0.436	0.504	0.416	0.400	0.356	0.415	0.361
C	0.378	0.417	0.357	0.349	0.311	0.352	0.296

^a min1 and sp1 are from an 8/6 CAS, while the remaining results are from a 10/10 CAS.

Table VI. Comparison of energetics with other calculations.

	present work					
	ICCI+Q + ZPE		BAC-MP4 ^c	ICCI+Q ^d	HMW ^e	CG ^f
	ref1 ^a	ref2 ^b				
NH ₂ + NO	0.0	0.0	0.0	0.0	0.0	
min1	-44.0	-38.1	-48.1	-45.7	-42.3	-28.9
sp1	-14.4	-8.5	-19.7	-13.3	-5.6	
min2	-45.7	-39.8	-47.5	-47.9	-42.1	-31.3
min3	-44.5	-38.6	-45.5	-46.5	-40.3	-30.4
sp3	-7.4	-1.5	-7.0	-6.9	2.8	
min4	-45.5	-39.6	-47.2	-47.3	-41.7	-31.7
sp4	-21.9	-16.1	-25.2	-19.5	-8.9	

^a Energies computed with respect to H₂ + N₂O and the NH₂ + NO asymptote positioned from experiment.

^b Energies computed with respect to NH₂ + NO.

^c Ref. 20.

^d Present results computed with respect to NH₂ + NO and without ZPE for comparison to the work of HMW.

^e Ref. 22.

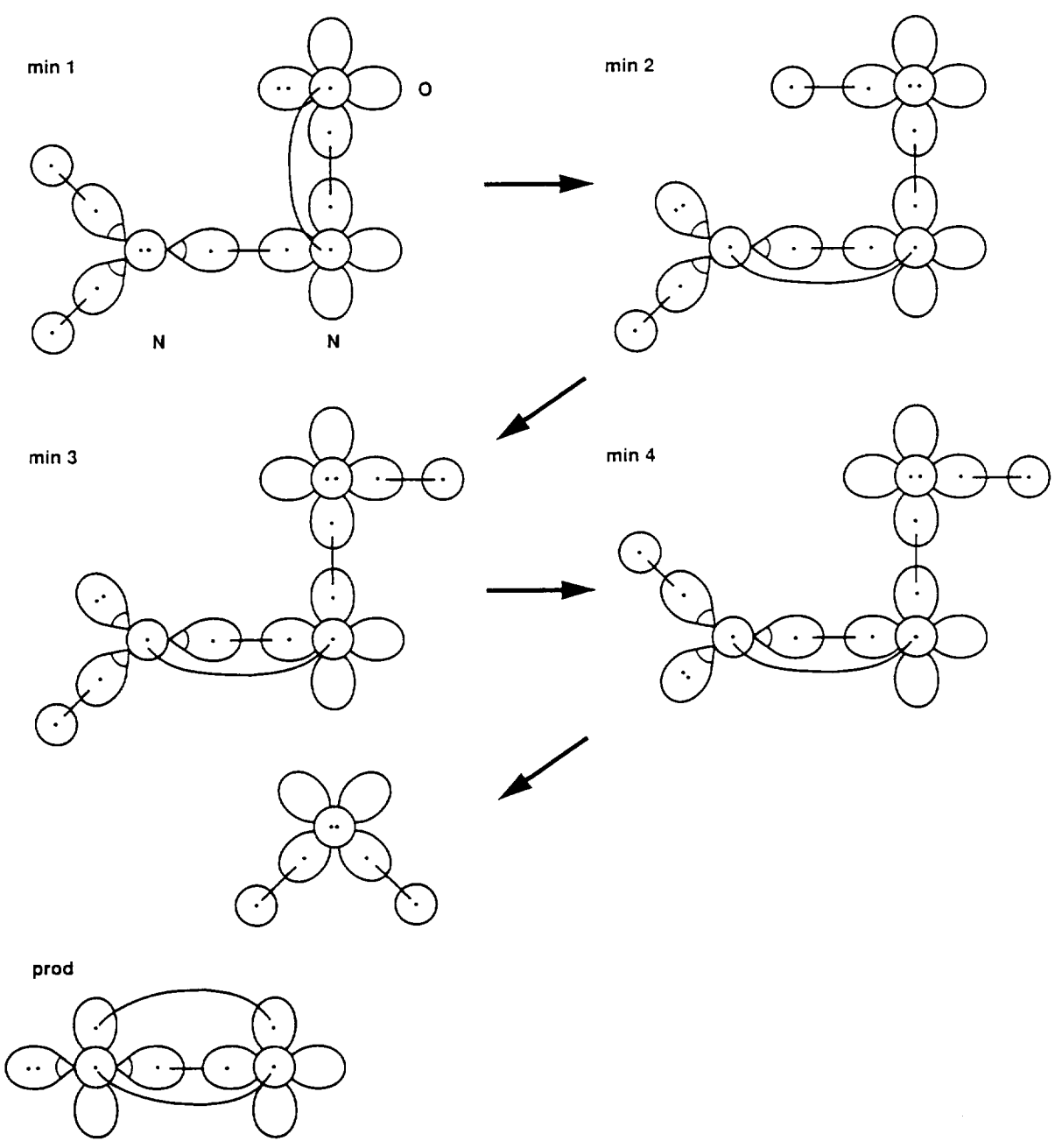
^f Ref. 18.

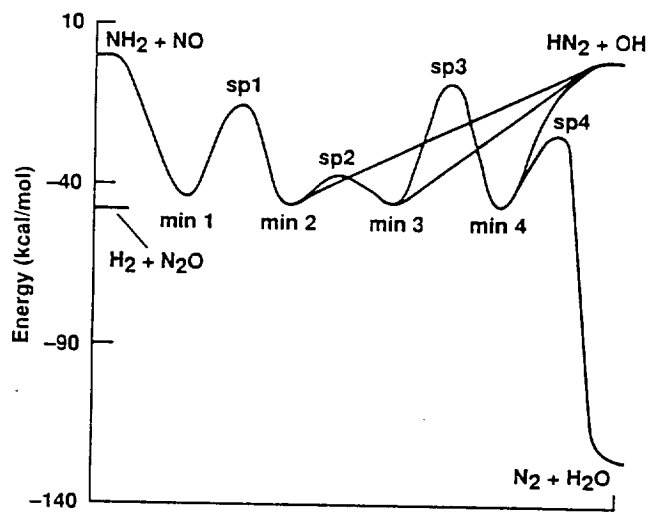
Figure Captions.

Fig. 1. The electronic structure of min1, min2, min3, min4, and $\text{N}_2 + \text{H}_2\text{O}$ (prod).

Fig. 2. Schematic representation of the minimum energy path for $\text{NH}_2 + \text{NO}$. The energies are from ICCI calculations (See the text.).

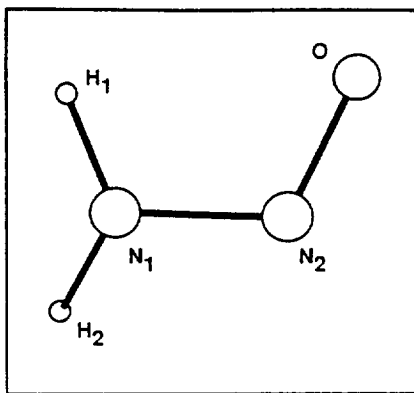
Fig. 3. Geometries for the stationary points for reaction (1) and reaction (2). Min1 is non-planar but the remaining structures are planar.



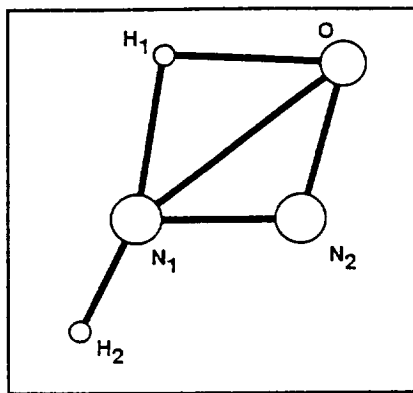


Walch-2

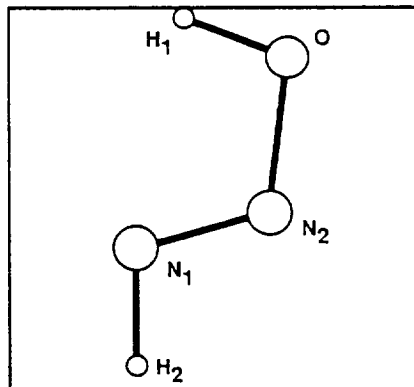
min 1



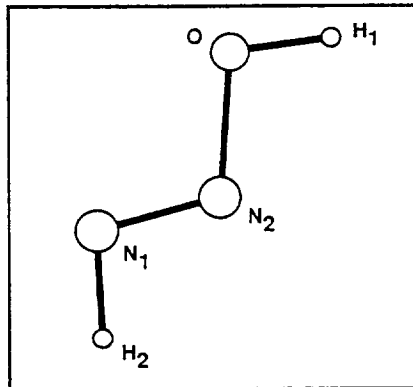
sp 1



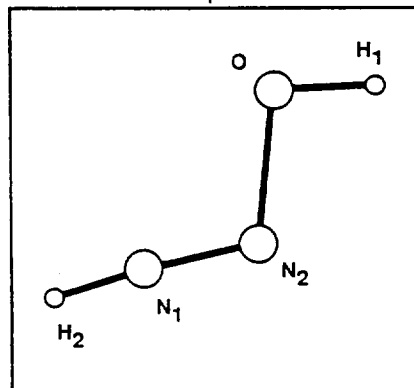
min 2



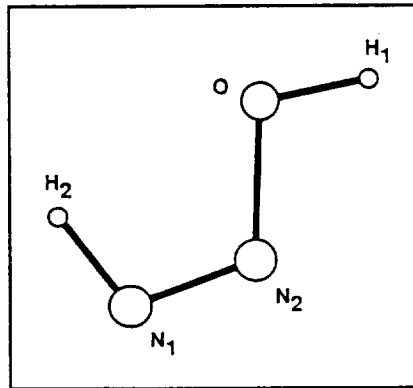
min 3



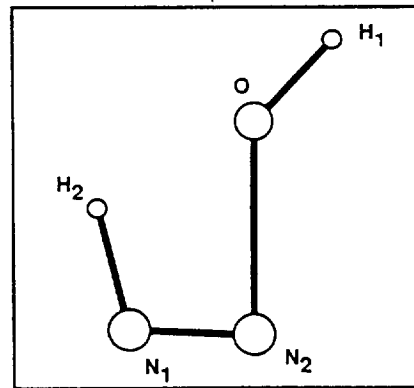
sp 3



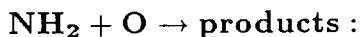
min 4



sp 4



Theoretical Characterization of the Reaction



Stephen P. Walch^a
ELORET Institute
Palo Alto, Ca. 94303

Abstract.

The potential energy surface for $\text{NH}_2 + \text{O}$ has been characterized using complete active space SCF (CASSCF)/ derivative calculations to determine stationary point geometries and frequencies followed by internally contracted configuration interaction (ICCI) calculations to determine the energetics. The calculations predict an NO bond strength of 85.8 kcal/mol for NH_2O . The barrier for isomerization of NH_2O to trans-HNOH is predicted to be 48.0 kcal/mol and the barriers for $\text{H} + \text{HNO}$ forming NH_2O and NHOH are predicted to be 2.1 and 8.3 kcal/mol, respectively (all corrected for zero-point energy).

The computed heats of formation for NH_2O and cis- and trans-HNOH reported by Soto, Page, and McKee are in good agreement with the present results. Our results also agree with those obtained by Melius and Binkley to within their stated ± 3 kcal/mol error limits.

The barrier for $\text{H} + \text{HNO} \rightarrow \text{H}_2 + \text{NO}$ is computed to be ≈ 0.3 kcal/mol which is about 0.7 kcal/mol lower than the value computed by Soto and Page (without correction for zero-point energy).

^aMailing Address: NASA Ames Research Center, Moffett Field, CA 94035.

I. Introduction

NH_2 and NH play important roles in the oxidation of nitrogen containing species as well as in the reduction of NO *e.g.* in the thermal de- NO_x process [1-4]. The reaction



may also be important in simulations of hypersonic flow, where heated air contains NO due to the thermal Zeldovich mechanism, and the reaction



followed by reaction (1) constitutes a pathway for recombination of H_2 with NO as a third body.

Recently Dagdigian and coworkers [5-6] have studied the internal energy distribution in the products for the reactions,



which occur on the same potential energy surface (PES) as reaction (1). In both cases the OH and HNO products show less internal excitation than predicted by statistical theories. These authors suggested that additional *ab initio* calculations were needed to help interpret the experimental results.

There have been a number of previous computational studies of the NH_2O PES. Most have focused on the geometry and energetics of the stable isomers of NH_2O . Melius and Binkley [7-8] used the bond additivity corrected Møller-Plesset perturbation theory through fourth-order (BAC-MP4) method to study the NH_2O and

HNOH (trans) isomers as well as some of the barriers to interconversion between the isomers of NH_2O and the barrier to the abstraction reaction, which yields the same products as reaction (3a), but occurs on the quartet PES. More recently Soto, Page, and McKee [9] (SPM) have carried out a careful study of the $^2A'$ and $^2A''$ states of H_2NO and the cis and trans isomers of HNOH, using Hartree-Fock (HF) plus configuration interaction (CI) wavefunctions with basis sets through correlation consistent polarized valence triple-zeta (cc-pVTZ) [10]. Soto and Page [11] (SP) also studied the minimum energy path for reaction (1) using a cc-pVDZ (double-zeta) basis set [10] and carried out calculations of the rate constant as a function of temperature using canonical variational transition-state-theory. Since completion of this work, we also became aware of recent calculations by Page and Soto [12] which characterized the barriers for addition of H to HNO to give H_2NO and HNOH.

In the present work, these earlier studies are extended to include additional saddle points connecting the various NH_2O isomers and the possible product channels. The technical details of the calculations are given in Section II, the results are presented in Section III, and the conclusions are given in section IV.

II. Computational Details.

Two different basis sets were used in this work. For the complete active space SCF (CASSCF) derivative calculations the polarized valence double-zeta set (PVDZ) of Dunning and Hay [13] was used. The basis set for N and O is a (9s5p)/[3s2p] basis augmented by a single set of 3d functions with exponents of 0.80 and 0.85 for N and O, respectively. The H basis is (4s)/[2s] augmented with a single set of 2p functions with exponent 1.00. The basis set used in the CI calculations is the Dunning correlation consistent triple-zeta natural orbital basis set (cc-pVTZ) [10]. This basis is [4s3p2d1f]. for N and O and [3s2p1d] for H and is described in detail in Ref. 10.

The CASSCF/derivative calculations had 11 electrons distributed among 9 orbitals (denoted by 11/9). Thus, all but the O 1s, N 1s, and O 2s like orbitals are included in the active space in the CASSCF calculations. In the subsequent internally contracted configuration interaction (ICCI) calculations, the N 1s and O 1s electrons were not correlated. These CI calculations were based on the 11/9 active space. The reference space for the ICCI calculations was restricted to no more than two electrons in the weakly occupied CASSCF orbitals.

The CASSCF/derivative calculations used the SIRIUS/ABACUS system of programs [14], while the ICCI calculations were carried out with MOLPRO [15-18]. A multi-reference analog of the Davidson's correction [19] was added to the ICCI energies and is denoted by +Q.

III. Discussion

Table I gives the ICCI and ICCI+Q energies, the zero-point energies (based on the harmonic CASSCF frequencies), and the relative energies with respect to $\text{NH}_2 + \text{O}$ and $\text{H} + \text{HNO}$. The energetics are also shown schematically in Fig. 1, while Fig. 2 shows the structures. The geometric parameters for each of the structures are given in Table II and the CASSCF harmonic frequencies and rotational constants are given in Table III.

The NH_2O minimum energy structure in the present calculations has the NO tilted by 35.6 degrees with respect to the NH_2 plane. This is very similar to what was found by SPM, who obtained values of 41.1 and 26.0 degrees for the same angle for HF and CI methods, respectively. As expected, the computed CASSCF bond lengths are found to be longer than the HF bond lengths reported by SPM. The computed $\angle \text{HNH}$ is 114.0 ° in the present work compared to 115.6° and 117.5° obtained by SPM for HF and CI, respectively. Calculations were also carried out for a planar structure, which is found to be a saddle point. From Table I it is

seen that the non-planar structure is slightly (≈ 0.6 kcal/mol) below the planar structure before correction for zero-point energy, but with inclusion of zero point energy the planar structure is 0.1 kcal/mol below the non-planar structure. Thus, in a one-dimensional model of the vibrational problem as a double-well minimum, even for the lowest vibrational level the zero-point energy is sufficient to surmount the barrier. For higher vibrational levels the vibrational energy is well above the barrier. This is consistent with the work of Pauzat et al. [20], where it is found that the vibrational levels for the NH_2O out-of-plane mode look much the same for a flat potential as for a double-minimum potential with a small inversion barrier.

The NH_2O minimum is computed to be 57.1 kcal/mol below $\text{H} + \text{HNO}$. This compares to 58.3 kcal/mol obtained by SPM. Melius and Binkley [8] find NH_2O to be 88.5 kcal/mol below $\text{NH}_2 + \text{O}$. Using the computed separation between $\text{H} + \text{HNO}$ and NH_2O from Table I plus the experimental separation between $\text{NH}_2 + \text{O}$ and $\text{H} + \text{HNO}$ leads to 85.8 kcal/mol as our best estimate of the latter energy difference (vide infra). Since the BAC-MP4 calculations include some rather large empirical corrections, this level of agreement is probably satisfactory and the present results are expected to be more reliable.

Table IV compares energetics obtained at the CASSCF level with those obtained at the ICCI level using several basis sets. As expected the CASSCF energetics do not agree well with the ICCI energetics. The significant point to be made with respect to Table IV is the comparison between the computed and experimental values of the locations of the $\text{NH} + \text{OH}$ and $\text{H} + \text{HNO}$ asymptotes. Here it is seen that the separation between $\text{NH}_2 + \text{O}$ and $\text{NH} + \text{OH}$ is accurately computed (error of 1.5 kcal/mol) with the cc-pVTZ basis set, but even with a cc-pVQZ basis set the separation between $\text{NH}_2 + \text{O}$ and $\text{H} + \text{HNO}$ is in error by 5.3 kcal/mol. This is expected since the former separation involves breaking an NH bond and

forming an OH bond. The OH bond is slightly more difficult to describe in the calculation but the errors in the two bond strengths approximately cancel. The latter separation involves breaking an NH bond and forming an NO multiple bond. Clearly the NO bond is much more difficult to describe than the NH bond and the error in the separation reflects an expected error of about 2 kcal/mol in the NH bond but about 7 kcal/mol in the NO bond. Another way of saying this is that the former separation is isodesmic, while the latter is not. This argument justifies the procedure used above for computing the energy of NH_2O with respect to $\text{NH}_2 + \text{O}$ as the computed separation between NH_2O and $\text{H} + \text{HNO}$ plus the experimental separation between $\text{H} + \text{HNO}$ and $\text{NH}_2 + \text{O}$.

The structure sp1 is a saddle point interconnecting the NH_2O minimum with trans-HNOH. The barrier is 48.0 kcal/mol with respect to NH_2O . Thus, this saddle point is below the $\text{NH}_2 + \text{O}$ energy. This barrier height compares well with the value of 50 kcal/mol obtained by Melius and Binkley [8].

From Table II it is seen that trans-HNNO is 5.2 kcal/mol below cis-HNNO. This is precisely the value obtained by SPM using the same basis set as used in the present calculations but with a CI based only on the HF reference configuration. The computed binding energies with respect to $\text{H} + \text{HNO}$ are 52.1 kcal/mol (trans) and 46.9 kcal/mol (cis). These compare very well with values of 52.2 kcal/mol (trans) and 47.0 kcal/mol (cis) obtained by SPM.

Saddle points sp2 and sp3 correspond to adding H to the O end of HNO to give trans-HNOH and to the N end of HNO to give NH_2O , respectively. The barrier heights with respect to $\text{H} + \text{HNO}$ are 5.9 kcal/mol and 0.4 kcal/mol, respectively, for ICCI calculations at the CASSCF saddle points. Page and Soto [12] carried out very similar calculations, which gave 5.8 kcal/mol and 0.2 kcal/mol, respectively, for MRCI calculations using a cc-pVTZ basis set at the CASSCF saddle point. How-

ever, they found that reoptimizing the saddle point using MRCI increased the barriers by 2.4 and 1.7 kcal/mol respectively. This leads to 8.3 kcal/mol and 2.3 kcal/mol as our best estimates of the barrier heights for forming trans-HNOH and NH₂O, respectively. Bozzelli and Dean [21] indicate a barrier of ≈ 10 kcal/mol for sp₂ and a lower barrier for sp₃ (taken from the work of Melius and Binkley [8]). They argue, based on analogy to other H addition reactions, that these barriers should be lower and use 3.5 kcal/mol for both sp₂ and sp₃. Our calculated results also indicate that the 10 kcal/mol barrier for sp₂ obtained by Melius and Binkley is too large, but should not be as small as 3.5 kcal/mol. Also our calculations indicate that a barrier height of 3.5 kcal/mol is too large for sp₃. Bozzelli and Dean used a barrier of 50.5 kcal/mol for sp₁ compared to 48.0 kcal/mol in the present results and barriers of 3.5 kcal/mol for sp₂ and sp₃ and obtained a branching ratio of 14 % NH + OH (3a) and 86 % H + HNO (3b) in good agreement with the experimental result by Dransfield et al. [22].

SPM speculate that there could be a saddle point connecting NH₂O or HNOH to H₂ + NO with energy below NH₂ + O. The structure denoted by sp₅ was obtained in an attempt to locate a saddle point for the process:



From Table III it is seen that sp₅ has two imaginary frequencies, thus it is not a saddle point. The larger one corresponds to dissociation to H₂ + NO, while the smaller one corresponds to removing the plane of symmetry. (Note that this calculation was carried out in C_s symmetry.) This structure is found to be 8.0 kcal/mol above NH₂ + O. This suggests that there is not a low energy pathway for reaction (5).

An attempt was also made to locate a saddle point for



The initial geometry for the search was obtained by rotating the H_2 moiety of sp5 about the H_2 center of mass to an orientation perpendicular to the plane. This search led to sp3. The failure to find a saddle point for this process, as well as simple qualitative considerations of the orbital changes in this reaction, suggest that there is not a low energy pathway for reaction (6).

The sp4 saddle point corresponds to reaction (1). The saddle point geometry which was obtained here using an 11/9 CASSCF has a longer $r_{H_1H_2}$ than that obtained by SP using a smaller 5/5 CASSCF ($r_{H_1H_2}$ of 1.41 Å in the present work compared to 1.21 Å obtained by SP). SP observed an elongation of $r_{H_1H_2}$ for CI as compared to CASSCF. The same effect is seen in our results. Table V shows CASSCF and ICCI results (without inclusion of zero-point effects) along the minimum energy path (MEP) from sp4 to $H + HNO$. This MEP was obtained by following the CASSCF gradient away from a starting geometry where the sp4 geometry was displaced slightly toward $H + HNO$ and an ICCI calculation was carried out at each step in the walk. These results are also shown in Fig. 3. From Table V it is seen that the barrier height on the ICCI surface is ≈ 0.3 kcal/mol and corresponds to an $r_{H_1H_2}$ of ≈ 1.6 Å. This barrier is significantly lower than the barrier of ≈ 1.0 kcal/mol obtained by SPM using MRCI (without inclusion of zero-point effects). The difference presumably arises from the larger basis set used in the present work.

SP predicted that the rate constant for reaction (1) should be about an order of magnitude larger than current experimental estimates. The lower barrier height

obtained in the present calculations would presumably mean that the computed rate is even larger, further increasing the discrepancy with experiment.

IV. Conclusions.

Calculations have been presented for the $\text{NH}_2 + \text{O}$ potential energy surface using complete active space SCF(CASSCF)/ derivative methods to characterize the stationary points and internally contracted configuration interaction (ICCI) to determine the energetics.

The results for the $^2A'$ state of NH_2O and for cis- and trans-HNOH are in good agreement with the work of Soto, Page, and McKee. In particular our results agree to within ± 1 kcal/mol with the heats of formation which they reported.

The agreement with the BAC-MP4 results of Melius and Binkley is poorer. They appear to overestimate the binding energy in NH_2O by ≈ 3 kcal/mol and overestimate barrier heights by ≈ 2 kcal/mol. However, these errors are within their stated error bars of ± 3 kcal/mol.

We predict barrier heights (zero-point corrected) of 2.1 and 8.3 kcal/mol for $\text{H} + \text{HNO}$ going to NH_2O and NHOH , respectively. We also predict a barrier height (zero-point corrected) of 48.0 kcal/mol for isomerization of NH_2O to trans-HNOH. This barrier height is less than the $\text{NH}_2\text{-O}$ bond strength which is computed to be 85.8 kcal/mol.

Production of $\text{H}_2 + \text{NO}$ from NH_2O or cis-HNOH is predicted to involve barriers which are above the $\text{NH}_2 + \text{O}$ asymptotic energy.

The barrier for $\text{H} + \text{HNO} \rightarrow \text{H}_2 + \text{NO}$ is predicted to be ≈ 0.3 kcal/mol (before zero-point correction). This is $\approx 1^{0.7}$ kcal/mol lower than the barrier used by Soto and Page in a canonical variational transition theory estimate of the rate of this reaction. Thus, the true rate may be even larger than predicted by Soto and Page, which in turn is about an order of magnitude larger than the experimental rate.

Thus, we concur with Soto and Page that a new experimental determination of this rate is needed.

Acknowledgement. SPW was supported by NASA cooperative agreement number NCC2-478.

References

1. J.A. Miller, M.C. Branch, and R.J. Kee, *Combust. Flame* **43**, 81 (1981).
2. R.K. Lyon, Sandia Laboratories Report No. SAND70-8635, 1970.
3. R.K. Lyon, U.S. Patent 3,900,544, August 1975.
4. R.K. Lyon, *Int. J. Chem. Kinet.* **8**, 315 (1976).
5. D. Patel-Misra, D.G. Saunder, and P.J. Dagdigian, *J. Chem. Phys.* **95**, 955 (1991).
6. D. Patel-Misra and P.J. Dagdigian, *Chem. Phys. Lett.* **185**, 387 (1991).
7. C.F. Melius and J.S. Binkley, *ACS Symp. Ser.* **249**, 103 (1984).
8. C.F. Melius and J.S. Binkley, 20th Symposium (Int.) on Combustion, The Combustion Institute, 1984, pp 575-583.
9. M.R. Soto, M. Page, and M.L. McKee, *Chem. Phys. Lett.* **187**, 335 (1991).
10. T.H. Dunning, Jr., *J. Chem. Phys.* **90**, 1007 (1989).
11. M.R. Soto and M. Page, *J. Chem. Phys.* **97**, 7287 (1992).
12. M. Page and M.R. Soto, personal communication
13. T.H. Dunning, Jr. and P.J. Hay in *Methods of Electronic Structure Theory*, H.F. Schaefer III ed., Plenum Publishing, 1977
14. SIRIUS is an MCSCF program written by H.J. Jensen and H. Agren and ABACUS is an MCSCF derivatives program written by T. Helgaker, H.J. Jensen, P. Jørgenson, J. Olsen, and P.R. Taylor.
15. H.-J. Werner and P.J. Knowles, *J. Chem. Phys.* **89**, 5803 (1988).
16. P.J. Knowles and H.-J. Werner, *Chem. Phys. Lett.* **145**, 514 (1988).
17. H.-J. Werner and P.J. Knowles, *J. Chem. Phys.* **82**, 5053 (1985).
18. P.J. Knowles and H.-J. Werner, *Chem. Phys. Lett.* **115**, 259 (1985).

19. S.R. Langhoff and E.R. Davidson, *Int. J. Quantum Chem.* **8**, 61 (1974).
20. F. Pauzat, H. Gritli, Y. Ellinger, and R. Subra, *J. Phys. Chem.* **88**, 4581 (1984).
21. J.W. Bozzelli and A.M. Dean, *J. Phys. Chem.* **93**, 1058 (1989).
22. P. Dransfield, W. Hack, H. Kurzke, F. Temps, and H.G. Wagner, 20th Symposium (Int.) on Combustion, The Combustion Institute, 1984, pp 655.

Table I. Computed energies and zero-point corrections.

	Energy ^a	ZPE ^b	ΔE_1^c	ΔE_2^d
NH ₂ + O	-130.74229(-.76506)	0.01848	0.0	28.7 ^e
NH ₂ O(minimum)	-130.87396(-.90028)	0.02659	-79.8	-57.1
NH ₂ O(planar)	-130.86878(-.89928)	0.02545	-79.9	-57.2
sp1	-130.78996(-.81750)	0.02021	-31.8	-9.1
NHOH(trans)	-130.86597(-.89218)	0.02645	-74.8	-52.1
NHOH(cis)	-130.85694(-.88319)	0.02569	-69.6	-46.9
sp2	-130.76365(-.78955)	0.01612	-16.8	5.9
sp3	-130.77316(-.79753)	0.01547	-22.3	0.4
NH + OH	-130.75192(-.77598)	0.01539	-8.8	13.9
sp4	-130.77216(-.79622)	0.01184	-23.7	-1.0
sp5	-130.72053(-.74861)	0.01472	8.0	30.7
H + HNO	-130.77387(-.79600)	0.01330	-22.7	0.0

^a Energy in E_H obtained with the cc-pVTZ basis set. The first energy is the ICCI energy, while the energy in parenthesis includes a multi-reference Davidson correction and is with respect to -130. E_H .

^b zero-point energy in E_H .

^c relative energy in kcal/mol with respect to NH₂ + O.

^d relative energy in kcal/mol with respect to HNO + H.

^e from experiment.

Table II. Computed CASSCF VDZP geometries^a.

	NH ₂ O	sp1	NHOH(t)	NHOH(c)	sp2	sp3	sp4	sp5
r_{NH_1}	1.037	1.049	1.049	1.053	1.068	1.079	1.150	1.289
r_{NH_2}	1.037	1.204				1.924	2.564	1.264
r_{NO}	1.298	1.448	1.396	1.393	1.265	1.230	1.211	1.351
r_{OH_2}		1.214	0.979	0.980	1.537			1.408
$r_{H_1H_2}$							1.414	0.963
$\angle H_1NH_2$	114.0	121.8						
$\angle H_2ON$		52.9	102.2	108.5	113.3			
$\angle ONH_2$		53.7						
$\angle NH_2O$		73.5						
$\angle H_1NO$		104.4	99.9	105.0	105.9	109.5	109.1	109.3
$\angle H_2NO$						119.6		
$\angle H_2H_1N$							174.5	
$\angle NH_1H_2$								66.5
$\angle H_1H_2O$								129.7
$\angle H_2ON$								54.5
α^b	35.6							
ϕ^c		138.6			131.9	116.2		

^a Bond lengths in Å and angles in degrees.

^b angle between the NO bond and the bisector of $\angle H_1NH_2$.

^c angle between the H₁NO and H₂NO planes.

Table III. Computed CASSCF VDZP frequencies and rotational constants (cm^{-1}).

	NH ₂ O	sp1	NHOH(t)	NHOH(c)	sp2	sp3	sp4	sp5
ω_1	3291	3242	3721	3675	2961	2800	1726	2380
ω_2	1656	2545	3261	3191	1493	1534	1524	1864
ω_3	1307	1305	1568	1505	1338	1504	1198	1297
ω_4	691	975	1266	1321	697	573	490	919
ω_5	3421	803	1066	1058	586	379	258	2278 <i>i</i>
ω_6	1304	2201 <i>i</i>	731	529	2013 <i>i</i>	1204 <i>i</i>	1724 <i>i</i>	750 <i>i</i>
A	9.94	8.93	9.50	9.41	6.48	5.01	3.46	6.87
B	1.01	0.98	1.03	1.02	1.10	1.07	1.07	1.11
C	1.01	0.93	0.93	0.92	0.99	0.94	0.82	0.96

Table IV. Computed relative energies (kcal/mol).

	CASSCF	ICCI	cc-VTZ	cc-VQZ ^a	Experiment
	VDZP	VDZP			
NH ₂ + O	0.0	0.0	0.0	0.0	0.0
NH ₂ O(minimum)	-57.3	-73.2	-79.8		
NH ₂ O(planar)	-56.9	-73.8	-79.9		
sp1	-10.0	-25.9	-31.8		
NHOH(trans)	-53.9	-68.4	-74.8		
NHOH(cis)	-48.2		-69.6		
sp2	-5.8		-16.8		
sp3	-15.7	-18.0	-22.3		
sp4	-18.4		-23.7		
NH + OH	-2.1	-7.8	-8.8		-10.3
H + HNO	-21.5	-19.1	-22.7	-23.4	-28.7
sp5			8.0		

^a This is a [5s4p3d2f/4s3p2d] basis set obtained from the cc-pVQZ basis set (Ref. 10.) by omitting the g function on N and O and the f function on H.

Table V. Computed energetics for reaction (1)^a.

r_{NH_1}	$r_{H_1H_2}$	CAS	ICCI+Q
1.150	1.414	4.41	0.14
1.106	1.493	4.12	0.24
1.097	1.562	3.63	0.33
1.091	1.629	3.15	0.33
1.088	1.694	2.69	0.28

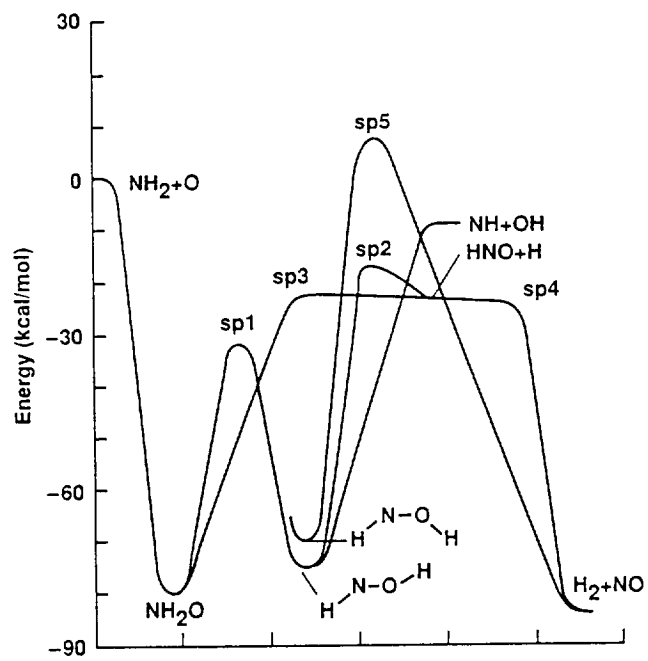
^a Bond lengths in Å and energies in kcal/mol relative to H + HNO.

Figure Captions.

Fig. 1. Schematic representation of the potential energy surface for $\text{NH}_2 + \text{O}$. The energies are from ICCI +Q calculations.

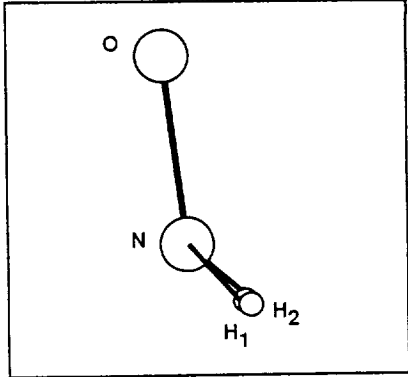
Fig. 2. Stationary point geometries for the $\text{NH}_2 + \text{O}$ surface. See also Table II.

Fig. 3. Potential for $\text{H} + \text{HNO} \rightarrow \text{H}_2 + \text{NO}$. The minimum energy path is from CASSCF/gradient calculations. The ICCI +Q energies were computed at the geometries at each step on the walk.

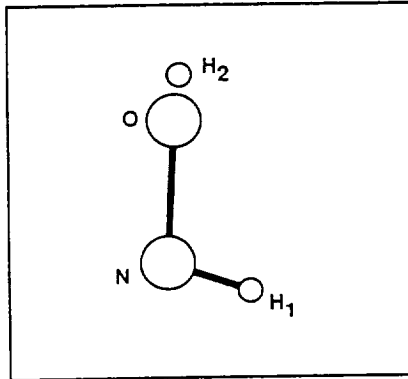


Walch-1

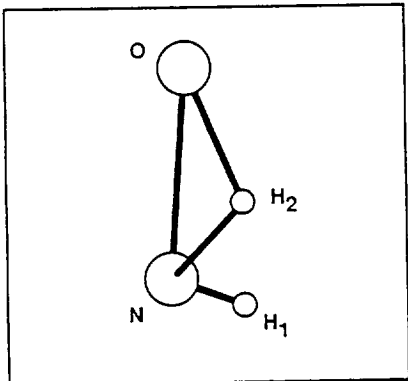
NH_2O



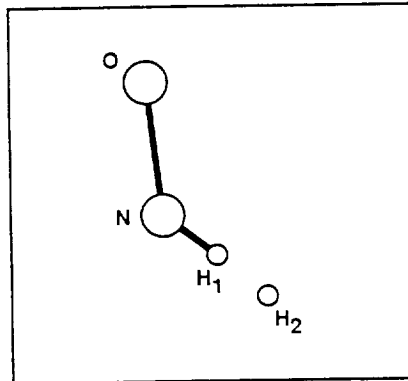
sp^2



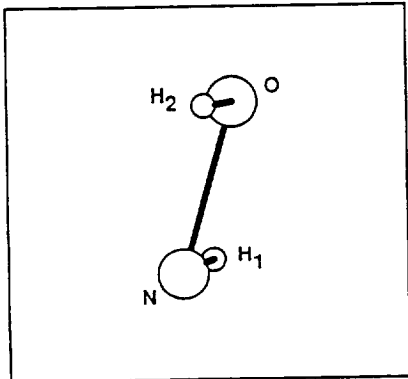
sp^1



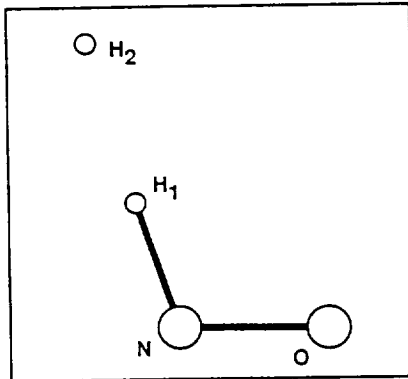
sp^3



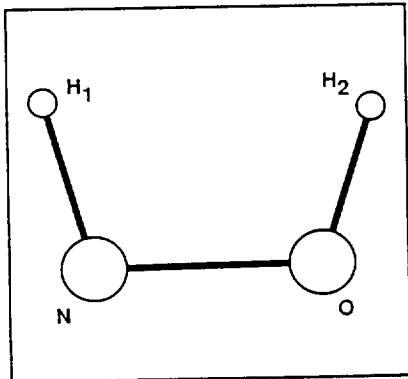
NHOH (t)



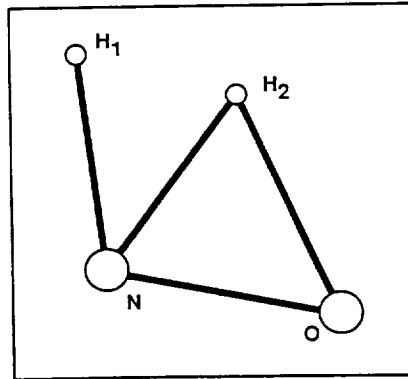
sp^4

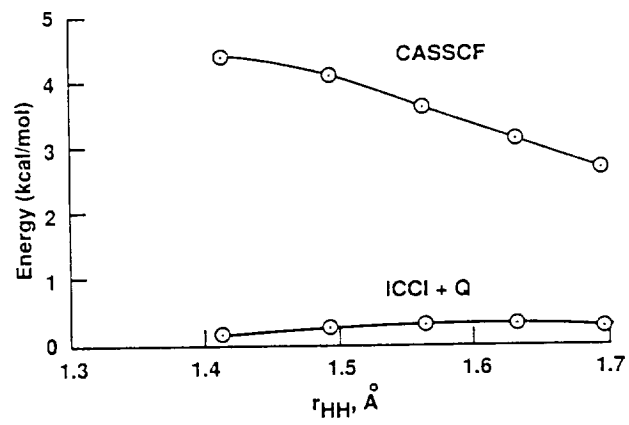


NHOH (c)



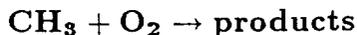
sp^5





Watch-3

Characterization of the Potential Energy Surface for



Stephen P. Walch^a
ELORET Institute
3788 Fabian Way
Palo Alto, Ca. 94303

Abstract. Complete active space SCF/internally contracted configuration interaction (CASSCF/ICCI) calculations using large atomic natural orbital (ANO) basis sets are reported for $\text{CH}_3 + \text{O}_2$. Two potential energy surfaces are found to be important in the $\text{CH}_3 + \text{O}_2$ reaction. In C_s symmetry, the lower ${}^2A''$ surface correlates with $\text{CH}_3 + \text{O}_2$ (${}^3\Sigma_g^-$) and connects to a bound CH_3OO species with no barrier, but leads only to $\text{CH}_3\text{O} + \text{O}$ products. A higher surface of ${}^2A'$ symmetry correlates with $\text{CH}_3 + \text{O}_2$ (${}^1\Delta_g$) and leads to $\text{CH}_2\text{O} + \text{OH}$ with a computed barrier of 13.7 kcal/mol (with respect to $\text{CH}_3 + \text{O}_2$ (${}^3\Sigma_g^-$)). Even in lower symmetry, two surfaces are involved leading to a more complex model for this reaction than had been previously considered.

I. Introduction.

The reaction



is believed to be an important chain branching reaction in hydrocarbon ignition processes [1]. The experimental situation has been discussed by Zellner and Ewig [2]. The various determinations of the rate coefficient for reaction (1a) are in reasonable agreement giving activation energies between 26.1 and 31.1 kcal/mol, which is consistent with the endothermicity of 28.7 kcal/mol [3]. However, there has been

considerable disagreement on the rate coefficient for reaction (1b). The determinations of K_{1b} vary by almost two orders of magnitude between 1500 and 2000K. A recent determination [4] of the rate of reaction (1b) gives an activation energy of only 9.1 kcal/mol. Zellner and Ewig have carried out RRKM calculations using a best estimate of the potential surface parameters for reaction (1) and assuming a model in which there is a common CH_3O_2 intermediate which can decompose to $\text{CH}_3\text{O} + \text{O}$ or rearrange to give $\text{CH}_2\text{O} + \text{OH}$. They conclude that channel 1b will dominate over channel 1a at all temperatures below 2800K. There still remains some uncertainty in the experimental situation, since Baldwin and Golden [5] failed to observe reaction (1b) in an experiment at 1220K in contrast to the results of Ref. 4.

Given the importance of this reaction and the remaining uncertainty in the experimental situation, we have carried out ab-initio calculations of the potential energy surface (PES) to better define the energetics, particularly the barrier to formation of $\text{CH}_2\text{O} + \text{OH}$. Section II describes some qualitative features of reaction (1). The technical details of the calculations are given in Section III. Section IV describes the results and the conclusions are given in Section V.

II. Qualitative Features.

Fig. 1 shows the electronic structure of the $^2A'$ and $^2A''$ surfaces of $\text{CH}_3 + \text{O}_2$. The presence of a mirror plane requires that one CH bond be in the C-O-O plane. Since the energy to rotate the CH_3 group is small, this constraint does not affect the energy significantly, but the use of a mirror plane reduces the size of the subsequent ICCI calculations considerably and this approximation was made here. As discussed in Section IV, the imposition of a plane of symmetry results in some stationary points in C_s symmetry which have small negative eigenvalues of the Hessian matrix corresponding to rotation of the CH_3 group. However, the effect on the energetics is small.

From Fig. 1 it is seen that the $^2A''$ surface correlates with the $X^3\Sigma_g^-$ ground state of O_2 . On this surface the distal O has an in plane doubly occupied 2p like orbital. Thus, 1,3-hydrogen migration to form CH_2OOH (and ultimately $\text{H}_2\text{CO} + \text{OH}$) is not favorable. Therefore the product is expected to be $\text{CH}_3\text{O} + \text{O}$. Note that CH_3O can form $\text{CH}_2\text{O} + \text{H}$ with a barrier of 23.3 kcal/mol [6].

The ${}^2A'$ surface correlates with CH_3 plus O_2 in the ${}^1\Delta_g$ state. On this surface the distal O has a singly occupied in plane O 2p like orbital and 1,3-hydrogen migration to give $\text{CH}_2\text{O} + \text{OH}$ is favorable.

III. Computational Details.

Two different basis sets were used in this work. For the CASSCF derivative calculations the polarized double zeta set of Dunning and Hay [7] was used. The basis set for C and O is a (9s5p)/[3s2p] basis augmented by a single set of 3d functions with exponents of 0.75 and 0.85 for C and O, respectively. The H basis is (4s)/[2s] augmented with a single set of 2p functions with exponent 1.00. The basis set used in the CI calculations is the Dunning correlation consistent triple zeta double polarization atomic natural orbital basis set [8]. This basis is [4s3p2d1f] for C and O and [3s2p1d] for H and is described in detail in Ref. 8.

The CASSCF/derivative calculations had 7 electrons distributed among 7 orbitals (denoted 7/7). The active electrons correspond to the electrons in Fig. 1. which are in singly occupied orbitals. In the subsequent internally contracted configuration interaction (ICCI) calculations, the C 1s and O 1s electrons were not correlated. These CI calculations were based on the 7/7 CAS calculation. The reference space for the ICCI calculations had the restriction that no more than two electrons were permitted in the weakly occupied CASSCF orbitals.

The CASSCF/derivative calculations used the SIRIUS/ABACUS system of programs [9], while the ICCI calculations were carried out with MOLPRO [10-13]. A multi-reference analog of the Davidson's correction [14] was added to the ICCI energies and is denoted by +Q.

IV. Discussion.

The computed energetics for the ${}^2A'$ and ${}^2A''$ surfaces are given in Tables I and II, respectively. The zero-point energies are obtained from the CASSCF harmonic frequencies (without scaling). The relative energies are computed with respect to $\text{CH}_3 + \text{O}_2$ (${}^3\Sigma_g^-$) on the ${}^2A''$ surface and include a multi-reference Davidson's correction and zero-point energy. In each case the ICCI calculations are carried out at the geometries obtained from the CASSCF/derivative calculations. For the $\text{CH}_3 + \text{O}_2$ asymptote a supermolecule calculation was carried out at geometries obtained at the CASSCF level (for the ${}^3\Sigma_g^-$ state in the case of O_2). The energetics are also

shown graphically in Fig. 2.

From Fig. 2 it is seen that, on the ${}^2A''$ surface, CH_3 adds to O_2 (${}^3\Sigma_g^-$) with no barrier to form CH_3OO . The calculated barrier is actually slightly negative (See Table II.), this indicates that the true barrier is nearly zero and probably occurs for larger r_{CO} than obtained at the CASSCF level. The CH_3OO species is bound by 27.6 kcal/mol, while the $\text{CH}_3\text{O} + \text{O}$ product channel is computed to be endothermic by 26.2 kcal/mol compared to 28.7 kcal/mol from experiment[3]. From Fig. 2 it is also seen that CH_3 adds to O_2 (${}^1\Delta_g$) with a 3.7 kcal/mol barrier, leading to a ${}^2A'$ excited state of CH_3OO , which is 19.7 kcal/mol above the ${}^2A''$ ground state. There is a barrier of 13.7 kcal/mol, with respect to $\text{CH}_3 + \text{O}_2$ (${}^3\Sigma_g^-$), to forming the $\text{CH}_2\text{O} + \text{OH}$ product channel, which is computed to be exothermic by 54.1 kcal/mol compared to 53.2 kcal/mol from experiment [3]. No minimum corresponding to CH_2OOH was found on this surface, rather the minimum energy path away from the saddle point proceeds directly to $\text{CH}_2\text{O} + \text{OH}$.

Formation of the $\text{CH}_2\text{O} + \text{OH}$ product channel from O_2 (${}^3\Sigma_g^-$) requires coupling between the initially formed ${}^2A''$ CH_3OO species and the exit channel portion of the ${}^2A'$ surface leading to $\text{CH}_2\text{O} + \text{OH}$. Thus, this problem involves two potential surfaces, which is more complicated than the model used by Zellner and Ewig [2]. The crossing region presumably involves geometries like those involved in the saddle point for 1,3-hydrogen migration. As discussed in Section II, on the ${}^2A''$ surface moving the hydrogen toward the distal O is a repulsive interaction. Therefore, if C_s symmetry is retained, the ${}^2A''$ surface should rise more rapidly than the ${}^2A'$ surface and the crossing would be expected to be before the saddle point. (This pathway is denoted by p2 in Fig. 2, while the pathway leading to $\text{CH}_3\text{O} + \text{O}$ is denoted by p1.) If symmetry breaking is allowed (by rotation of the CH_3 group), the ${}^2A'$ minimum energy path would be displaced toward slightly higher energy, while the ${}^2A''$ minimum energy path would be less repulsive. Therefore, the crossing would occur further along the reaction coordinate in the absence of symmetry. In this picture, the bottleneck would be the barrier to $\text{CH}_2\text{O} + \text{OH}$ formation on the ${}^2A'$ surface, which is 13.7 kcal/mol. This is larger than the value of ≈ 9 kcal/mol obtained in the recent experiments of Saito et al. [4], and which was also used by Zellner and Ewig [2] in their RRKM calculations. The ab initio calculations

reported here should be accurate to $\approx \pm 2$ kcal/mol, based on the accuracy of the computed heats of reaction for (1a) and (1b). This implies that the true barrier is larger than that used by Zellner and Ewig [2]. An additional complication is the need to treat the crossing of the two surfaces. Both of these factors would suggest that the true rate for formation of channel 1b is smaller than estimated by Zellner and Ewig [2].

The $\text{CH}_3 + \text{O}_2$ energy given in Table I corresponds to the O_2 ($^1\Delta_g$) state. The computed excitation energy to the O_2 ($^1\Delta_g$) state is 24.6 kcal/mol, which may be compared to the T_0 value [15] of 22.5 kcal/mol. Table I also gives the energy of the $\text{CH}_2\text{O} + \text{OH}$ asymptote with respect to $\text{CH}_3 + \text{O}_2$ ($^3\Sigma_g^-$). Here it is seen that the computed separation is within 1 kcal/mol of experiment.

There is also a reported heat of formation of CH_3O_2 of 4.1 kcal/mol at 298K [16]. Our calculated value at 0K is 7.2 kcal/mol, or about 5.1 kcal/mol at 298K [17], which is in reasonable agreement. This is especially true since the C_s minimum in this case has a small imaginary frequency corresponding to symmetry breaking which would give a slightly lower value of the computed heat of formation if the geometry were fully optimized (vide infra).

Tables III and IV give computed vibrational frequencies and rotational constants obtained for stationary points on the $^2A'$ and $^2A''$ surfaces. As mentioned in Section II forcing C_s symmetry results in stationary points in C_s symmetry which have small imaginary frequencies corresponding to symmetry breaking. This is seen in the case of the $^2A'$ surface both for the $\text{CH}_3\text{-OO}$ saddle point and for the CH_3OO minimum ($\omega_{12} = 82 i$ and $235 i$). However, the saddle point for $\text{CH}_2\text{O} + \text{OH}$ production is a true saddle point in C_s symmetry with an imaginary frequency of $2278 i$. Similar effects are seen for the $^2A''$ surface in which there is a small imaginary frequency of $192 i$ for the CH_3OO minimum. An estimate of the effect of symmetry breaking involving rotation of the CH_3 group can be obtained from the results of calculations on CH_2OH at the SCF level. Here there are two C_s symmetry structures with imaginary frequencies of $445 i$ and $338 i$. These are 1.9 and 2.4 kcal/mol above the low symmetry true minimum. Thus, these effects introduce uncertainties as large as 2 kcal/mol in the CH_3OO minima and one of the $\text{CH}_3\text{-OO}$ saddle points. This would make these stationary points slightly deeper than calculated here, but would

have no significant effects on the rates for 1a or 1b, which depend on the barrier heights of the saddle points, which do not exhibit these symmetry breaking effects. Another minor problem with the frequency analysis is that the CH₃OO saddle point on the ²A'' surface has a nearly zero frequency. This corresponds to a very floppy torsional mode.

V. Conclusions.

Complete active space SCF/ internally contracted configuration interaction (CASSCF/ICCI) calculations using large atomic natural orbital (ANO) basis sets have been carried out for CH₃ + O₂. The calculations were carried out in C_s symmetry, which requires that one CH bond be in the plane defined by the C atom and two O atoms. Some of the stationary points obtained in C_s symmetry have small imaginary frequencies corresponding to symmetry breaking. However, by comparison to calculations on CH₂OH these symmetry breaking effects would have only small (<1-2 kcal/mol) effects on the energetics and do not effect the saddle point leading to the CH₂O + OH product channel which is the main concern in this paper.

Two potential energy surfaces are found to be important in the CH₃ + O₂ reaction. In C_s symmetry, the lower ²A'' surface correlates with CH₃ + O₂ (³Σ_g⁻) and connects to a bound CH₃OO species with no barrier, but leads only to CH₃O + O products. A higher surface of ²A' symmetry correlates with CH₃ + O₂ (¹Δ_g) and leads to CH₂O + OH with a computed barrier of 13.7 kcal/mol (with respect to CH₃ + O₂ (³Σ_g⁻)). Production of CH₂O + OH requires a surface hopping from the ²A'' to the ²A' surface. This crossing is predicted to occur before the saddle point. The saddle point for formation of CH₂O + OH is predicted to be the bottleneck to reaction. The computed barrier is larger than the barrier height of ≈ 9 kcal/mol used by Zellner and Ewig in their RRKM calculations for this system. Both the higher barrier found here and the need for surface hopping would lead to a lower probability for formation of CH₂O + OH than predicted by Zellner and Ewig.

The computed heat of formation of CH₃O₂ is 7.2 kcal/mol at 0K and is estimated to be 5.1 kcal/mol at 298K in good agreement with an experimental value of 4.1 kcal/mol.

ACKNOWLEDGMENTS

S.P. Walch was supported by a NASA grant(NCC2-478).

References

- ^a Mailing Address: NASA Ames Research Center, Moffett Field, CA 94035.
1. Combustion Chemistry, ed. W.C. Gardiner, Jr. (Springer-Verlag, 1984).
 2. R. Zellner and F. Ewig, *J. Phys. Chem.*, **92** (1988)2971.
 3. M.W. Chase, Jr., C.A. Davies, J.R. Downey, Jr., D.J. Frurip, A.A. McDonald, and A.N. Syverud, *J. Phys. Chem. Ref. Data*, **14**, Suppl. 1(1985).
 4. K. Saito, R. Ito, T. Kakumeto, and A. Imamura, *J. Phys. Chem.*, **90** (1986)1422.
 5. A.G. Baldwin and D.M. Golden, *Chem. Phys. Lett.*, **55** (1978)350.
 6. S.P. Walch, *J. Chem. Phys.*, **98** (1993)3076.
 7. T.H. Dunning, Jr. and P.J. Hay, in: *Methods of Electronic Structure Theory*, ed. H.F. Schaefer III (Plenum Publishing, 1977)
 8. T.H. Dunning, Jr., *J. Chem. Phys.*, **90** (1989)1007.
 9. SIRIUS is an MCSCF program written by H.J. Jensen and H. Agren and ABACUS is an MCSCF derivatives program written by T. Helgaker, H.J. Jensen, P. Jørgensen, J. Olsen, and P.R. Taylor.
 10. H.-J. Werner and P.J. Knowles, *J. Chem. Phys.* **89** (1988)5803.
 11. P.J. Knowles and H.-J. Werner, *Chem. Phys. Lett.* **145** (1988)514.
 12. H.-J. Werner and P.J. Knowles, *J. Chem. Phys.* **82** (1985)5053.
 13. P.J. Knowles and H.-J. Werner, *Chem. Phys. Lett.* **115** (1985)259.
 14. S.R. Langhoff and E.R. Davidson, *Int. J. Quantum Chem.* **8** (1974)61.
 15. *Spectroscopic Data Relative to Diatomic Molecules*, ed. B. Rosen (Pergamon Press, 1970)
 16. L. Batt and R.D. McCulloch, *Int. J. Chem. Kinet.*, **8** (1976)491.
 17. Based on a correction of $-7/5 RT$, which includes RT for the PV product, $3/2 RT$ for translation, $3/2 RT$ for rotation for non-linear and RT for rotation for linear.

Table I. Computed energies and zero-point corrections ($^2A'$ surface).

	Energy ^a	zero-point energy ^b	ΔE^c	Exp.
CH ₃ + O ₂	-189.77857(-.83292)	0.03314 ^d	24.6	22.5
CH ₃ -O ₂	-189.77189(-.83048)	0.03678	28.4	
CH ₃ O ₂	-189.83686(-.89447)	0.04295	-7.9	
CH ₃ OO → CH ₂ OOH	-189.79296(-.85440)	0.03735	13.7	
CH ₂ O + OH	-189.90756(-.96144)	0.03632	-54.1	-53.2

^a The energies are in E_H and are in the form ICCI(ICCI+Q +189.).

^b Zero-point energy in E_H based on the CASSCF harmonic frequencies.

^c Energy in kcal/mol relative to CH₃ + O₂ ($^3\Sigma_g^-$) based on the ICCI+Q energies plus zero-point energy.

^d The O₂ zero point energy is obtained as $1/2 \omega ^3\Sigma_g^-$ (CAS) - $1/2 (\omega ^3\Sigma_g^-$ (Exp.) - $\omega ^1\Delta_g$ (Exp.))

Table IIa. Computed energies and zero-point corrections ($^2A''$ surface).

	Energy ^a	zero-point energy ^b	ΔE^c
CH ₃ + O ₂	-189.78797(-.87226)	0.03330	0.0
CH ₃ -O ₂	-189.79599(-.87394)	0.03421	-0.5
CH ₃ O ₂	-189.86187(-.92649)	0.04354	-27.6

^a The energies are in E_H and are in the form ICCI(ICCI+Q +189.).

^b Zero-point energy in E_H based on the CASSCF harmonic frequencies.

^c Energy in kcal/mol relative to CH₃ + O₂ ($^3\Sigma_g^-$) based on the ICCI+Q energies plus zero-point energy.

Table IIb. Computed energies and zero-point corrections (${}^4A''$ surface).

	Energy ^a	zero-point energy ^b	ΔE^c	Exp.
CH ₃ + O ₂	-189.79849(-.87421)	0.03330	0.0	0.0
CH ₃ O + O	-189.78571(-.83822)	0.03905	26.2	28.7

^a The energies are in E_H and are in the form ICCI(ICCI+Q +189.).

^b Zero-point energy in E_H based on the CASSCF harmonic frequencies.

^c Energy in kcal/mol relative to CH₃ + O₂ (${}^3\Sigma_g^-$) based on the ICCI+Q energies plus zero-point energy.

Table III. Computed stationary point frequencies and rotational constants(cm^{-1}).
 $^2A'$ surface.

	CH ₃ -OO	CH ₃ OO	CH ₃ OO → CH ₂ OOH
ω_1	3343	3363	3263
ω_2	3082	3027	1885
ω_3	1517	1592	1563
ω_4	1054	1515	1156
ω_5	899	1213	1070
ω_6	557	988	727
ω_7	265	776	565
ω_8	700 <i>i</i>	421	2278 <i>i</i>
ω_9	3441	3330	3390
ω_{10}	1466	1531	1210
ω_{11}	522	1199	1135
ω_{12}	82 <i>i</i>	235 <i>i</i>	431
A	1.4049	1.4483	1.1196
B	0.2492	0.3705	0.4533
C	0.2213	0.3129	0.3459

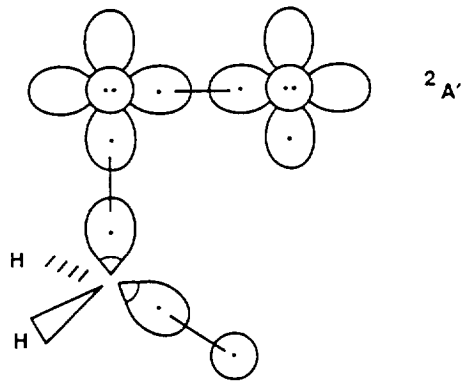
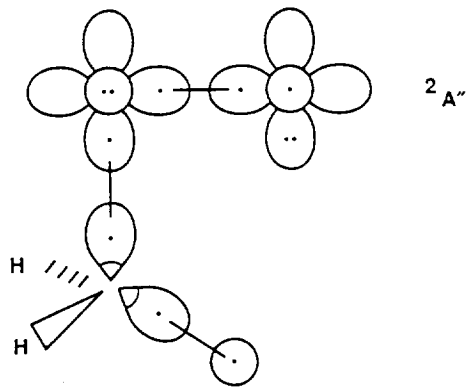
Table IV. Computed stationary point frequencies and rotational constants(cm^{-1}).
 ${}^2A''$ surface.

	$\text{CH}_3\text{-OO}$	CH_3OO
ω_1	3350	3261
ω_2	3099	3053
ω_3	1504	1597
ω_4	1084	1511
ω_5	495	1219
ω_6	248	1041
ω_7	138	850
ω_8	$156i$	534
ω_9	3444	3320
ω_{10}	1449	1532
ω_{11}	203	1196
ω_{12}	≈ 0	$192i$
A	1.4988	1.6532
B	0.1720	0.3661
C	0.1594	0.3180

Figure Captions.

Fig. 1. The electronic structure of the ${}^2A'$ and ${}^2A''$ surfaces of $\text{CH}_3 + \text{O}_2$.

Fig. 2. Schematic representation of the lowest two potential energy surfaces of $\text{CH}_3 + \text{O}_2$. The ${}^2A''$ surface is denoted by a solid curve, while the ${}^2A'$ surface is denoted by a dashed curve. For the ${}^2A''$ surface two product pathways are indicated. The pathway leading to $\text{CH}_3\text{O} + \text{O}$ is denoted by p1, while the pathway denoted by p2 leads toward $\text{CH}_2\text{O} + \text{O}$ and is the region of crossing between the ${}^2A''$ and ${}^2A'$ surfaces.



Walch-1

Ab initio potential energy surface for H-H₂

Harry Partridge, Charles W. Bauschlicher, Jr., and James R. Stallcop

Computational Chemistry Branch, Thermosciences Division

NASA Ames Research Center

Moffett Field, CA 94035-1000

and

Eugene Levin[†]

ELORET Institute^a

Palo Alto, CA 94303

Abstract

Ab initio calculations employing large basis sets are performed to determine an accurate potential energy surface for H-H₂ interactions for a broad range of separation distances. At large distances, the spherically-averaged potential determined from the calculated energies agrees well with the corresponding results determined from dispersion coefficients; the van der Waals well depth is predicted to be $75 \pm 3 \mu E_h$. Large basis sets have also been applied to reexamine the accuracy of theoretical repulsive potential energy surfaces (25-70 kcal/mol above the H-H₂ asymptote) at small interatomic separations; the Boothroyd, Keogh, Martin, and Peterson (BKMP) potential energy surface is found to agree with results of the present calculations to within the expected uncertainty (± 1 kcal/mol) of the

^a Mailing address: NASA Ames Research Center, Moffett Field, CA 94035-1000

fit. Multipolar expansions of the computed H-H₂ potential energy surface are reported for four internuclear separation distances (1.2, 1.401, 1.449, and 1.7 a_0) of the hydrogen molecule. The differential elastic scattering cross section calculated from the present results is compared with the measurements from a crossed beam experiment.

†Work supported by Cooperative Agreement NCC 2-478 of the National Aeronautics and Space Administration (NASA) with ELORET Institute.

I. Introduction

The transport properties of H atoms in H₂ molecules are required for studies of the preliminary heating of the fuel and subsequent combustion processes in a hydrogen-burning supersonic ramjet engine for the proposed National Aero-Space Plane (NASP). The accuracy of these transport properties is limited by the H-H₂ potential energy surface. While this potential energy surface is irrefutably the best characterized polyatomic potential energy surface available [1-9], the potential at large H-H₂ separation distances r , needed to determine diffusion and viscosity coefficients, is far less well studied than for small separations ($r < 4 a_0$). In addition, the potential energy surface for shorter interatomic separation distances is of considerable interest for the theoretical determination of reactive scattering cross sections. Furthermore, there are discrepancies between calculated and measured results [10-13]. For example, the state resolved differential scattering cross sections for the D+H₂ → DH+H reaction shows a large discrepancy between the calculated and measured ratios of the backward-scattered to the forward-scattered intensities [11-13]; an analysis [11] of the difference in the cross sections led to questions of

the accuracy of the high-energy potential energy surface (at about 1 eV above the $\text{H}+\text{H}_2$ asymptote), particularly for bent configurations. In this work we reinvestigate the H_3 potential energy surface using a much larger basis set than those used in previous work [1-9]. Our goals are to characterize the surface for longer $\text{H}-\text{H}_2$ separation distances and to calibrate the existing potential energy surfaces in the repulsive region (25 to 70 kcal/mol above the $\text{H}-\text{H}_2$ asymptote), which has been suggested [10-11] as the important region for comparisons of theoretical results with measurements from reactive scattering experiments.

II. Existing Potential Energy Surfaces

The best available potential energy surface is that of Boothroyd, Keogh, Martin, and Peterson (BKMP) [9], which is thought to be accurate to within about 1 kcal/mol. This potential is based on 772 *ab initio* points from several different sets of calculations. In order to include the different sets of computed points in their fitting procedure, BKMP developed a semiempirical basis set correction to adjust the calculated energies onto an equal footing. Hence, the BKMP potential energy surface supersedes the earlier Liu-Siegbahn-Truhlar-Horowitz (LSTH) [3] and double many-body expansion (DMBE) [7] surfaces as it incorporates the *ab initio* energies on which these potentials were based and includes several hundred additional points. It should be noted, however, that while only the DMBE potential behaves properly in the vicinity of the conical interaction, the BKMP, LSTH, and DMBE potentials yield similar results for the scattering calculations [10].

While 772 points are used in the fit, none of the *ab initio* energies correspond to $\text{H}-\text{H}_2$ distances greater than $4 a_0$. The range $4.0 < r < 6.0 a_0$ defines an interpolation region between the *ab initio* data and an empirical potential energy function that is constructed from the spherically-averaged potential $V_0(r)$ of

Gengenbach *et al.* [14] and the anisotropic V_2 model potential of Dalgarno, Henry, and Roberts [15]. The spherical (Born-Mayer-spline-van der Waals (BMSV) type) potential of Gengenbach *et al.* [14] was derived from their measurements of absolute integral cross sections for D-H₂ scattering using the dispersion coefficients, C_6 obtained by Langhoff and Karplus [15] and C_8 from the results of Margenau [17]. The uncertainty in the measured cross sections (large error bars at low collision energies [14]) and the difficulty in obtaining a unique potential fit [18,19] (e.g., changes in the van der Waals attraction can be compensated for by shifting the repulsive wall) limit the accuracy of their potential at large r . Gengenbach *et al.* [14] estimated that the uncertainty in the well depth of the BMSV potential is $\pm 30\%$. The uncertainty in the van der Waals region is illustrated by the difference between the BMSV potential and the Born-Mayer dispersion (BMD) and modified BMD (MBMD) potentials. The latter two potentials were derived by Torello and Dondi [20] from their measurements of the differential cross sections for D-H₂ scattering using a crossed beam experiment and the combined data from their measurement and that of Ref. 14, respectively, and the values of the dispersion coefficients calculated by Meyer, reported in Ref. [20]. The potential fit to the differential cross section is likewise not unique [18], but, nevertheless, is expected to be more sensitive to the van der Waals region since the rainbow structure in the scattering cross section has been resolved by their measurements.

We compare the available spherically-averaged potentials in Figs. 1 and 2. Clearly, there is significant variation; this is disconcerting because this uncertainty would not allow a definitive determination of the transport properties that are described above. The BKMP potential [9] closely follows the BMSV potential as expected, but is unrealistic at large r because it falls below the interaction energies determined from the dispersion coefficients. The DMBE potential is much too

repulsive because it was constrained in the van-der Waals region by six, scaled *ab initio* energies [4] that are not accurate. In addition to questions as to the accuracy of the existing van der Waals spherically-averaged potential, there has been no accurate determination of the leading anisotropic term V_2 (which is important for determining the inelastic contribution to the scattering from rotational transitions at low collision energies or large impact parameters [21]), but the general functional form has been predicted (see Sec. V below).

III. Methods

The coordinate system used in this work (pictured in Fig. 3) is that employed in our previous study [8]. It is specified by the internuclear separation distance for the hydrogen molecule r_{H_2} , the distance from the H atom to the center of mass of the H_2 molecule r and χ (the angle between a line from H to the H_2 center of mass and the H_2 internuclear axis). Note that although r_{H_2} refers to a molecule it is longer than r for some of our calculations. For convenience, selected calibration points were also performed using the coordinate representation used by BKMP [9], that is the coordinates r_1 , r_2 and θ_{12} , where r_1 is H_a-H_b , r_2 is H_b-H_c , and θ_{12} is the angle between them.

The determination of accurate potential energy surfaces for weakly interacting systems is in general a very demanding computational problem. The theoretical description must be able to describe the dispersion interaction and the basis set superposition error (BSSE) must be sufficiently small that it does not significantly affect the results. This puts severe demands on both the one- and n -particle basis sets. In this work we employ the multireference configuration interaction (MRCI) procedure used in our previous study [8] of H_3 that was shown to be essentially equivalent to a full configuration-interaction (FCI); test calculations have demon-

strated that the MRCI energies are within $1 \mu E_h$ of the FCI energy. First a MRCI calculation is performed (in the self-consistent-field (SCF) molecular orbital basis), which includes all single and double excitations away from all distributions of the three electrons among 12 a' and 3 a'' orbitals. This is followed by the same MRCI treatment using the natural orbitals (NOs) of the first MRCI. For all geometries the reference space comprises more than 99.9% of the final CI wave function.

While we use the same n -particle treatment, the previous basis sets [8] are unsuitable for the present study. The $[5s\ 4p\ 1d]$ basis set, which is essentially equivalent to the basis sets used to generate all of the *ab initio* points employed in the BKMP fit, is not flexible enough to describe the dispersion terms; it significantly underestimates the van der Waals well depth and is too repulsive in the region $r = 3$ to $6 a_0$. Even the larger $[6s\ 5p\ 2d\ 1f]$ set is unsuitable because the $\text{H}(\text{H}_2)$ BSSE is unacceptably large. Note that while these limitations make the basis sets unsuitable for the present study, they do not affect the previous results [8] to within their stated accuracy.

Most of the current calculations are performed with a hydrogen one-particle basis set that is derived from the 10s set optimized for the 2S state [22] supplemented with a diffuse s (0.02486). The innermost 6s functions are contracted based on the SCF orbital and the outer five functions are uncontracted. This is supplemented with the three p , two d , and one f function optimized by Dunning [23] and augmented with two diffuse p (0.1168 and 0.0467) and a diffuse d (0.2648) function, thus yielding a final basis set of the form $(11s\ 5p\ 3d\ 1f)/[6s\ 5p\ 3d\ 1f]$. The supplementary diffuse functions are required to accurately describe the van der Waals region. However, the diffuse functions introduce linear dependency problems at the shorter r values. This occurs even for H_2 by itself at the shortest r values considered (0.8 and 0.9 a_0). Thus, the linear dependency problems restrict, to some extent,

the geometries considered. For selected calibration calculations a diffuse f (0.32) is also added. The final basis sets employed replace the (3*p* 2*d* 1*f*) set with Dunning’s (4*p* 3*d* 2*f*) H polarization set. This basis set is again augmented with two diffuse p (0.0984 and 0.0394) and a diffuse d (0.1972) function, giving a basis set of the form (11*s* 6*p* 4*d* 2*f*)/[6*s* 6*p* 4*d* 2*f*]. The final basis set includes a diffuse f (0.35) and Dunning’s optimized g (2.358) giving a [6*s* 6*p* 4*d* 3*f* 1*g*] basis set. Only the pure spherical harmonic components of the basis function are used.

The basis sets employed in this work yield an energy for H that is only 0.64 μE_h above the exact result. The H₂ potential energy curve (given in Table I) is in good agreement with the known non-relativistic limit [24] and the error in the H₂ dissociation energy is only 0.3 kcal/mol. The errors in the total energies are smaller than for the Slater basis used by Liu [1] to calculate the linear H₃ potential. The basis sets are sufficiently complete as to provide an accurate description of the dispersion terms. In addition, at $r = 6.0 a_0$, the BSSE for all of the basis sets employed is less than 1 μE_h . This is sufficiently small that the BSSE [H(H₂)+H₂(H)] is insignificant even in the van der Waals region; hence, we do not correct for BSSE in this work unless otherwise noted.

IV. Calibration Points

In the following discussion, we compare our computed results with the BKMP potential [9] and the data used for its construction; one major goal being to test the BKMP semiempirical basis set correction which allowed them to merge the *ab initio* energies from various groups in a consistent manner and to approximately correct for the known error in the H₂ interaction energies. The correction, δ_{bas} , is obtained by using the London equation to provide a procedure for combining the H₂ basis set correction for the 3 interatomic distances in H₃. On the basis of

test calculations, they estimated that the extrapolation energies were accurate to about $0.15 mE_h$ for the linear symmetric conformations and about $0.3 mE_h$ for the other conformations. In Table II we compare the basis set corrected energies compiled by BKMP from different authors with the results of this work. The basis set correction for our computed points is about 2.5 times smaller than for the points computed by BKMP and about 1.7 times smaller than for the linear points of Liu. The agreement for the linear points, and particularly the symmetric points, is extremely good. Our extrapolated energies are slightly (0.07 kcal/mol) below the Monte Carlo energies [25], suggesting that the basis set correction is slightly overestimated for the linear points, but the difference is within the estimated uncertainty of the correction. For the nonlinear geometries, the agreement between the extrapolated energies decreases with increasing θ_{12} . At $\theta_{12}=120^\circ$, our calculated energies are lower than BKMPs extrapolated values. The increase in the error in the BKMP extrapolated values with θ_{12} is due to using a basis set correction that is independent of θ_{12} for the case $r_1=r_2$; intuitively, however, the basis set correction must increase with the angle.

Defining the correlation energy as the difference between the reference energy and the MRCI energy (both in the natural orbital basis), we find that there is $\frac{1}{3}$ more correlation energy at 120° than at 0° . Because of the very large basis sets used, it is logical to assume that the error in the correlation treatment is proportional to the correlation energy; this suggests that the basis set correction at 120° should be 33% larger than for 0° . We expect the underestimation of the correction to be true for all non-linear geometries; therefore the energies calculated in this work and those used to generate the BKMP potential are expected to differ the most for the large angle structures.

In Table III, we compare a subset of the calculated energies that are more

than 25 kcal/mol above the H-H₂ asymptote with the LSTH, DMBE, and BKMP potential energy surfaces. The root mean square (rms) differences for the 200 structures that are more than 25 kcal/mol above the H-H₂ asymptote are 0.64, 0.49, and 0.27 kcal/mol, respectively, for three potentials with the maximum differences being 1.39, 1.94, and 0.85 kcal/mol. The London basis set correction relative to the H-H₂ asymptote is also reported. As for the calibration points, the extrapolated energies are in excellent agreement with the BKMP potential for small angles. The basis set corrected values give an rms difference of 0.65, 0.54, and 0.34 kcal/mol with the maximum errors being 1.39, 2.15 and 1.02 kcal/mol. The largest errors occur for the large angle structures as previously discussed. The rms error for the 484 points computed in this work are 0.44(0.47), 0.37(0.40), and 0.19(0.23) kcal/mol for the three potentials with the basis set corrected results in parentheses. All the computed energies and the comparisons with the three potential functions are available as a PAPS document [26]. Selected cuts for a small value of r are compared with the corresponding results for the BKMP potential in Fig. 4; note that the agreement is very good and that the largest error lies within the claimed uncertainty of the BKMP potential.

As discussed by Liu [1] it is difficult to assess the accuracy of the calculated H₃ potential surfaces. The best procedure is to compare the calculated energy differences with improved treatments. As the basis set errors in the current work (either δ_{bas} , or the error in the H₂ energies) are about 40% smaller than those for the linear potential computed by Liu, we can assess the reliability of the data upon which the previous fits are based. Unfortunately, the same geometries were computed for only a few points. Following Liu's [1] arguments, we expect our calculated H₃ surface to lie between 0.1 and 0.5 kcal/mol above the true surface in the region $1.0 \leq r \leq 4.0 a_0$. Relative to the calculated saddle point energies, the current

linear points appear to be within 0.1 kcal/mol of the energy separations computed by Liu over the specified range; the largest errors occurring for the larger r values. Comparing with the calculations of Siegbahn and Liu [2], the energy separations from the saddle point energy differ by as much as 0.5 kcal/mol for the large angle structures. While the errors are larger than the 0.1 kcal/mol estimated by Siegbahn and Liu [2], the errors are still relatively small. Also note, that the differences between our computed points and the BKMP fit (for the large angle structures) is about twice that compared with the differences in the *ab initio* calculations. We estimate that the current *ab initio* energies with respect to H+H+H are accurate to within about 0.5 kcal/mol, 1.5 times the error in our H₂ dissociation energy. The relative energies with respect to the saddle point should be considerably more accurate, probably to within 0.2 kcal/mol. Basis set incompleteness is still the principal source of error in the calculations; corrections for relativistic effects and Born-Oppenheimer corrections will be smaller.

V. Classical Barrier Height

The classical barrier height is the energy difference between the saddle point and the H-H₂ asymptote. This quantity is an important aspect of the surface and has been extensively studied [1,5,8,25]. We calculate the barrier height to be 9.654, 9.649, and 9.632 kcal/mol in the [6s 5p 3d 1f], [6s 6p 4d 2f], and [6s 6p 4d 3f 1g] basis sets, respectively (the [6s 6p 4d 3f 1g] result is based on a single point calculation at $r_1 = r_2 = 1.75 a_0$). Corrected for BSSE, the barrier heights are 9.670, 9.663, and 9.643 kcal/mol. The computed barrier height may be compared with the 9.65 kcal/mol calculated by Liu [5] (extended basis II) and is in very good agreement with the 9.59 ± 0.06 kcal/mol estimate of Liu [5]. The computed results are also in good agreement with the Monte Carlo results of Diedrich and Anderson [25]

of 9.61 ± 0.01 kcal/mol where the error bar gives one standard deviation. The calculated total energies for the $[6s\ 5p\ 3d\ 1f]$ and $[6s\ 6p\ 4d\ 2f]$ basis sets are 0.37 and 0.26 kcal/mol respectively, above the Monte Carlo energies at $r_1 = r_2 = 1.7 a_0$. We note that the reduction in the computed barrier height is not linear with the error in the H_2 energy so it difficult to extrapolate our results to predict the “true” barrier height. However, our results are consistent with Monte Carlo estimates. The London basis set correction for the $[6s\ 5p\ 3d\ 1f]$ basis set is 0.12 kcal/mol giving an estimate of 9.53 kcal/mol; this is consistent with the observation that the London correction slightly overestimates the basis set correction.

VI. H–H₂ potential energy

The potential energy surface describing H–H₂ interactions can be conveniently determined using the expansion

$$V(r, r_{H_2}, \chi) = V_0(r, r_{H_2}) + V_2(r, r_{H_2})P_2(\cos \chi) + V_4(r, r_{H_2})P_4(\cos \chi) + \dots \quad (1)$$

where $P_{2n}(\cos \chi)$ is a Legendre polynomial. The *ab initio* points have been computed on a grid to facilitate the calculation of the expansion coefficients V_{2n} . The values of V_{2n} were determined by a least squares fit of the calculated energies for fixed r and r_{H_2} . We have tested the convergence of V_{2n} and the stability of the fit using additional data points. The fitting error is small ($\leq 0.02\%$) for $r \geq 2 a_0$, but it increases rapidly at smaller r to a maximum value of 0.5% at $r=1.6 a_0$. The results for V_{2n} are presented in Tables IVa–d. For consistency, the expansions (1) of the BKMP potential for comparison with the present results were generated with the same procedure as that described above. The leading anisotropic term of the expansion (1) vanishes at the angle $\chi_0 = \cos^{-1}(1/\sqrt{3}) = 54.73561^\circ$ for which $P_2(\cos \chi) = 0$; as would be expected from Tables IV, we find that the calculated values of the potential energy for this particular angle χ_0 yield a good approximation to the

spherically-averaged potential for a broad range of large r values.

One expects that the potential energy deduced from the scattering measurements corresponds to an average separation distance for the hydrogen molecule that is about the same as the expectation value of the first vibrational state (i.e., $r_{H_2} = 1.449 a_0$) rather than the equilibrium separation distance $1.401 a_0$. The highest collision energy of the scattering measurements by Gengenbach *et al* [14]. corresponds to about 34 kcal/mol; from Tables IV one finds that the spherically-averaged potentials for these two choices of r_{H_2} differ by a few percent at the smallest value of r ($\approx 2 a_0$) probed by the experiment. On the other hand, the average potentials for these two choices are about the same for large r ($\geq 4 a_0$).

Our calculated V_0 is compared with other potentials in Figs. 1 and 2. The agreement between the repulsive wall of our computed V_0 and that of the BKMP potential is very good for small r . The value of $66 \mu E_h$ for the van der Waals well depth D_e of our calculated V_0 potential agrees very well with value $67 \mu E_h$ from the MBMD potential of Torello and Dondi [20]. Furthermore, our calculated V_0 agrees well with the prediction of the asymptotic dispersion terms; for example, at $r = 10 a_0$ it is only 4 % lower than the slightly damped dispersion interaction energy (as described below). Thus overall, our computed spherically-averaged potential agrees very well with the best available data. We point out, in passing, that the repulsive wall of the LSTH potential in the van der Waals region agrees remarkably well with the results of the present calculation (see Fig. 2), notwithstanding the disclaimer stated in Ref. 3.

Further improvement in the one-particle basis set will unquestionably yield a larger value for D_e and also is expected to shorten r_e , the position of the minimum of the potential well. It is difficult, a priori, to estimate the error in the calculations. The BSSE, which often can be used as a measure of basis set error, is negligible;

at $r = 6.0 a_0$, the BSSE is less than $1 \mu E_h$. Supplementing the basis set with a diffuse f function lowers V_0 slightly, by 1, 8, 19, and $34 \mu E_h$ at $r=7.5, 6.0, 5.0,$ and $4.0 a_0$, respectively. Expanding the polarization set, going from the $(5p 3d 1f)$ to the $(6p 4d 2f)$ set has a slightly smaller effect; the $(6p 4d 2f)$ results are $-0.1, 4.7,$ and $9.1 \mu E_h$ (at $r=7.5, 6.0,$ and $4.0 a_0$) above the diffuse f basis set results. The results indicate that the $[6s 5p 3d 1f]$ basis set employed in this work is reasonably complete even for the van der Waals region—the error in the H_2 energy will largely cancel. The largest deficiencies in the basis sets are the lack of diffuse f and g functions necessary to describe the higher-order polarizabilities. However, based on the calibration results we estimate that the true van der Waals well depth to be no more than about 20% deeper than the present value $66 \mu E_h$; that is, we estimate D_e to be $72 \pm 6 \mu E_h$. To improve upon this estimate, we have employed the larger $[6s 6p 4d 3f 1g]$ basis set. Using the modified potential energy fit derived below and our estimated D_e of $72 \mu E_h$, we predict a bond length of $6.54 a_0$. At this predicted bond length, we obtain a D_e value of $72.4 \mu E_h$, which is unquestionably a lower bound (the BSSE is only $0.23 \mu E_h$). These results lead to our recommended value of $75 \pm 3 \mu E_h$. From the foregoing discussion, we conclude that the values of both r_e and D_e from the BMSV potential are too large.

As mentioned above, the anisotropic coefficient V_2 is of particular significance for rotational excitation by collisions. The general functional form was deduced by Tang [27] based upon a semiempirical potential by Tang and Karplus [28] and the asymptotic long-range form. $V_2(r, r_{H_2})$ for values of r_{H_2} near the equilibrium distance has 3 sign changes; the long-range V_2 is negative and is determined by the anisotropy of the dispersion interaction. At large r , including the van der Waals region, as well as the region of the long-range dispersion forces, the interaction potential is monotonically increasing from 0 to 90° (with r and r_{H_2} fixed,

e.g., see Fig. 5). In the range $3.7 \leq r \leq 5.2 a_0$, V_2 is positive indicating that a 90° approach is the most favorable. At slightly smaller r values, V_2 is negative and sizable (e.g., see Fig. 6) and a linear approach is strongly favored. This occurs because the repulsion between the H_2 and the H is smallest for this orientation; the quadrupole moment of H_2 is positive. At shorter range, $r \leq 1.9 a_0$, V_2 is positive again and increases sharply; this is to some extent an artifact of the coordinate system employed as the minimum H–H distance is now much smaller than r_{H_2} for a linear approach.

In Fig. 6, we compare V_2 and V_4 deduced from this work with the corresponding results from the BKMP potential. The agreement is excellent for small r ; for example, the inner minimum of V_2 is only slightly more shallow than that derived from the BKMP fit. The *ab initio* values are more realistic (smoother), however, in the interpolation region at large r as would be expected. Improvements in the basis set are expected to have only a small effect on the anisotropic coefficients as the errors cancel in the H_2 energy differences.

The *ab initio* results for the van der Waals region at large r are shown in Fig. 5. Note the uniform spacing of the potential energy curves with respect to χ ; this is consistent with equal differences from the leading term (note that $\Delta P_2 = 3/8$ for adjacent angles) of the expansion (1) when the higher-order terms are negligible.

We have found that the potential energy in the van der Waals region can be described well by a modified version [29] of the potential form developed by Tang and Toennies [30] that can be written

$$V(r, \chi) = V_{SR}(r, \chi) + V_{DLR}(r, \chi) \quad (2)$$

where the short-range repulsive potential V_{SR} has the Born-Mayer form

$$V_{SR}(r, \chi) = A(\chi) \exp[-\alpha(\chi)r] \quad (3)$$

and the long-range attractive dispersion energy is obtained from

$$V_{DLR}(r, \chi) = - \sum_{n=3} f_{2n}[\alpha(\chi)r] \frac{C_{2n}}{r^{2n}} \quad (4)$$

using the universal form of the damping function that can be related to an incomplete gamma function [31]

$$f_{2n}(x) = 1 - \exp(-x) \sum_{k=0}^{2n} \frac{x^k}{k!}. \quad (5)$$

The parameters A and α^{-1} characterize the strength and range, respectively, of the repulsive interaction. The long-range forces are determined by the dispersion coefficients that are approximated by the expansion

$$C_{2n}(\chi) = \bar{C}_{2n}[1 + \Gamma_{2n}P_2(\cos \chi)]. \quad (6)$$

The isotropic components \bar{C}_{2n} calculated by Meyer (reported in Ref. [20]) are $8.813 a_0^6 E_h$, $163.87 a_0^8 E_h$, and $4232.2 a_0^{10} E_h$ for $n = 3-5$, respectively. The theoretical value of \bar{C}_6 agrees with the corresponding value deduced by Zeiss and Meath [32] from measured oscillator strengths, photoabsorption, and scattering data. Higher-order values can be obtained from the recursion relations [30,33]

$$\bar{C}_{2n+4} = \Omega_n (\bar{C}_{2n+2}/\bar{C}_{2n})^3 \bar{C}_{2n-2} \quad (7)$$

with the values of Ω_n calculated for hydrogen [33].

We have calculated the leading anisotropic contribution Γ_6 from the combining relations developed by Fuchs *et al.* [34] using polarizability data (exact results for H [35] and calculated/measured data for H₂ [36]) and the calculated dispersion coefficients for H-H and H₂-H₂ interactions. The value of C_6 for H₂ has been determined exactly [33]; the values of $C_6^{L_A L_B M}$ for the molecular interactions were

obtained from a transformation [37] of the results for the angular representation $C_6^{L_A L_B L}$ calculated by Riyks and Wormer [38]. We obtain the result $\Gamma_6 = 0.100$, which agrees well with the value 0.114 determined by Langhoff *et al.* [39] from optical dispersion, absorption, and scattering data. By comparing the contribution from the leading anisotropic dispersion term described above with the values of V_2 determined from the *ab initio* data at large r , we can estimate the contribution from the next higher-order term. Thus we obtain the result $\Gamma_8 \approx 0.40$ from the data for r in the range 8.5–10.0 a_0 .

Following the discussion of Ref. 29, we can readily determine the repulsive parameters from the *ab initio* data for the parallel and perpendicular orientations ($\chi = 0^\circ$ and 90° , respectively); i.e., we obtain

$$\ln A(\chi) = 1.390 + 0.233P_2(\cos \chi) \quad (8)$$

and

$$\alpha(\chi) = 1.629 + 0.018P_2(\cos \chi). \quad (9)$$

We find that the result obtained with $\chi = \chi_0$ from the modified Tang-Toennies (MTT) potential energy surface of this work (i.e., Eqs. (2–9) with the above data for the dispersion coefficients) agrees well with the spherically-averaged potential (i.e., V_0 of Table IVc). In addition, if we constrain the spherically-averaged potential to the *ab initio* results of Table IVc for the upper region of the repulsive wall, the long-range behavior described by the dispersion interaction described above, and the expected value of $D_e \doteq 75 \mu E_h$ from the above analysis; we obtain $A = 5.05 \mu E_h$ and $\alpha = 1.669 a_0^{-1}$. The value of r_e from this predicted potential is 6.51 a_0 which is slightly less than the value of 6.54 a_0 deduced by Torello and Dondi [20] from their measured differential scattering data. The results for the predicted upper and lower bounds for D_e are also reported in Table V with those for

the calculated and measured potentials described above. The MTT potential for $\chi = \chi_0$ is compared with the calculated data and also the predicted potential with the deeper potential well in Fig. 7.

As described above, the potentials obtained from the differential scattering measurements agree well with the present results in the region of the van der Waals minimum; the repulsive wall of these potentials is, however, considerably weaker (see Fig. 2). Because potentials fitted to scattering data may not be unique, it is of interest to compare the scattering from the present potential data with the measured results.

We have calculated the differential elastic scattering cross section using the sudden approximations of Parker and Pack [40] from scattering phase shifts that have been determined by direct numerical integration of the Schrödinger equation. The potential energies for these calculations were constructed from spline fits to the *ab initio* data of Table III and the long-range tails from the MTT potential for the values of χ specified in Fig. 5. In addition, we have also calculated the scattering from the spherically-averaged potential (i.e., the values of V_0 from Table IVc and the long-range tails from the MTT potential with $\chi = \chi_0$). The cross sections from these two different approaches are found to be nearly identical, as would be expected when the anisotropic terms of the potential energy (1) are small.

The theoretical scattering results are compared with the experimental data of Ref. 20 in Fig. 8. We have averaged the cross section over the velocity profile of the primary beam, but the theoretical results represent a high-resolution cross section, in that, we have not taken the beam size, detector area, etc. into account; unfortunately, sufficient data was not provided by the authors to allow this averaging of the scattering. In light of this difference, the agreement between theory and experiment can be considered satisfactory.

VII. Conclusions

Ab initio calculations have been performed using a very large basis set to calibrate the H-H₂ surface. The basis set incompleteness is much smaller than in all previous calculations. The results confirm the accuracy of the recent Boothroyd, Keogh, Martin, and Peterson (BKMP) potential and their scheme for correcting the H₃ calculations using the error in the H₂ potential. Our calculations do show, however, that the accuracy of the correction decreases with increasing angle, as some of our computed points are below their extrapolated energies. Our computed data fill in a region of the potential that has been left out of previous theoretical studies; that is, the region of large r from $4 a_0$ out to about $8-10 a_0$ where the long-range dispersion interaction energies are sufficiently accurate. The differential elastic scattering cross section calculated from the present results for the potential energies agrees well with the measured data. We have derived a potential energy function for the van der Waals region at large r to augment the available potential energy fits that cover the small r region. The present results will allow an accurate determination of the contribution from H-H₂ interactions to transport properties; collision integrals for hydrogen will be reported in a future publication.

Acknowledgements

The authors gratefully acknowledge helpful discussions with A. I. Boothroyd.

REFERENCES

- ¹B. Liu, J. Chem. Phys. **58**, 1925 (1973).
- ²P. Seigbahn and B. Liu, J. Chem. Phys. **68**, 2457 (1978).
- ³D. G. Truhlar and C. J. Horowitz, J. Chem. Phys. **68**, 2466 (1978); **71**, 1514E (1979).
- ⁴A. J. C. Varandas and J. Tennyson, Chem. Phys. Lett. **77**, 151 (1981).
- ⁵B. Liu, J. Chem. Phys. **80**, 581 (1984).
- ⁶M. R. A. Blomberg and B. Liu, J. Chem. Phys. **82**, 1050 (1985).
- ⁷A. J. C. Varandas, F. B. Brown, C. A. Mead, D. G. Truhlar, and N. C. Blais, J. Chem. Phys. **86**, 6258 (1987).
- ⁸C. W. Bauschlicher, S. R. Langhoff, and H. Partridge, Chem. Phys. Lett. **170**, 345 (1990).
- ⁹A. I. Boothroyd, W. J. Keogh, P. G. Martin, and M. R. Peterson, J. Chem. Phys. **95**, 4343 (1991).
- ¹⁰. a) J. Z. H. Zhang and W. H. Miller, J. Chem. Phys. **91**, 1528 (1989), b) M. Zhao, D. G. Truhlar, D. J. Kouri, Y. Sun, and D. W. Schwenke, Chem. Phys. Lett. **156**, 281 (1989), c) M. Zhao, D. G. Truhlar, D. W. Schwenke, and D. J. Kouri, J. Chem. Phys. **94**, 7074 (1990), d) N. C. Blais and D. G. Truhlar, H. Chem. Phys. **88**, 5457 (1988), e) N. C. Blais, M. Zhao, M. Mladenovic, D. G. Truhlar, D. W. Schwenke, Y. Sun, and D. J. Kouri, J. Chem. Phys. **91**, 1038 (1989), f) N. C. Blais, M. Zhao, D. G. Truhlar, D. W. Schwenke, and D. J. Kouri, Chem. Phys. Lett. **166**, 11 (1990), g) S. L. Mielke, R. S. Friedman, D.

- G. Truhlar, and D. W. Schwenke, Chem. Phys. Lett. **188**, 359 (1992), and h)
W. J. Keogh, A. I. Boothroyd, P. G. Martin, S. L. Mielke, D. G. Truhlar, and
D. W. Schwenke, Chem. Phys. Lett. **195**, 144 (1992).
- ¹¹R. E. Continetti, B. A. Balko, and Y. T. Lee, J. Chem. Phys. **93**, 5719 (1990).
- ¹²S. A. Buntin, C. F. Giese, and W. R. Gentry, J. Chem. Phys. **87**, 1443 (1987);
Chem. Phys. Lett. **168**, 513 (1990).
- ¹³D. A. V. Kliner and R. N. Zare, J. Chem. Phys. **92**, 2107 (1990) and D. A.
V. Kliner, D. E. Adelman, and R. N. Zare, J. Chem. Phys. **95**, 1648 (1991).
- ¹⁴R. Gengenbach, Ch. Hahn, and J. P. Toennies, J. Chem. Phys. **62**, 3620 (1975).
- ¹⁵A. Dalgarno, R. J. W. Henry, and C. S. Roberts, Proc. Phys. Soc. **88**, 611
(1970).
- ¹⁶P. W. Langhoff and M. Karplus, J. Chem. Phys. **53**, 233 (1970).
- ¹⁷H. Margenau, Phys. Rev. **66**, 303 (1944).
- ¹⁸J. P. Toennies, Chem. Soc. Faraday Discuss. **55**, 129 (1973).
- ¹⁹N. Hishinuma, J. Phys. Soc. Japan **41**, 1733 (1976).
- ²⁰F. Torello and M. G. Dondi, J. Chem. Phys. **70**, 1564 (1979).
- ²¹J. R. Stallcop, J. Chem. Phys. **61**, 5085 (1974).
- ²²H. Partridge, J. Chem. Phys. **87**, 6643 (1987).
- ²³T. H. Dunning, J. Chem. Phys. **90**, 1007 (1989).
- ²⁴W. Kolos and L. Wolniewicz, J. Chem. Phys. **43**, 2429 (1965).
- ²⁵D. L. Diedrich and J. B. Anderson, Sci. **258**, 786 (1992).

- ²⁶PAPS reference
- ²⁷K. T. Tang, Phys. Rev. **187**, 122 (1969).
- ²⁸K. T. Tang and M. Karplus, J. Chem. Phys. **49**, 1676 (1968).
- ²⁹J. R. Stallcop, H. Partridge, S. P. Walch, and E. Levin, J. Chem. Phys. **97**, 3431 (1992).
- ³⁰K. T. Tang and J. P. Toennies, J. Chem. Phys. **80**, 3786 (1984).
- ³¹A. Erdélyi, W. Magnus, F. Oberhettinger, and F. G. Tricomi, *Higher Transcendental Functions* (McGraw-Hill, New York, 1953), Vol. II, Chap. 9.
- ³²G. D. Zeiss and W. J. Meath, Mol. Phys. **33**, 1155 (1977).
- ³³A. J. Thakkar, J. Chem. Phys. **89**, 2092 (1988).
- ³⁴R. R. Fuchs, F. R. W. McCourt, A. J. Thakkar, and F. Grein, J. Phys. Chem. **88**, 2036 (1984).
- ³⁵A. Dalgarno, Adv. Phys. **11**, 281 (1962).
- ³⁶D. M. Bishop and L. M. Cheung, J. Chem. Phys. **72**, 5125 (1980).
- ³⁷F. Visser, P. E. S. Wormer, and P. Stam, J. Chem. Phys. **79**, 4973 (1983).
- ³⁸W. Riyks and P. E. S. Wormer, J. Chem. Phys. **88**, 5704 (1982).
- ³⁹P. W. Langhoff, R. G. Gordon, and M. Karplus, J. Chem. Phys. **55**, 2126 (1971).
- ⁴⁰G. A. Parker and R. T. Pack, J. Chem. Phys. **68**, 1585 (1978).

Table I. Total energies (E_h) for the $X^1\Sigma_g^+$ state of H_2 .

$r(a_0)$	Basis set		
	[6s 5p 3d 1f]	[6s 6p 4d 2f]	[6s 6p 4d 3f 1g]
0.8	-1.01964331 ^a	-1.01964589 ^a	
0.9	-1.08290665 ^a		
0.95	-1.10569977		
1.0	-1.12388052	-1.12417145	
1.05	-1.13825085		
1.1	-1.14945650		
1.15	-1.15802352		
1.2	-1.16438212	-1.16459398	
1.25	-1.16888723		
1.3	-1.17183355		
1.4	-1.17399454	-1.17416126	-1.17424203
1.401	-1.17399505		
1.449	-1.17360611	-1.17376375	-1.17384418
1.5	-1.17240057		
1.6	-1.16815089	-1.16828665	
1.7	-1.16204450		
1.75	-1.15848532	-1.15860666	-1.15868356
1.8	-1.15466972	-1.15478735	
1.9	-1.14646449		
2.0	-1.13775776	-1.13786438	
2.2	-1.11977532	-1.11987628	
2.4	-1.10208144	-1.10218103	
2.6	-1.08546434		
2.8	-1.07037029		
3.0	-1.05702837	-1.08556502	
3.4	-1.03581724		
3.8	-1.02134469		
4.0	-1.01621290		
4.5	-1.00787702		
5.0	-1.00371123		
5.5	-1.00172715		
6.0	-1.00080524	-1.00081273	
6.5	-1.00038078		
7.0	-1.00018488		
8.0	-1.00004951	-1.00005118	
9.0	-1.00001649		
10.	-1.00000661		

12.	-1.00000106		
100.	-0.99999868	-0.99999868	-0.99999868

^a The CI vectors in the MRCI procedure were picked based on overlap with the previous iteration to avoid “collapse” due to linear dependence in the basis set; the values might therefore be less accurate than the others.

Table II. Comparison of the basis set corrected Π_3 energies.

Geometry ^a		BKMP ^b		SL ^b		Liu ^b		Present		Monte Carlo ^c
r_1	r_2	θ_{12}	δ_{bas}	E_{fin}	E_{fin}	δ_{bas}	E_{fin}	δ_{bas}	E_{fin}	
1.40	1.40	0.	1779	-0.129432	-0.158724	1187	-0.158719	749	-0.12945002	
1.70	1.70	0.	1760		-0.159283	1193	-0.159276	698	-0.15873850	-0.158636(024)
1.75	1.75	0.	1759	-0.159317	-0.159011	1199	-0.159012	686	-0.15929055	
1.80	1.80	0.	1757		-0.130421	1197	-0.130437	691	-0.15902244	-0.158910(029)
2.30	2.30	0.	1757	-0.130436	-0.173377	959	-0.173317	637	-0.13043051	
1.43	3.87	0.	1483		-0.174174	901	-0.174122	567	-0.17330991	
1.41	4.33	0.	1390		-0.146280			545	-0.17413289	
1.38	1.74	30.	1776	-0.146188	-0.160280			725	-0.14633800	
1.53	2.17	30.	1746	-0.160253	-0.027042			685	-0.16028835	
1.00	1.40	60.	1978	-0.026894	-0.164342			837	-0.02729276	
1.45	2.80	60.	1748	-0.164379	-0.121720			657	-0.16434564	
2.10	2.10	90.	1736	-0.121634	-0.074010			657	-0.12201356	
1.90	1.90	120.	1746	-0.073715	-0.073400			676	-0.07500499	
2.10	2.10	120.	1736	-0.073224				657	-0.07420926	

^a r in a_0 , θ in degrees, and E_{fin} are the basis set corrected energies are in E_h relative to $E(\text{H}+\text{H}+\text{H})=-1.5E_h$. δ_{bas} is the London H_3 basis set correction in μE_h .

^b Values from Ref. 9. Note, the basis set corrections are the same for the BKMP and SL calculations because the same basis sets are used.

^c Values from Ref. 25.

Table III. Comparison of computed H_3 energies with the LSTH, DMBE, and BKMP potentials.

r	Geometry ^a		Present	LSTH		DMBE		BKMP		$\delta_{ba,s}^c$
	r_{H_2}	χ^b		E	ΔE	E	ΔE	E	ΔE	
1.8000	1.4490	0.0000	61.9485	62.1060	-0.1575	62.5439	-0.5954	61.8494	0.0991	-0.1964
1.9000	1.4490	0.0000	46.0014	46.1700	-0.1686	46.1294	-0.1280	45.8739	0.1275	-0.1759
2.0000	1.4490	0.0000	34.8774	35.0360	-0.1586	34.7923	0.0851	34.7319	0.1455	-0.1642
1.5000	1.4490	30.0000	100.8240	101.3518	-0.5278	101.6174	-0.7934	101.1330	-0.3090	-0.1680
1.7000	1.4490	30.0000	58.3027	58.1623	0.1404	58.1595	0.1432	58.3193	-0.0166	-0.1811
1.8000	1.4490	30.0000	45.3848	45.1113	0.2735	44.9875	0.3973	45.4108	-0.0260	-0.1692
2.0000	1.4490	30.0000	29.1930	28.9542	0.2388	28.6997	0.4933	29.1666	0.0264	-0.1522
1.4000	1.4490	54.7356	73.4545	74.7217	-1.2672	74.2363	-0.7818	73.3932	0.0613	-0.1813
1.6000	1.4490	54.7356	51.4333	52.0565	-0.6232	51.6748	-0.2415	51.6364	-0.2031	-0.1595
1.7000	1.4490	54.7356	43.8260	44.3678	-0.5418	43.9179	-0.0919	43.9642	-0.1382	-0.1527
1.8000	1.4490	54.7356	37.7542	38.2901	-0.5359	37.7889	-0.0347	37.8426	-0.0884	-0.1470
1.9000	1.4490	54.7356	32.8328	33.3884	-0.5556	32.8801	-0.0473	32.9005	-0.0677	-0.1424
2.0000	1.4490	54.7356	28.7775	29.3411	-0.5636	28.8746	-0.0971	28.8396	-0.0621	-0.1388
1.3000	1.4490	90.0000	83.5794	83.8257	-0.2463	83.8226	-0.2432	84.2654	-0.6860	-0.1486
1.4000	1.4490	90.0000	73.0910	72.4861	0.6049	73.6377	-0.5467	73.8381	-0.7471	-0.1452
1.6000	1.4490	90.0000	56.3564	55.0349	1.3215	57.1668	-0.8104	56.9114	-0.5550	-0.1402
1.8000	1.4490	90.0000	43.6898	42.3429	1.3469	44.3444	-0.6546	44.0929	-0.4031	-0.1363
2.0000	1.4490	90.0000	33.9232	32.7971	1.1261	34.1869	-0.2637	34.2512	-0.3280	-0.1319
2.2000	1.4490	90.0000	26.3270	25.4670	0.8600	26.1849	0.1421	26.5959	-0.2689	-0.1284
1.6000	1.4010	54.7356	53.9335	54.6348	-0.7013	54.1675	-0.2340	54.1360	-0.2025	-0.1620
1.8000	1.4010	54.7356	39.6090	40.1412	-0.5322	39.6550	-0.0460	39.7129	-0.1039	-0.1501
2.0000	1.4010	54.7356	30.0763	30.5878	-0.5115	30.1924	-0.1161	30.1609	-0.0846	-0.1424
2.2000	1.4010	54.7356	23.3273	23.7618	-0.4345	23.5276	-0.2003	23.3868	-0.0595	-0.1371
1.8000	1.4010	30.0000	46.8835	46.5890	0.2945	46.4028	0.4807	46.9050	-0.0215	-0.1703

2.0000	1.4010	30.0000	30.8384	30.5781	0.2603	30.3292	0.5092	30.8158	0.0226	-0.1543
1.8000	1.4010	0.0000	61.3948	61.5576	-0.1628	61.7429	-0.3481	61.2871	0.1077	-0.1897
2.0000	1.4010	0.0000	35.8981	36.0459	-0.1478	35.7348	0.1633	35.7368	0.1613	-0.1648
2.2000	1.4010	0.0000	23.0166	23.1561	-0.1395	22.8816	0.1350	22.8648	0.1518	-0.1505
1.4000	1.4010	90.0000	74.2394	73.4048	0.8346	74.9068	-0.6674	75.0375	-0.7981	-0.1498
1.5000	1.4010	90.0000	65.0024	63.7953	1.2071	65.8484	-0.8460	65.6923	-0.6899	-0.1470
1.6000	1.4010	90.0000	57.0399	55.6786	1.3613	57.9416	-0.9017	57.6167	-0.5768	-0.1447
1.8000	1.4010	90.0000	44.0767	42.7745	1.3022	44.7870	-0.7103	44.5115	-0.4348	-0.1407
2.0000	1.4010	90.0000	34.1105	33.0665	1.0440	34.4054	-0.2949	34.4785	-0.3680	-0.1363
2.2000	1.4010	90.0000	26.3753	25.6148	0.7605	26.2546	0.1207	26.6848	-0.3095	-0.1329
1.8000	1.2000	0.0000	67.4410	67.5794	-0.1384	67.1991	0.2419	67.2915	0.1495	-0.1919
1.8000	1.2000	30.0000	58.9098	58.6820	0.2278	58.4286	0.4812	58.9394	-0.0296	-0.1809
1.8000	1.2000	90.0000	52.6910	52.0918	0.5992	53.4303	-0.7393	52.7328	-0.0418	-0.1648
2.0000	1.2000	30.0000	43.1358	42.8944	0.2414	42.8996	0.2362	43.1595	-0.0237	-0.1695
2.0000	1.2000	60.0000	41.1952	41.6744	-0.4792	41.5038	-0.3086	41.3155	-0.1203	-0.1626
2.2000	1.2000	30.0000	33.2532	33.0881	0.1651	33.2542	-0.0010	33.2180	0.0352	-0.1625
1.8000	1.2000	54.7356	52.6470	53.3013	-0.6543	52.8763	-0.2293	52.7659	-0.1189	-0.1691
2.0000	1.2000	54.7356	41.1806	41.5936	-0.4130	41.4075	-0.2269	41.3046	-0.1240	-0.1634
2.2000	1.2000	54.7356	32.8886	33.1792	-0.2906	33.0565	-0.1679	32.9799	-0.0913	-0.1590
2.0000	1.2000	0.0000	46.4505	46.6219	-0.1714	46.4374	0.0131	46.3178	0.1327	-0.1753
2.2000	1.2000	0.0000	34.4108	34.5394	-0.1286	34.6152	-0.2044	34.2501	0.1607	-0.1656
1.4000	1.2000	90.0000	86.0419	85.8218	0.2201	87.5600	-1.5181	86.8880	-0.8461	-0.1749
2.0000	1.2000	90.0000	41.8861	41.4672	0.4189	42.0620	-0.1759	41.9107	-0.0246	-0.1603
2.2000	1.2000	90.0000	33.5664	33.3889	0.1775	33.3001	0.2663	33.6086	-0.0422	-0.1571
1.8000	1.0000	54.7356	82.4654	83.5510	-1.0856	82.9128	-0.4474	82.8051	-0.3397	-0.2065
1.8000	1.0000	90.0000	80.4567	81.1450	-0.6883	80.3585	0.0982	80.0827	0.3740	-0.2068
2.0000	1.0000	90.0000	68.8447	69.3022	-0.4575	68.1756	0.6691	68.6057	0.2390	-0.2025
2.2000	1.0000	90.0000	59.9629	60.4822	-0.5193	58.9996	0.9633	59.8966	0.0663	-0.1992
3.0000	1.0000	90.0000	40.6327	41.4271	-0.7944	40.5409	0.0918	40.4239	0.2088	-0.1742
2.0000	1.0000	54.7356	69.7394	70.3390	-0.5996	70.0438	-0.3044	69.9952	-0.2558	-0.2025

2.2000	1.0000	54.7356	60.4320	60.8577	-0.4257	60.5279	-0.0959	60.5508	-0.1188	-0.1991
2.5000	1.0000	54.7356	50.5918	51.0079	-0.4161	50.2886	0.3032	50.4572	0.1346	-0.1928
3.0000	1.0000	54.7356	40.8201	41.4019	-0.5818	40.4428	0.3773	40.4170	0.4031	-0.1756
4.0000	1.0000	54.7356	33.3113	33.6065	-0.2952	33.7213	-0.4100	33.0042	0.3071	-0.1264
2.1000	2.0000	0.0000	33.4399	33.3284	0.1115	33.6443	-0.2044	33.0849	0.3550	-0.1706
4.0000	2.0000	0.0000	23.1157	23.1235	-0.0078	22.9558	0.1599	22.9544	0.1613	-0.0542
1.8000	2.0000	90.0000	59.2657	59.9967	-0.7310	60.1255	-0.8598	59.9680	-0.7023	-0.1030
2.0000	2.0000	90.0000	51.5860	51.2737	0.3123	51.7744	-0.1884	51.8902	-0.3042	-0.1002
2.2000	2.0000	90.0000	45.4442	44.6770	0.7672	45.1051	0.3391	45.4729	-0.0287	-0.0959
2.5000	2.0000	90.0000	38.4920	37.6212	0.8708	37.7364	0.7556	38.3476	0.1444	-0.0877
3.0000	2.0000	90.0000	31.0973	30.6983	0.3990	30.6110	0.4863	31.0234	0.0739	-0.0682
4.0000	2.0000	90.0000	24.7072	25.2353	-0.5281	25.3967	-0.6895	24.9315	-0.2243	-0.0202
1.7000	2.0000	54.7356	28.5990	28.5296	0.0694	28.8350	-0.2360	28.8485	-0.2495	-0.1372
1.8000	2.0000	54.7356	26.0691	26.1723	-0.1032	26.2704	-0.2013	26.2312	-0.1621	-0.1299
2.0000	2.0000	54.7356	23.9792	24.4992	-0.5200	24.1658	-0.1866	24.0439	-0.0647	-0.1180
2.2000	2.0000	54.7356	24.1512	25.0106	-0.8594	24.4537	-0.3025	24.2727	-0.1215	-0.1103
2.5000	2.0000	54.7356	25.6432	26.6003	-0.9571	26.2061	-0.5629	25.8273	-0.1841	-0.1010
3.0000	2.0000	54.7356	26.7395	27.1905	-0.4510	27.3103	-0.5708	26.6686	0.0709	-0.0839
3.5000	2.0000	54.7356	25.7639	26.0024	-0.2385	26.1353	-0.3714	25.6444	0.1195	-0.0581
4.0000	2.0000	54.7356	24.4389	24.7242	-0.2853	24.7653	-0.3264	24.4310	0.0079	-0.0313
2.5000	3.0000	54.7356	31.1834	31.2006	-0.0172	31.2049	-0.0215	31.1180	0.0654	-0.0644
3.0000	3.0000	54.7356	50.0705	50.6318	-0.5613	50.9231	-0.8526	50.1478	-0.0773	-0.0463
4.0000	3.0000	54.7356	71.5128	72.3076	-0.7948	72.5326	-1.0198	71.5372	-0.0244	0.0054
2.0000	3.0000	90.0000	56.8189	56.6814	0.1375	56.7374	0.0815	57.1568	-0.3379	-0.0707
2.5000	3.0000	90.0000	80.4800	80.1217	0.3583	80.2068	0.2732	80.6851	-0.2051	-0.0308
3.0000	3.0000	90.0000	80.3416	80.4414	-0.0998	80.3939	-0.0523	80.3958	-0.0542	-0.0040
4.0000	3.0000	90.0000	75.1651	76.3451	-1.1800	76.4082	-1.2431	75.3179	-0.1528	0.0426
1.7000	1.7000	54.7356	35.7438	36.1077	-0.3639	36.0126	-0.2688	35.9454	-0.2016	-0.1431
1.8000	1.7000	54.7356	31.4075	31.9138	-0.5063	31.5703	-0.1628	31.5300	-0.1225	-0.1363
2.0000	1.7000	54.7356	25.6804	26.4625	-0.7821	25.8006	-0.1202	25.7408	-0.0604	-0.1258

1.8000	1.7000	30.0000	42.3703	42.2702	0.1001	42.4690	-0.0987	42.3979	-0.0276	-0.1709
2.0000	1.7000	30.0000	24.5299	24.4231	0.1068	24.3449	0.1850	24.5151	0.0148	-0.1468
2.0000	1.7000	60.0000	27.8952	28.5693	-0.6741	28.0136	-0.1184	28.0067	-0.1115	-0.1229
1.8000	1.7000	0.0000	75.8030	75.8015	0.0015	77.7417	-1.9387	75.6816	0.1214	-0.2160
2.0000	1.7000	0.0000	36.1085	36.1861	-0.0776	36.5051	-0.3966	35.9110	0.1975	-0.1694
1.4000	1.7000	90.0000	66.3677	66.6319	-0.2642	66.9446	-0.5769	67.0610	-0.6933	-0.1293
1.7000	1.7000	90.0000	52.9062	52.3866	0.5196	53.5288	-0.6226	53.3793	-0.4731	-0.1197
1.8000	1.7000	90.0000	47.6675	46.8231	0.8444	48.1344	-0.4669	47.9850	-0.3175	-0.1181
2.0000	1.7000	90.0000	38.9108	37.8186	1.0922	38.9724	-0.0616	39.0104	-0.0996	-0.1142
2.2000	1.7000	90.0000	32.0181	30.9448	1.0733	31.6760	0.3421	32.0055	0.0126	-0.1103
2.3000	2.0000	90.0000	42.8577	41.9989	0.8588	42.3258	0.5319	42.8007	0.0570	-0.0932
2.5000	2.0000	90.0000	38.4920	37.6212	0.8708	37.7364	0.7556	38.3476	0.1444	-0.0877
2.1000	1.4000	0.0000	28.4216	28.5716	-0.1500	28.2527	0.1689	28.2696	0.1520	-0.1568
1.4000	1.5000	90.0000	72.3722	72.1422	0.2300	72.8458	-0.4736	73.0841	-0.7119	-0.1407
1.7000	8.0000	90.0000	101.0327	101.2859	-0.2532	100.7703	0.2624	101.1116	-0.0789	0.1791
2.3000	-2.3000	0.0000	27.7361	27.9575	-0.2214	28.1351	-0.3990	27.6967	0.0394	-0.0866
3.0000	-3.0000	0.0000	63.9537	64.1158	-0.1621	64.0924	-0.1387	63.9627	-0.0090	-0.0205
1.0000	-1.4000	60.0000	92.5805	93.5497	-0.9692	93.0723	-0.4918	92.8342	-0.2537	-0.2117
1.0000	-1.2000	45.0000	112.4147	113.2808	-0.8661	112.7839	-0.3692	112.2328	0.1819	-0.2246
1.9000	-1.9000	120.0000	62.5400	63.9029	-1.3629	63.6481	-1.1081	63.3915	-0.8515	-0.1106

^a τ in a_0 , θ in degrees, and energies are in kcal/mol relative to energy of $\text{H}+\text{H}_2(r=1.401)$, $-1.673994390 E_h$. A negative τ_{H_2} value is used to specify that the coordinate is τ_1 , τ_2 , and θ_{12} .

^b $\chi=54.7356$ corresponds to 54.73561032.

^c δ_{bas} is the London basis set correction for the present calculations relative to $\text{H}+\text{H}_2$. One measure of the agreement between the calculated energies and the fits, particularly the BKMP potential, is obtained by adding $\Delta E + \delta_{\text{bas}}$ —see the text. The basis set correction for H_2 is -0.3133 kcal/mol.

Table IVa. Expansion coefficients^a V_n (kcal/mol) for $r_{H_2} = 1.2 a_0$

$r(a_0)$	V_0	V_2	V_4	V_6	V_8
1.8	48.477	7.206	5.113	0.509	0.102
2.0	35.987	1.861	2.302	0.237	0.032
2.2	27.216	0.045	0.993	0.112	0.012
2.5	18.176	-0.331	0.251	0.035	0.003
3.0	9.183	0.059	0.016		
4.0	1.934	0.102	0.000		
5.0	0.253	0.009	-0.001		
6.0	-0.020	-0.008	0.000		
7.0	-0.033	-0.006	0.000		
8.0	-0.019	-0.003	0.000		

^aBlank entries indicate that the term was not included in the fit.

Table IVb. Expansion coefficients V_n (kcal/mol) for $r_{H_2} = 1.401 a_0$

$r(a_0)$	V_0	V_2	V_4	V_6	V_8
1.8	43.386	6.051	10.473	1.049	0.430
2.0	31.794	-1.320	4.766	0.530	0.129
2.2	24.036	-3.332	1.995	0.275	0.043
2.5	16.322	-2.793	0.391	0.093	0.011
3.0	8.633	-0.858	-0.055		
4.0	1.960	0.048	-0.010		
5.0	0.266	0.007	-0.002		
6.0	-0.023	-0.011	-0.001		
7.0	-0.038	-0.008	0.000		
8.0	-0.022	-0.004	0.000		

Table IVc. Expansion coefficients V_n (kcal/mol) for $r_{H_2} = 1.449 a_0$

$r(a_0)$	V_0	V_2	V_4	V_6	V_8
1.6	60.2286	26.9028	25.7629	2.9543	1.9716
1.7	49.9297	13.9850	17.8003	1.8156	1.0662
1.8	41.9195	5.7196	12.2588	1.2063	0.5942
1.9	35.6059	0.6223	8.3590	0.8430	0.3225
2.0	30.5564	-2.3270	5.6128	0.6115	0.1764
2.2	23.0717	-4.4369	2.3519	0.3294	0.0570
2.5	15.7320	-3.6383	0.4373	0.1144	0.0151
3.0	8.4351	-1.2047	-0.0880	0.0092	0.0027
3.5	4.2592	-0.1971	-0.0468	-0.0004	0.0000
4.0	1.9579	0.0239	-0.0145	-0.0002	-0.0004
4.5	0.7985	0.0295	-0.0046	-0.0002	-0.0004
5.0	0.2684	0.0061	-0.0020	-0.0002	-0.0003
5.5	0.0514	-0.0077	-0.0013	-0.0001	-0.0002
6.0	-0.0240	-0.0115	-0.0010	0.0001	-0.0001
6.5	-0.0417	-0.0107	-0.0007	0.0001	0.0000
7.0	-0.0389	-0.0083	-0.0005	0.0002	0.0000
7.5	-0.0309	-0.0061	-0.0003	0.0001	0.0000
8.0	-0.0230	-0.0043	-0.0002	0.0001	0.0000
8.5	-0.0167	-0.0030	-0.0001	0.0000	0.0000
9.0	-0.0120	-0.0020	-0.0001	0.0000	0.0000
10.0	-0.0064	-0.0010	0.0000	0.0000	0.0000

Table IVd. Expansion coefficients V_n (kcal/mol) for $r_{H_2} = 1.7 a_0$

$r(a_0)$	V_0	V_2	V_4	V_6	V_8	V_{10}
1.8	32.857	4.962	25.585	2.265	2.843	0.270
2.0	22.657	-8.380	12.465	1.083	0.813	0.029
2.2	16.657	-11.898	5.486	0.665	0.244	0.013
2.5	11.563	-9.961	0.949	0.308	0.050	
3.0	6.885	-4.042	-0.427	0.019	0.008	
4.0	1.884	-0.219	-0.068			
5.0	0.276	-0.009	-0.006			
6.0	-0.029	-0.017	-0.002			
7.0	-0.045	-0.012	-0.001			
8.0	-0.027	-0.006	0.000			

Table V. Summary of the results for the H-H₂ van der Waals potential well.

	$r_e(a_0)$	$D_e(\mu E_h)$	$A(E_h)$	$\alpha(a_0^{-1})$
<i>ab initio</i> ($r_{H_2}=1.449 a_0$)	6.62	67	4.01	1.629
lower bound	6.54	72	4.55	1.652
predicted	6.51	75	5.05	1.669
upper bound	6.48	78	5.57	1.686
BMD ^a	6.54	61.4		
MBMD ^a	6.56	66.8		

^aRef. 20.

Figure Captions

Fig. 1. A comparison of the spherically-averaged H-H₂ interaction energy for $r_{H_2} = 1.401 a_0$ from the present calculation (solid line) with the corresponding averages for various fitted potentials (dotted lines) and the potential energies deduced from measured scattering cross sections (dashed lines).

Fig. 2. A comparison of the spherically-averaged H-H₂ interaction energy from the present calculation (solid line) with the corresponding averages for various fitted potentials (dotted lines) and the potential energies deduced from measured scattering cross sections (dashed lines).

Fig. 3. The coordinate system used for most of the energy calculations.

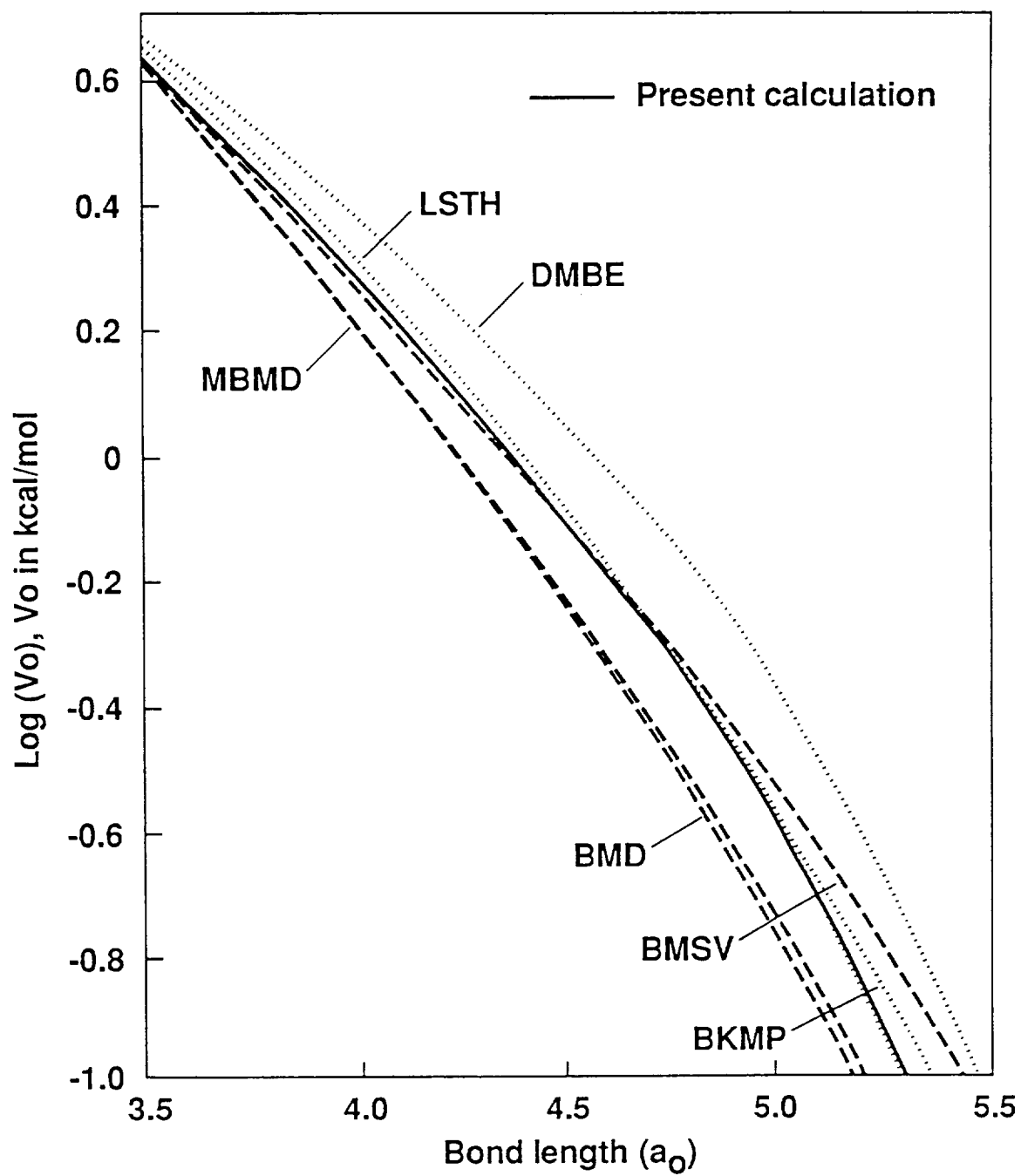
Fig. 4. Selected cuts through the potential energy from the present calculation (data points with a spline curve fit) obtained for $r = 1.8 a_0$ and certain values of r_{H_2} . The corresponding cuts for the BKMP potential (dashed line) are shown for comparison.

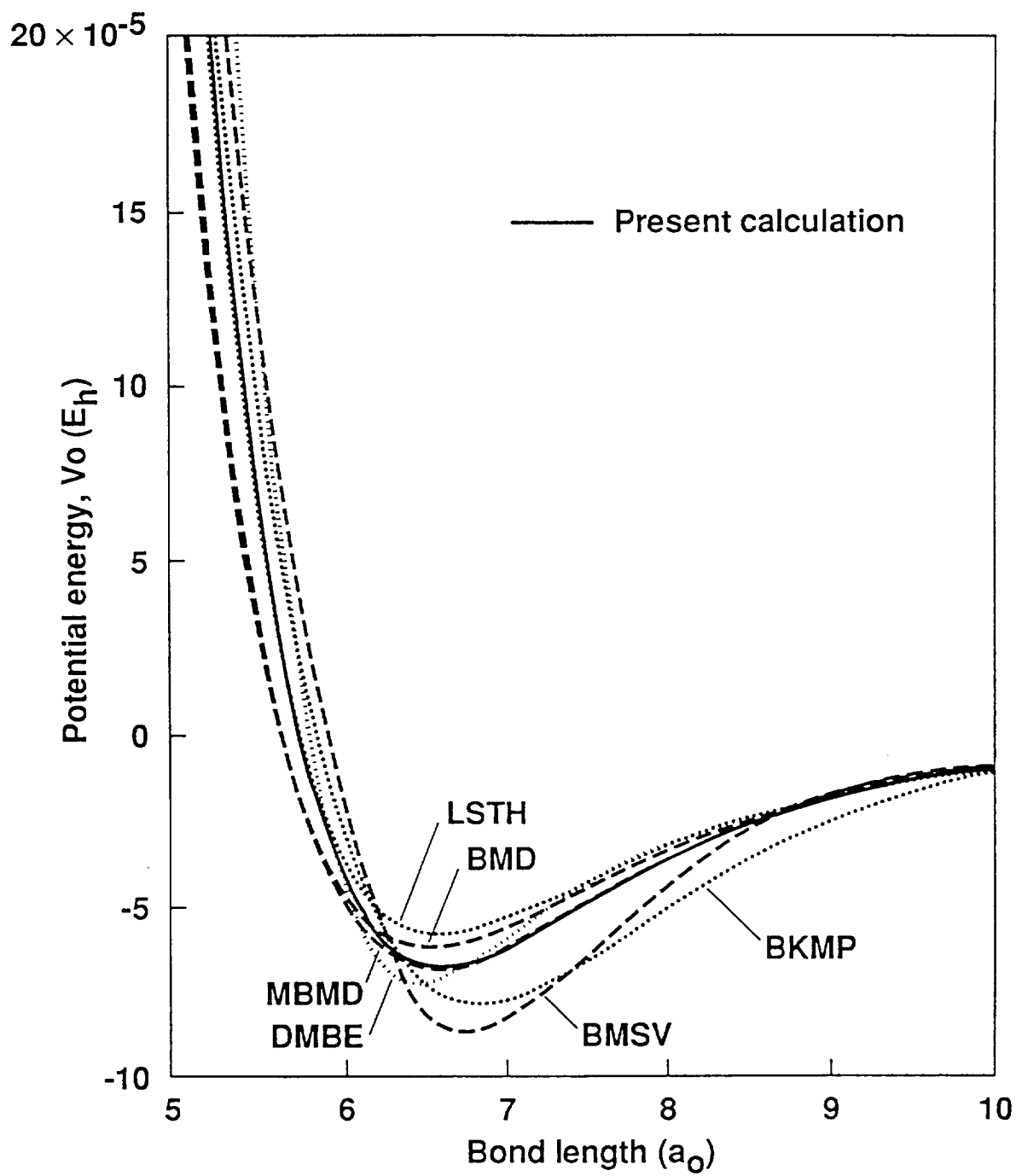
Fig. 5. Van der Waals potential energy curves for $r_{H_2} = 1.449 a_0$ and certain values of χ ; the curves were constructed from spline fits to the discrete data.

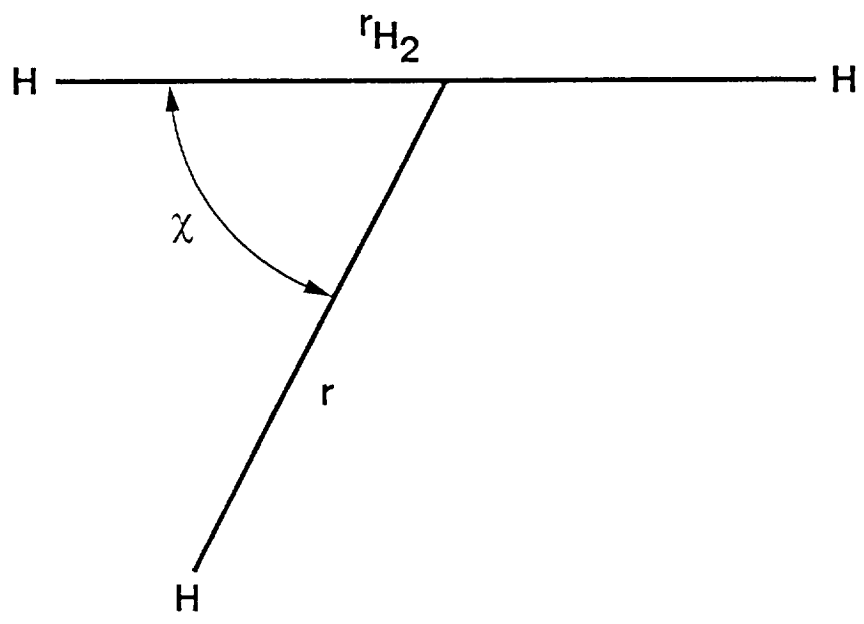
Fig. 6. A comparison of the potential coefficients from the present calculation (data points with a spline curve fit) for $r_{H_2} = 1.449 a_0$ with the corresponding results for the BKMP potential (dashed lines).

Fig. 7. A comparison of the values of $V_0(r, r_{H_2} = 1.449 a_0)$ from Table IVc (data points) with the values obtained from the MTT potential for $\chi = \chi_0$ (dashed line) and the predicted potential (solid line) with $D_e = 75 \mu E_h$, which is like the MTT potential for $\chi = \chi_0$ except that the repulsive parameters have the values indicated in the figure.

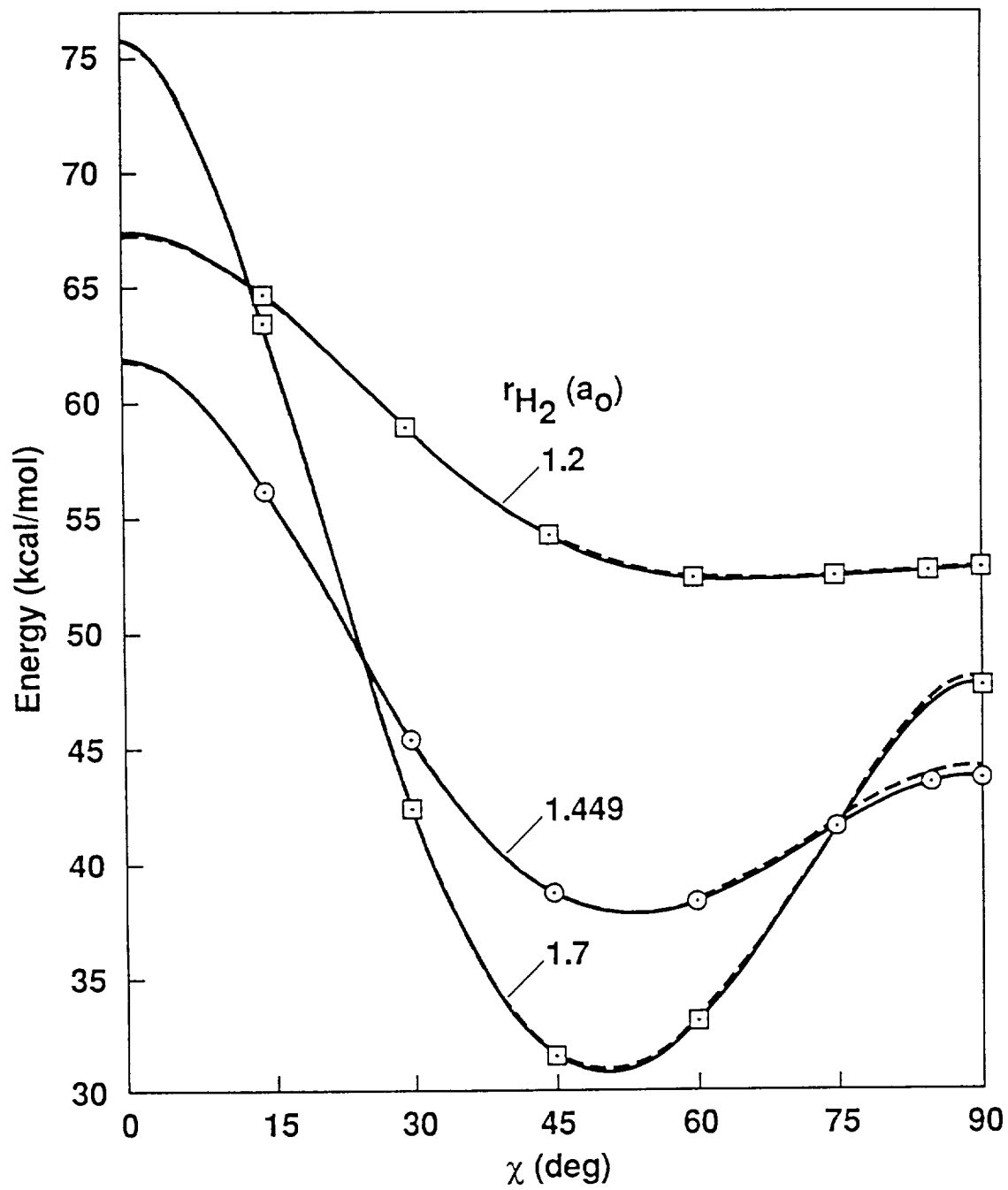
Fig. 8. A comparison of the theoretical high-resolution D-H₂ differential elastic scattering cross section (solid line) calculated from the present results for the interaction energy (see text) with the measured data (represented by the data points with error bars) from the crossed beam scattering experiment of Ref. 20. The cross sections are shown for the laboratory system for a peak collision energy = 35.8 meV. The measured cross sections have been normalized to the theoretical results at large scattering angles since absolute cross sections were not obtained in the experiment.







Partridge-3



Partridge-4

